Mathematical Approach of MSE in Thermo-poro-elastic Conditions Improves Decision Making to Use Bore Hole Enlargement (BHE)

By

Abbas Roohi

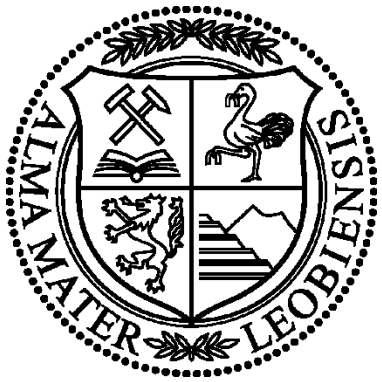

A Thesis Submitted to the Department of Petroleum Engineering

Chair of Drilling and Completion Engineering

Montanuniversität Leoben

In Partial Fulfilment of the Requirements for the Degree of Doktor der montanistischen Wissenschaften

January 2017

Affidavit

I declare in lieu of oath, that I wrote this thesis and performed the associated research myself, using only literature cited in this volume.

……..

Abbas Roohi, 2017

Acknowledgments

All glory and honour goes to God, the Almighty, as nothing would have been possible without his abundant grace and love.

I would like to express my deep and sincere gratitude to my supervisor, Professor Dr. Gerhard Thonhauser, Chair for Department Petroleum Engineering, Montanuniversität Leoben, for the opportunity and continuous support for my PhD study and research, for his patience, motivation, enthusiasm, and immense knowledge. His outstanding guidance helped me during the time of research and writing of this thesis. I wish to also thank him for providing extra funding through the University for my study when it was needed.

My profound gratitude goes to Dr. Thomas Finkbeiner for accepting to be the second referee for my thesis.

I am very grateful to Dr. Samiullah Baig, Department of Simulation and Modelling of Metallurgical Processes, for his kind support, guidance, constructive and valuable comments and suggestions throughout my work. In addition, I would in particular like to thank Dr. Michael Prohaska, for his special supports.

I owe a lot of gratitude to Dipl. Ing. Manfred Frenzl, Technical Manager of TDE Equipment and Manufacturing GmbH. I also give thanks to my workers at TDE E&M for their kind support and the lovely interactions.

Many thanks must go to my colleagues at the Department Petroleum Engineering (DPE) in general and the Statistics Group in particular not forgetting our awesome Secretary, Frau Patrizia Haberl; for the immense contributions and wonderful working atmosphere and environment.

Finally, I owe my loving thanks to my wife Mahsoomeh for her amazing love and support especially through the hard times. Her soothing words always made me feel better and urged me on. Therefore, it is not surprising that I dedicate this thesis to her and our miraculous kids, Amir Hossein, Amir Mohammad and Hadis. Since their birth, they have brought a lot of energy, joy and blessings to our home. I wish to thank my lovely mum, dad, siblings and all friends. Without their encouragement, understanding, support and prayers it would have been impossible for me to finish this work.

Abstract

Historically Bore Hole Enlargement (BHE) operations have been restricted to softer formations. However, when including thermoporoelasticity as part of deriving Mechanical Specific Energy (MSE) for BHE more informed decisions can be made for BHE for a specific formation in the sense of optimizing reamer-pilot size ratio.

This thesis focuses on the development of a thermoporoelastic model of rock mechanics for quantifying the stress distribution around the wellbore and the Apparent Rock Strength (ARS) after drilling a pilot hole. This is intrinsically linked to fluid and heat diffusion due to the effects of the drilling fluid. Indeed, ARS of the rock in the Depth of Cut (DOC) zone beneath the reamer can be determined by using Mohr-Coulomb theory. Additionally, the MSE is analytically estimated in different rock formations which is named as Analytical Mechanical Specific Energy (AMSE), for varying permeability values, in the presence of non-hydrostatic in-situ stress.

Following these parameters, a set of laboratory drilling tests were carried out on sandstone formation. The rock samples were drilled and reamed, and the MSE calculated by using measured drilling parameters. Prior to the test, the rock samples were either pressurized by circulating highly pressurized mud; or heated up in an oven. The rock underwent confining and overburden pressure, a circulation of high pressure, and it was exposed to high or low temperature mud. The effects of stress alteration, pore pressure, temperature, time, distance between the pilot and a hole enlargement tool on the rock weakening around the wellbore and the performance of the hole enlargement operation, were studied. MSE was calculated and compared for different test conditions to determine the hole enlargement performance.

To conclude, as the pilot hole is created, stress alteration will occur around the wellbore and the rock will weaken due to stress alteration, mud diffusion and heat diffusion. This simulation can help to estimate the optimum reamer/pilot size ratio, as well as the positioning of the reamer in order to take advantage of rock weakening around the wellbore.

Considering that so far in the market there is no evidence of a specific model to predict rock strength below the reamers, this research and study shows its degree of novelty since it proposes a model to fill this gap by estimating AMSE applying thermoporoelastic approach. The model can be fine-tuned and used as a reference application in the petroleum industry to facilitate decision making and project cost analysis.

Kurzfassung

Traditionell wird die Bohrlocherweiterung (engl.: „Borehole Enlargement“ – BHE) nur beim Bohren durch weiche Formationen angewandt. Wenn man jedoch die Thermoporoelastizität in die Bestimmung der spezifischen mechanischen Energie (MSE) miteinbezieht, hat man eine bessere Entscheidungsgrundlage zu Verfügung, wann bzw. ob man BHE anwendet, insbesondere wenn es darum geht, das Größenverhältnis Räumer/Pilot zu optimieren.

Der Fokus dieser Arbeit liegt auf der Entwicklung eines thermoporoelastischen Modells, das in der Felsmechanik angewandt werden kann, um sowohl die Spannungsverteilung um ein Bohrloch herum als auch die Bruchfestigkeit der Formation nach dem Bohren der Pilotbohrung zu quantifizieren. Diese steht in unmittelbarer Verbindung zur Flüssigkeits- und Temperaturverteilung durch die Einwirkung der Bohrspülung. Tatsächlich kann die Bruchfestigkeit des Gesteins direkt unterhalb des Räumers mit dem Mohr-Coulomb Kriterium bestimmt werden. Zusätzlich wird die spezifische mechanische Energie in verschiedenen Formationsarten, bei variabler Permeabilität und unter realitätsnahen, Spannungen im Gestein bestimmt.

Mit den gewonnen Parametern eine Reihe an Bohrversuchen mit Sandsteinproben im Labor durchgeführt. Die Gesteinsproben wurden gebohrt und ausgeweitet. Im Anschluss wurde mit den gemessenen Daten die spezifische mechanische Energie bestimmt. Vor den Tests wurden die Proben entweder in einem Ofen erhitzt oder unter Druck gesetzt, indem Bohrspülung unter Hochdruck zirkuliert wurde. Während der Versuche waren die Proben allseits eingespannt und gezielt temperierte Bohrspülung wurde unter Hochdruck zirkuliert. Dabei wurden die Auswirkung von Spannungsänderung, Porendruck, Temperatur und Abstand zwischen Pilot und Räumer auf die Schwächung der Formation rund um die Bohrung und die Performance des Ausweitungsvorgangs untersucht. Die spezifische mechanische Energie wurde berechnet und mit verschiedenen Testszenarien verglichen um die Performance des Ausweitungsvorganges zu ermitteln.

Zusammengefasst kann festgestellt werden, dass es durch die Pilotbohrung zu Spannungsänderungen rund um die Bohrung kommt, was, zusätzlich zum Eindringen von Spülung und Hitze, zu einer Schwächung der Formation führt. Diese Simulation kann bei sowohl der Bestimmung des optimalen Größenverhältnisses zwischen Räumer und Pilot als auch beim Positionieren des Räumers hinter dem Piloten helfen, um die Schwächung der Formation möglichst gut auszunutzen.

Bisher gibt es am Markt keine Anzeichen für ein solches spezifisches Modell, das die Bruchfestigkeit der Formation unterhalb des Räumers vorhersagt. Der verwendete, thermoporoelastische Ansatz zur analytischen Bestimmung der spezifischen mechanischen

Energie stellt auf jeden Fall eine neuartige Herangehensweise an das Problem dar. Das Modell kann anwendungsspezifisch angepasst und als Referenzanwendung in der Öl- und Gasindustrie herangezogen werden, sowohl um Entscheidungen während der Bohrphase als auch im Rahmen der Projektkostenanalyse zu fällen.

Table of Contents

1 Introduction and Problem Statement 1-1

1.1 Goal of the Thesis 1-1

1.2 Analytical Modelling 1-2

1.3 Experimental Proofing 1-3

2 Bore Hole Enlargement (BHE) Tools 2-1

2.1 Introduction 2-1

2.2 Values of BHE 2-2

2.3 BHE Tool Challenges 2-3

2.3.1 Bit and Reamer Matching 2-3

2.3.2 Drilling Parameters 2-4

2.3.3 Drilling Dynamics 2-5

2.3.4 The BHA's Neutral Point (NP) 2-6

2.3.5 Formation Scenarios 2-7

2.4 Operational Considerations 2-8

2.4.1 Formation Parameters 2-8

2.4.2 Trajectory 2-9

2.4.3 Hole Quality 2-9

2.4.4 Drill Out Casing Shoe 2-9

2.4.5 Reliability 2-9

2.4.6 Drilling Parameters 2-9

2.4.7 Weight and Torque Sharing 2-10

2.4.8 Cutting Structure Matching 2-11

2.4.9 Vibration Mitigation 2-12

3 Specific Energy Concept 3-1

3.1 Introduction 3-1

3.2 Properties Used as Drillability Index 3-1
3.3 Specific Energy (SE) Concept 3-2
3.4 MSE Background Knowledge 3-3
3.5 MSE Model 3-5
4 Thermoporoelastic Theory 4-1
4.1 Introduction 4-1
4.2 Problem Definition 4-2
4.3 Governing Equations 4-5
4.3.1 Conservative Laws 4-5
4.3.2 Constitutive Laws 4-5
4.3.3 Diffusivity Laws 4-6
4.4 Field equations 4-6
4.4.1 Deformation Equation 4-7
4.4.2 Fluid Diffusion Equation 4-7
4.4.3 Heat Diffusion Equation 4-7
4.5 The Fully Coupled in Polar Coordinates 4-8
4.6 Loading Decomposition 4-10
4.6.1 Problem I 4-10
4.6.2 Problem II 4-11
4.6.3 Problem III 4-12
4.7 Semi-Analytical Solutions 4-12
4.7.1 Problem I 4-13
4.7.2 Problem II 4-22
4.7.3 Problem III 4-22
4.8 Superposition 4-23
4.9 Result in Time Domain 4-23
5 Experimental Design 5-1
5.1 Experiment Goal 5-1
5.2 Hypothesis 5-1

5.3 Lab Facility 5-6
5.4 Parameters 5-7
5.5 Proposed Design of Pilot-Reamer Arrangement 5-7
5.6 Test Procedure 5-8
6 Results and Discussions 6-1
6.1 1st test 6-3
6.2 2nd test 6-9
6.3 Third, fourth and fifth tests 6-12
6.4 6th and 7th test 6-16
6.5 8th and 9th test 6-20
7 Summary and Conclusions 7-1
8 Further Work 8-1
9 List of Abbreviations 9-1
10 References 10-1

List of Figures

Figure 2-1 Borehole Enlargement (BHE) *2-2*
Figure 2-2 Bit ROP/Torque response at constant RPM *2-4*
Figure 2-3 Neutral Point (NP) location on the BHA, after Mensa [4] *2-7*
Figure 2-4 Bit-Reamer critical scenarios,after Mensa [4] *2-8*
Figure 2-5 A simple analogy of Concept of Depth of Cut (DOC) control technology *2-12*
Figure 3-1 Power Graph, [56], [57] *3-9*
Figure 4-1 Problem definition *4-3*
Figure 4-2 Loading decomposition scheme *4-13*
Figure 4-3 (a) Relationship between the two local coordinate systems, (b) stress components acting in the plane perpendicular to the borehole in cylindrical coordinate system *4-14*
Figure 5-1 Rock strength estimation in the vicinty of wellbore *5-3*
Figure 5-2 Low permeable thermoporoelastic induced transient pore pressure distribution (a) and AMSE profile (b) [84], [85] *5-4*
Figure 5-3 Medium/high permeable thermoporoelastic induced transient pore pressure distribution (a) and AMSE profile (b). *5-5*
Figure 5-4 Very High permeable formation pore pressure distribution (a) and AMSE distribution (b). *5-6*
Figure 5-5 Principle of the Drilling Test Facility (DTF) *5-7*
Figure 5-6 Cross-section of the drilled sample *5-7*
Figure 5-7 Drilling Test Facility *5-7*
Figure 5-8 The XOS, Pilot bit and Reamer arrangment *5-8*
Figure 5-9 XOS, Pilot bit and Reamer *5-8*
Figure 5-10 Problem definition (First scenario) *5-9*
Figure 5-11 Problem definition (Second scenario) *5-9*
Figure 6-1 Drilling parameters: RPM, Depth *6-3*
Figure 6-2 Drilling parameters: ROP (ROPc: calculated) was increased to different levels *6-4*
Figure 6-3 Drilling parameters: WOB, TOB *6-4*
Figure 6-4 Mechanical Specific Energy (MSE) and Pressures *6-5*
Figure 6-5 ROP vs MSE: Zones 6, 7 and 8 show higher performance, any zone placed on a particular power curve which means power loss is very low *6-6*
Figure 6-6 Depth of Cut vs MSE: there is a riverse relation between DOC and MSE *6-7*
Figure 6-7 Torque vs WOB: Beyond the critical depth of cut, any WOB increase transfers into the bit's matrix body *6-8*
Figure 6-8 Wear ring on body bit indication of high WOB *6-8*
Figure 6-9 Smooth bottom hole, indicates very low vibration frequency/rate *6-9*

Figure 6-10 2nd test plan: Maintain RPM, increase ROP, WOB will be adjusted by machine to reach target ROP6-10
Figure 6-11 2nd pilot and reamer: larger cutter size which leads to lower MSE 6-10
Figure 6-12 Test 2: Full hole, High Pore pressure, High Temperature (A): ROP, Depth, WOB, TOB vs Time, (B) MSE, Confine, Overburden, Pore and Mud pressure vs Time 6-11
Figure 6-13 Test 3: Full Hole bit, High Pore pressure, High Temperature (A): ROP, Depth, WOB, TOB vs Time, (B) MSE, Confine, Overburden, Pore and Mud pressure vs Time 6-13
Figure 6-14 Test 4: Full Hole, High Pore pressure, High Temperature (A): ROP, Depth, WOB, TOB vs Time, (B) MSE, Confine, Overburden, Pore and Mud pressure vs Time 6-14
Figure 6-15 Test 5: Full Hole, High Pore pressure, High Temperature (A): ROP, Depth, WOB, TOB vs Time, (B) MSE, Confine, Overburden, Pore and Mud pressure vs Time 6-15
Figure 6-16 Pilot and Reamer configuration: The pilot set 10-cm ahead of the reamer 6-16
Figure 6-17 The sample was enlarged and broken due to long period of time off-bottom rotation at the same depth 6-17
Figure 6-18 test 6: Pilot - Reamer 10-cm distance, No Pore pressure, High Temperature: MSE reduces as the combination of the pilot-reamer drill and over time. Time can be translated to distance between the pilot and the reamer. It was shown before in section 5.2 6-18
Figure 6-19 test 7: Pilot - Reamer 10-cm distance, No Pore pressure, High Temperature: Reduction of MSE confirms the Hyptothesis in section 5.2 6-19
Figure 6-20 Test 8: Pilot - Reamer 10-cm distance, High Pore pressure, Ambient Temperature: The rock sample was broken due to high vibrations, ... 6-21
Figure 6-21 Test 9: Pilot - Reamer 10-cm distance, High Pore pressure, Ambient Temperature: One cutter was broken, therefore MSE higher than former test 6-22
Figure 6-22 the pilot bit balling (test 9) 6-23
Figure 6-23 Broken cutter (test 9) 6-23
Figure 6-24 Extreme vibration while rotating off bottom (test 8), unsmooth wellbore is a good indication of viberation 6-23

List of Tables

Table 2-1 - Ranking of application dificulty for BHE [4] *2-8*

Table 5-1 Test Key Parameters (Lab operational condition, [60], [62]) *5-3*

Table 5-2 Sample cells *5-7*

Table 6-1 Summary of the test condition (Rock sample: Sandstone Vosges) *6-2*

1 Introduction and Problem Statement

1.1 Goal of the Thesis

Bore Hole Enlargement (BHE) technology falls into two main categories, eccentric and concentric reamers. Generally, eccentric types include fixed cutter tools such as bi-center drill bits. The second group comprises a broader variety of models. This includes fixed blades as well as more complex tools, operating either hydraulic or mechanical controls on demand. These techniques are utilized when an operator is required to enlarge the hole, but it is necessary for the tool to pass through a limited diameter restriction, as compared with the planned hole size.

Regardless of whether an eccentric reaming tool or a concentric under-reamer is utilized, there are generally three BHE techniques used. These are Casing-While-Drilling (CWD), Dual Body Bit (DBB) and a hole opener, along with a pilot bit.

The mentioned techniques, BHE, provide several advantages to operators:

- ✓ Setting larger casing strings deeper into holes, where wellbore stability, high-pressure sections and lost circulation are encountered as typical problems. This is decided typically so as to eliminate numerous trips, which would leave open-hole formations exposed to fluid interactions for a shorter period of time.
- ✓ Greater clearance between the casing and the wellbore is provided by the reamer, which can render an improved cement job.
- ✓ Providing a sufficiently large bore hole and more complex completion string access to reservoir has several advantages for exploration and production wells [1], [2].

However, the deployment of two cutting tools, pilot bit and reamer, in-hole opening BHAs lead to additional drill string vibration [3]. As a consequence of these challenges, hole enlargement usage generally suffers from the following detrimental issues: downhole tool

failures, shorter BHA life time, lower drilling performance, poor borehole quality, and comprised directional efficiency [4]. These drilling problems, which have profound negative effects on AFE, and are even more magnified in deep water drilling [5].

It is crucial to first understand the effects of drilling a well into rock to understand the performance improvements that can be achieved using the BHE compared to conventional full-hole bits. When a drill bit penetrates the formation, the stress state – as well as the pore pressure and temperature of the rock – surrounding the bit and the wellbore will significantly alter from their original in situ state. In effect, the rock becomes stress alteration; however, most conventional drill bits gain little advantage from this effect [6]. In contrast, BHE tools effectively apply this stress alteration due to their configuration. The pilot hole, which is initially drilled by the pilot section of the BHE, performed very similarly to when using a conventional bit; nevertheless, as a result of its smaller diameter, less rock volume has to be removed. The smaller pilot leads to a slight improvement in the rate of penetration in comparison to a larger diameter bit. After making this pilot hole, the stress state, pore pressure and temperature in the surrounding rock change due to the stress alteration effect, drilling fluid diffusion and thermal diffusion. Consequently, when the succeeding reamer section continues enlarge the hole, it does so through this stress-altered rock; which will weaken further. The consequence of this effect is that the reamer section requires less power to destroy the remaining rock to the full extent of the hole's diameter, which leads to a further improvement in ROP.

Bencic, A. 1998, addressed further investigation into the distance that the pilot bit projects ahead of the following reamer bit (hole opener) [7]. It is believed that for different rock strengths a variation of pilot lengths might be required for an optimized drilling performance. Therefore, the main aim of this work is to investigate the optimum pilot length.

1.2 Analytical Modelling

This thesis illustrates a coupled thermo-poroelastic model, taking into account the compressibility and thermal expansion of components, convective temperature diffusion and porosity variation and related properties of a saturated rock.

Mechanical Specific Energy (MSE) is the energy required to destroy a given volume of the rock during the drilling process. Note that lower specific energy renders a more efficient drilling process in a given drilling environment. The MSE measured at atmospheric pressure conditions could have an approximate value of the Unconfined Compressive Strength (UCS) of the rock when drilling with maximum efficiency [8], [9], [10]. The least possible MSE is approximately equal to the compressive strength of the formation being drilled [11]. However, the calculated specific energy is practically rarely equal to the strength of the rock due to

inefficiencies within the drilling system like friction and drilling vibration (axial, lateral, and torsional).

In this thesis, concentration is on the estimation of the least value of MSE by calculating Apparent Rock Strength (ARS) redistribution using Mohr-Coloumb theory. More precisely, it is concentrated on the reamer/pilot configuration for BHE application and bit design in certain formation in order to get advantage of rock weakening around the wellbore after creating the pilot hole. For this purpose, two different formations properties and in-situ stress have been considered. Then, the data served as input to a thermoporoelastic model to analysis the borehole wall behaviour and reamer performance. In addition, compressive strength for rock in the Depth of Cut (DOC) zone just below the pilot bit were estimated in order to compare and illustrate the significance of a weakened section/interval surrounding the wellbore (base on method is developed by [12], [13]).

This research also explores the theoretical relationship between bit and reamer size and models a minimum MSE for predicting an optimal reamer / bit size ratio. The method enables selecting the reamer size that best complements a given bit size as well as estimate an optimum distance between reamer and bit based on best time elapsed to destroy wellbore rock by reamer in relation with Rate of Penetration (ROP).

1.3 Experimental Proofing

In final part of the research, a PDC pilot bit was set up and a reamer test procedure was performed to verify analytical modelling. Since this work was a continuation study of Dr. Antonio Bencic [14], the pilots and reamers have been left from his research were used in drilling facility test at Mines De Paris. Meanwhile, another part was to identify weak spots and to modify any designs concern. Thus, it was essential to establish and set up a continuous feedback loop. The configurations of pilot and reamer were planned, and evaluated.

Afterwards, the visual quality control procedure was established, mainly to address the bit and the PDC cutters. The new bits have been checked and additional inspections have been performed after each individual test run. This was targeted to determine e.g. the wear stage of the individual cutters and body.

The following chapters give a detailed overview of the Multi - diameter's classifications, challenges and implemented, geomechanic, MSE and thermoporoelastic theory.

The primary outcome of the research was to evolve the weakening zone around the wellbore using thermoporoelastic model. The method enables the engineers to select the reamer size that best complements the bit to be properly utilized.

The next outcome of the research is to estimate optimum distance between reamer and bit based on the best time elapsed to destroy wellbore rock by reamer in relation with ROP.

2 Bore Hole Enlargement (BHE) Tools

2.1 Introduction

Generally, hole opener or enlargement tool is defined as simultaneous multi-diameter drilling, with bit and reamer in a single Bottom Hole Assembly (BHA) pass. Furthermore, the diameter of the hole drilled is anticipated to be bigger than the internal diameter (ID) of the last set casing.

Hole openers are about a century old. This technology was initially designed as fixed-blade concentric tools employed to clean up or enlarge existing drilled wellbores. Since almost 45% of wells drilled take advantage of some kind of Bore Hole Enlargement (BHE) technology, this technology has become commonplace [15]. It grants for tighter tolerance casing pass through in an existing casing string and also provides larger annulus clearances in the open hole sections to mitigate practical challenges such as swab/surge pressures, improved cementing jobs, complicate completion string, meet production target and wellbore stability. Generally, hole opener tool, falls into two main categories, ***Eccentric*** and ***Concentric*** reamers, each of these with their own design aspects. Both of them comprise tools that can be positioned higher up in the drill string at some distance from the bit or alternatively directly at the bit. A variety of enlargement tools exist nowadays, each of them designed for a special usage. Figure 2-1 illustrates BHE classification.

Regardless of whether an eccentric reaming tool, or a concentric under-reamer is utilized, there are generally three BHE techniques used in addition to conventional rotary drilling. These are Casing-While-Drilling (CWD), Dual Body Bit (DBB), (this concept was developed by Bencic and de Sousa in 1990's [16], [17] for slim hole drilling), and using a hole opener and a pilot bit simultaneously.

The following sub-sections summarize values, challenges and some operational considerations of BHE tools.

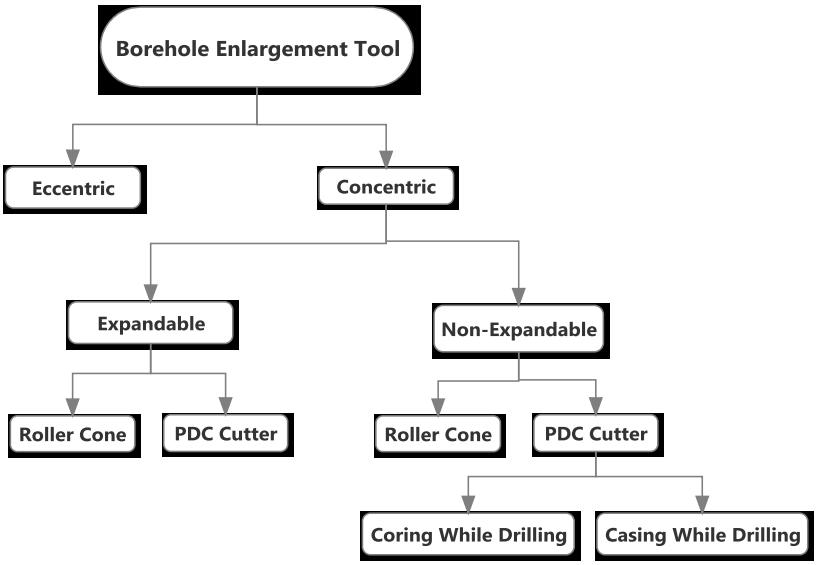

Figure 2-1 Borehole Enlargement (BHE)

2.2 Values of BHE

The merits of the hole opening systems are well documented. Csonka et al. (1996) show an example of the cost effectiveness of BHE drilling technology in offshore wells in Australia [18]. Dewey et al (1996) present the benefits of under reaming during drilling operations, according to two parameters': efficiency and cost effectiveness [19]. Hyatt et al. (1997) discuss another successful example of under reaming drilling in Egypt [20]. Miller et al. (2003) presented a concentric reamer as a supersession of the bi-center bit in order to enlarge holes [21]. According to the authors, although using a concentric bit is a cost-effective approach to enlarge hole, the tool suffers from mechanical deterioration. Courville et al. (2004) presented the major issue of hole opening a well in deep water, thereby facilitating a multiple casing string [22]. The authors argued that their new technology is reliable and improves wellbore quality. Mason et al. (2007) discusses drilling and under reaming apart from the hole cleaning of extended reach wells, drilled from an offshore Platform [23]. Applying a rotary steerable system (RSS) to drill five directional wells with Multidiameter BHAs resulted in lower vibration (Jones et al., 2008) [24]. The authors also conclude that the concentric under reaming systems provide a cost-effective approach. T. Ho et al. (2013) describes a successful case study of drilling an offshore well in GOM with an under reamer and RSS [25]. The authors explain this favourable experience in different aspects: ROP, MSE, Lateral vibration and stick slip, hole verticality and dog leg severity. The bit and the under-reamer selections were based on the knowledge and information of offset well analysis drilled in the area. The application of DOC control facilitated

the bit and under reamer synchronization that was implemented in the bit design and was introduced first time by Thomson et al. (2008) [26].

BHE Applications are:

- ✓ Control ECD
- ✓ Manages pore pressure anomalies
- ✓ Ensure that casing and string and liners reach total depth (TD)
- ✓ Executing a proper cement job

2.3 BHE Tool Challenges

Traditionally, borehole enlargement has faced numerous challenges. Some of those challenges, such as tool failure, were not robust enough and likely to fail downhole, finally led to costly fishing operation. Some reamers' designs include several sliding mandrels with close tolerances. These features cause difficulties closing post-job due to solid particles settling. In some cases, lower flow rates are required while drilling out the casing shoe and plug, and a higher flow rate can be required to activate the reamer, which is sometimes unable to activate and stay closed during the whole section. Some existing types of concentric reamers have complicated operational conditions, including a fine sharing of flow, pressure drops and WOB in order to work properly. Some hydraulically activated reamers deploy pistons for cutter blades that are tough to close and pull into their casing after drilling. Some reamers on the market are dressed with smaller and fewer effective cutter blocks, leading to only a few PDC cutters, shortening their life and shrinking efficiency. Tool failures regularly occur leaving parts in the wellbore, seal failures and even twist-offs. In the following sections, some of these challenges will be discussed in more detail.

2.3.1 Bit and Reamer Matching

In the oil drilling industry, there is an erroneous assumption that matching the bit to the reamer means having the same cutter size on both tools. This assumption does not take into consideration several other aspects of the drilling process. Due to the rock weakening in the vicinity of the wellbore and the aggressiveness of bit and reamer, both interact with the formation differently. Thus, the drilling dynamics differ from one hole to the next. Even mechanical rock properties may differ because of changes in stress, pore pressure, temperature profile around the wellbore. However, for BHAs without reaming devices, bit aggressiveness is a widely-used term to describe how much weight on bit (WOB) is needed to generate a certain amount of torque on bit (TOB).

Bits and hole openers were traditionally selected as an isolated system and not as part of a whole system. Indeed, the bit was selected regardless of the under-reamer in the BHA, and focused only when placed on the Confined Compressive Strength (CCS) and the formation properties to be drilled. However, this approach has been determined to result in vibrations-related drilling failures and downhole tools damage, was less effective. Consequently, Non-Productive Time (NPT) is increased sharply, and finally it can be translated to high AFE and drilling costs [25].

2.3.2 Drilling Parameters

Drilling parameters such as RPM, flow rate, W_r, are crucial in drilling operations due to their direct impact drilling efficiency. For instance, by applying optimum drilling parameters, drilling dynamics could be managed, and consequently, higher drilling efficiency can be reached. In addition, the pilot bit and enlargement tool could show favourable dull grades and less damage on cutters. In contrast, if a set of sub-optimal drilling parameters is applied, it might lead to drilling dynamics, drilling errors, as well as low ROP. In some cases, the vibrations and drilling dysfunction also result in downhole tool damage and ultimately increase NPT sharply and greater drilling expenses [25].

In terms of drilling parameters, different BHA designs prescribe different practical situations. In spite of that, this fact there is no definite correlation with actual drilling operations. As drilling parameters, regarding their impacts and contributions to hole enlargement performance, are considered as the prism of traditional drilling practice. In other words, the impact of WOB and RPM on ROP and Torque are traditionally assumed similar to pilot bit and enlargement tool (Figure 2-2).

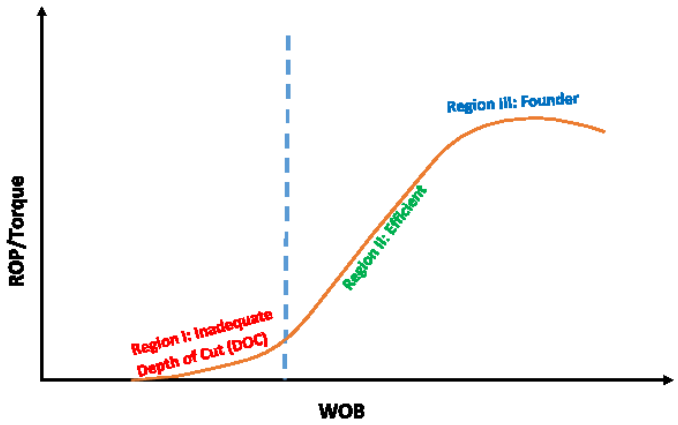

Figure 2-2 Bit ROP/Torque response at constant RPM

Both bits and reamers have some different responses and mechanisms in terms of:

- ✓ Rock failure mechanisms
- ✓ Dissimilar response to WOB and RPM
- ✓ Dynamic behavior
- ✓ Vibrational tendencies
- ✓ Tool failure mechanisms

In addition, one of the over-arching issues in the industry is the distribution of weight and torque over bit and reamer cutting structure, especially when both are a certain distance apart, and, drill different formations. It can happen, that one reamer/bit would out- perform the other (defined here as out-drilling). However, understanding the weight and torque distribution inside the BHA certainly allows a better estimation of the durability of the tools. This will result in optimized downhole performance. Reich (2003) assumes equal MSEs at the bit and reamer [27]. However, his approach does not provide an accurate description of the tool's aggressiveness. Meyer-Heye et al (2010) developed bit aggressiveness by introducing the concept of new blade aggressiveness [28]. In their work, they introduce an analytical approach to estimate load distribution on the BHA, based on ROP and MSE. Furthermore, the authors demonstrate changes in ROP and weight distribution caused by different formations and drilling parameters. They conclude that the torque distribution is only dependent on the cross sectional areas, although the weight distribution varies with tool penetration parameters and cross sectional areas. Too much weight and torque due to deep depth of cut (DOC) result in severe damage to the reamer. The authors relate lower efficiency of the reamer rather than the bit to higher lateral vibrations. Therefore, in order to decrease vibrations, using a stabilizer above reamer was one recommendation suggested. In addition, according to this model it is possible to optimize the cutter layout and cutter density for a given bit and reamer diameter ratio by calculating the loads applied on each tool. The optimized cutter layout results in improved durability.

2.3.3 Drilling Dynamics

It is well-documented that the vibration and stick-slip (SS) are common Key Performance Indicators (KPIs) that the drilling company needs to apply to benchmark drilling operation efficiency. This is related to the fact that drilling performance improves when there are fewer vibrations. It is worth emphasizing that vibrations are unfavourable as they lead to greater damage to the bit and hole opener, cutting structure and a decrease in the ROP. In some instances, the vibrations can also result in directional tool, LWD and MWD tools, and other drillstring failures that can lead to trip out of hole. Sometimes, vibrations also can damage bore hole quality and wellbore integrity which can lead to NPT and in some cases, even the complete loss of the well [25].

In addition, this problem to some extent relates to the fact that full gauge stabilizers cannot be run above the bit. For instance, the largest diameter of a stabilizer is the same as the pilot size, which can be placed immediately above the bit without altering the passage through diameter [29]. Although larger stabilizers, restricted by the casing ID, can be used a couple of drill collars above the enlargement tool, these stabilizers will still be significantly smaller than the final borehole size.

A non-symmetrical mass of eccentric tools can lead to a dynamic imbalance of force that is considerable for large bits. For example, the mass imbalance force for one matrix body 9 7/8" x 13-3/4" bi-center bit was determined to be 240-lbs at 120-RPM, but it will increase fourfold at double RPM. In fact, this will exacerbate if DHM is used in the BHA [29]. In short, the main causes of vibrations are: non-optimized drilling practices, sub-optimal drilling parameters, poor pilot bit and underreamer matching, and non-optimal BHA design. However, these parameters are highly inter-dependent, meaning that non-optimal or sub-optimized efficiency from one set can cast inefficiencies into the other parameter.

2.3.4 The BHA's Neutral Point (NP)

As there are several types of cutting tools in the BHA, one of the greatest challenges is drilling dynamics. Therefore, vibration control, regarding prevention and/or mitigation, is crucial for evaluation. Vibration sources can be identified as drilling system modeling, downhole dynamics measurements and field practices. BHA design as one of the most important factor has to be evaluated accurately. The following parameters must be identified in order to eliminate reamer free loading, which is known to be the main cause of vibration:

- ✓ Single neutral point (NP)
- ✓ Preferable NP location
- ✓ Least WOB to move NP above reamer

Reamer free loading occurs when the NP (Figure 2-3) is moved below the reamer as a result of BHA design or operation. In this situation, tensile loads (defined as free loading) act on the reamer and lead it to be pulled down and damaged beyond repair. This condition is suggested as an initial source of vibrations. This is caused by failing to provide enough WOB, required to place the NP above the reamer. Therefore, in order to expel free loading, there are some critical considerations concerning BHA design and operation. These include factors such as well profile, formation hardness, mud weight (MW), bit to reamer distance and bit type [4].

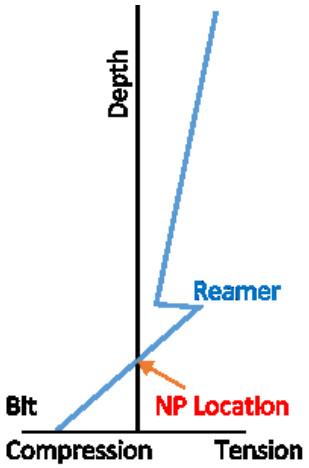

Figure 2-3 Neutral Point (NP) location on the BHA, after Mensa [4]

2.3.5 Formation Scenarios

In addition to in conventional drilling all cutting elements of the bit are in contact with one and the same formation. However, when drilling with hole enlargement tools, the tools may sometimes end up in different formations during the drilling operation. Three different scenarios have been identified with a potential for vibration while drilling transition zones with variations of hard and soft formations. These include the following situations [25], [30], [31]:

(1) Bit and reamer drill in homogenous formations: Due to stresses redistribution and alteration around the wellbore, the reamer is typically more aggressive than the bit. Thus, it is less likely that the reamer will out-drill the bit. Furthermore, the reamer requires less W_r but because of a relatively larger diameter hole, it needs higher percentage of total torque (Figure 2-4-a & c)

(2) Drilling from soft to hard formations: The bit controls the ROP as the reamer will not hold up ROP. In addition, the bit will demand much more W_r because of it is in hard formations. Further, the reamer will need less torque than to the bit since it is in soft formation. Based on this analysis, this scenario is the worst situation for a bit (Figure 2-4-d).

(3) Drilling from hard to soft formations: The bit will likely out-drill the reamer. This means that not enough weight transfers to the pilot to keep the pilot stable, which leads to lateral vibrations and whirl. Of the three scenarios, this is the worst case and most challenging situation for the whole system since the reamer takes the higher proportion of WOB and is exposed to higher torque (Figure 2-4-b). Over-torqueing the reamer is more likely, which can rapidly lead to stick-slip motion of the string.

The aforementioned cases lead to various performance challenges; they also have differing outcomes concerning project success and costs. The rate of success strongly depends on the remedy action being taken. Historically the solutions mainly focused on drill bit parameter reactions and behaviours, which are not the same as for the reamer. Mensa-Wilmot et al. (1999), gave different application severity grades base on rock drillabilty and its impact on BHA design (Table 2-1). Thus, Thomson et al. (2008) introduced DOC control to the industry [26].

Table 2-1 - Ranking of application dificulty for BHE [4]

Item	Bit	Reamer	Difficulty rank
Drillability of rock	Hard	Hard	2
	Hard	Soft	4
	Soft	Hard	1
	Soft	Soft	3

Other risks associated with the reamer are: potential lost time, premature activation and casing damage, and failure to actuate or failure to open the hole. The most serious hazards would include a tool that fails to retract while pulling up into the casing.

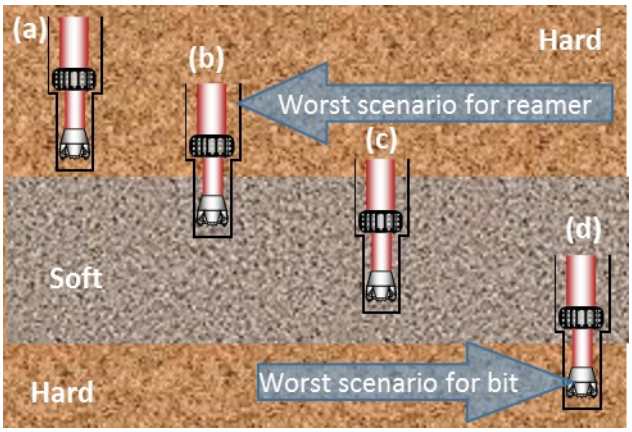

Figure 2-4 Bit-Reamer critical scenarios,after Mensa [4]

2.4 Operational Considerations

Like other tools, when dealing with a range of multi-diameter tools, there are many operational considerations that must be addressed.

2.4.1 Formation Parameters

Full awareness of the formations to be drilled (such as depth, the rock strength before a bit and reamer selecting and designing for a particular application), is crucial. In addition, this information allows predictions for potential depths where greater shocks or drilling vibrations could arise.

Eccentric tools are more suitable for well-known formations with fewer challenges, while concentric types are appropriate for more problematic formations due to blade count, stability characteristics etc. In addition, a reservoir's complexity and its properties that determine the well trajectory and the formation to be drilled, influence the decision making process.

2.4.2 Trajectory

Vertical hole sections often deploy a conventional rotary BHA. Current BHE technology presents few limitations. However, deviated wellbores are more challenging. PDM can deliver higher DLS than RSS. If DLS increases to higher values than 10^{o}/100ft then a bi-center is often the only option. As most RSS assemblies are restricted to lower values than 10^{o}/100ft, then concentric tools are the best option.

2.4.3 Hole Quality

The eccentric systems are typically more dependent on pilot holes. The concentric tools deliver maximum flexibility in a full gauge enlarged hole.

2.4.4 Drill Out Casing Shoe

Bi-center and concentric bits can be employed to drill out the shoe. However, some eccentric tools primarily due to their very large expansion ratio (usually 50%) can have many challenges. It may cause eccentric tools or casing damage. Bi-center tools do not exhibit such dysfunction. Furthermore, concentric tools can be kept in a locking position while drilling out the shoe.

2.4.5 Reliability

Since concentric tools are very complex and have moving parts, they are more susceptible to fail than eccentric systems. However, if both types are used within their design criteria, they are reliable. The primary issues with eccentric drills include cutting structure damage and under gauge hole. This is because of either inappropriate drilling parameters or poor pilot hole geometry. Concentric tool failures include seals, mechanisms, expansion/retraction components, etc.

2.4.6 Drilling Parameters

Currently, there is a variety of methods to extend a set of optimized drilling parameters. Post-well-evaluation results, drilling failures, vibrations occurrences, or any favourable performance cases are transferrable to the drilling parameters applied. In addition, the drilling performance

correlates with the rocks drilled and the drilling parameters. The outcome of these observations and the results lead to develop a set of optimized drilling parameters and best drilling operations. Moreover, Mechanical Specific Energy (MSE) is currently used as a powerful key performance indicator (KPI) to find out optimum drilling parameters in real time. There is extensive research on the applications of MSE, Low MSE tendencies during smooth drilling operations are favourable and interpreted as having greater drilling efficiency (For more information refer to 3). Furthermore, as stated in 2.3.5, drilling engineers attain crucial insight by analysing the dull grading of the pilot bit and hole opener. This information combines with the formations drilled, and contributes to determining the cutters or any other kind of failures on the pilot bit or enlargement tool, and choosing optimized drilling parameters based on the best-in-class approach.

Although optimizing pre-drilling design and drilling parameters is crucial before starting a drilling project, these factors must also be examined in the field. The *Drilloff* test is an old and effective method that can be applied to develop drilling parameters optimization on rig site. In reality, the driller can perform this test to fine-tune the drilling parameters by real time ROP and the drilling efficiency [32]. Monitoring the real time drilling parameters is a highly effective method to improve the drilling efficiency. As part of the process, if any drilling dysfunctions are observed in the drilling mechanics plot, appropriate mitigation approaches should be pursued. In this instance, the drilling parameters should be changed to find out the optimum function.

Both of the enlargement tools (concentric and eccentric) are in the same situation regarding drilling parameters, except the eccentric tool cannot be used to enlarge a predrill hole. In fact, parameter selections must consider performance improvement, and not only the reamer protection. In addition, the free loading consequences should always be considered.

2.4.7 Weight and Torque Sharing

Ma Rutao at el, 2012, introduced a dual factor approach to calculate weight sharing in reaming while drilling by substituting ratio of the ROP/RPM with the depth of cut per bit rotation in the specific energy equation [33].

$$W_b = \frac{\sigma_b A_b}{1 + \frac{120\pi k_b}{\Delta h_b}} \qquad \text{Eq. 2-1}$$

Where k_b is bit sharpness, Δh illustrates depth of cut per rotation of the bit (m), σ_b is the compressive strength of the rock, which with reference to Passier's research, is approximately equal to the specific energy. A similar equation is defined for a reamer. Then, weight distribution factor is derived as:

$$f_w = \frac{W_r}{W_b} = \left(\frac{A_r \sigma_r}{A_b \sigma_b}\right)\left(\frac{\Delta h_r}{\Delta h_b}\right)\left(\frac{\Delta h_b + 120\pi k_b}{\Delta h_r + 120\pi k_r}\right) \quad \text{Eq. 2-2}$$

According to this equation, a ratio of the weight on the reamer to the total weight applied from the surface is derived as follows:

$$F_r = \frac{W_r}{W_r + W_b} = \left(1 - \frac{1}{f_w + 1}\right) \times 100\% \quad \text{Eq. 2-3}$$

f_w depends upon drilling tool's geometry, the bit and reamer's sharpness and formation strength. Currently, the maximum reamer's diameter is dictated by the drilling technology, and cannot be arbitrarily modified. Therefore, this factor is deemed as a constant. However, the other two factors, sharpness and formation stress, may vary with operational conditions. Consequently, the two factors are the main variables influencing weight distribution in BHE. Properly matching the factors will render a stable and secure enlargement process.

2.4.8 Cutting Structure Matching

Improper selection or location of the bit or drill string components used in the string can lead to vibrations, leading to catastrophic drilling problems. Many profiosnals in the field beliefs that the cutting elements must come from the identical manufacturer company. It is highly recommended that product engineers for bits and reamers improve matching tools. While this may be true to some extent, the focus must not be placed on preventing different manufacturers from developing good bits and reamers. In terms of the functional and developmental differences between pilot bits and enlargement tools, it is logical to engage different companies should need be.

Depth of Cut (DOC) control technology was recently introduced to match a PDC bit to the underreamer [26]. The focus of this approach is on adjusting the bit cutter exposure and blade geometry, governing the bit drills up to a limited target DOC. After hitting the target DOC, a bearing surface will expose the formation and decrease the aggressiveness of bit (Figure 2-5). The primary aim of this feature is to govern ROP maximums and prevents out-drilling the reamer by the bit. This is achieved by the bearing surface having engaged with the rock. Consequently, extra DOC will be restricted, and the bit will be prevented from out-drilling the underreamer when the final DOC is achieved. In fact, in case of additional WOB being applied to the BHA, this extra weight will act on the bearing surface, and the underreamer does not take the additional weight. The bit is hence continuously loaded on the bottom and is devoid of any destructive backward whirl and lateral vibration. Such destructive forces would be exacerbated when drilling through interbedded formations, composed of both soft and hard rock. The total weight used to the system will oscillate from the moving of a neutral point (NP). As a result of this, the structural integrity of BHA could be affected and cause to element or

drillstring damage. In such instances, a pilot bit, which equipped with DOC control technology, highly recommended to be selected in order to maximize matching [25].

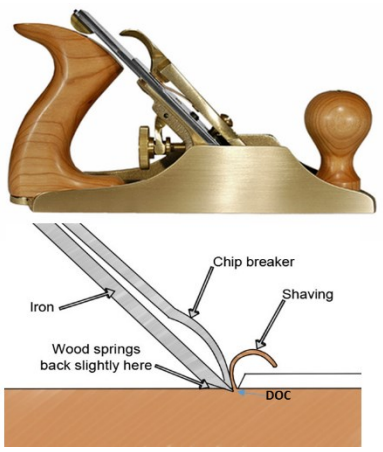

Figure 2-5 A simple analogy of Concept of Depth of Cut (DOC) control technology

When the bit with the DOC controls is pulled out of the hole, typically, the bit body shows circumferential marks on the cone, nose, and shoulder areas. This sort of indication is evident when the final DOC is reached. This is the primary role of the DOC control technology that prevents the pilot bit from outdrilling the hole opener. Therefore, the harmful lateral vibration is mitigated and the total system becomes more stable. Barton, et al, 2010, developed and assessed many concepts concerning matching bit and reamer [30]. There was initially a misunderstood vision to identify bits and reamers with the same design features such as cutter size, side rakes and back rakes. The authors classified this approach of element/feature designation as a bit and reamer matching process. Finally, sophisticated software was developed to accelerate decision making and matching processes. In another approach, the mechanical efficiency differences between reamers and bits were taken into account. Generally, a bit normally drills faster than the reamer. The authors were left with costly mistakes and a less aggressive bit tan the comparable reamer ROP.

2.4.9 Vibration Mitigation

It is well documented that vibration diminishes drilling performance and heightens NPT.

With minimal vibrations, the ROP, drilling efficiency, MSE, drilling performance, pilot bit and reamer dull condition will improve. Additionally, downhole tool failures, that would cause losses of millions of $, are mitigated. There are different schools of thought that must be considered to reduce vibrations:

- ✓ Proper matching pilot bit and reamer: DOC control technology able to prevent the PDC bit from outdrilling the reamer, which highly affect vibrations reduction.
- ✓ Optimum drilling parameters

- ✓ Improve BHA design: V-shaped stabilizer delivers a mechanism for disrupting resonant vibration modes, reducing the number and magnitude of shocks which occur during the drilling process [30], [34], [35].

3 Specific Energy Concept

3.1 Introduction

It is known that because of high expenses incurred, drilling operation is often the highest cost item during field development. As a result of its sensitivity to daily oil prices, the drilling process is a critical candidate for optimization. A little improvement can result in great savings and make the venture a success.

MSE is being used as a measurable to enhance the drilling operation due to its sensitivity to all the essential parameters of the drilling process. It can be applied to help drilling engineering recognize bottom hole balling, bit balling, excessive vibrations, and bit dulling. Owing to a better understanding of the bottom hole conditions and a proactive approach to correcting any inefficient parameters, it is encouraged to employ MSE as a drilling process efficiency indicator on the rig site.

3.2 Properties Used as Drillability Index

In the literature, several parameters have been applied to explain the drillability characteristic of the formation. Drillability is often defined as a parameter to describe how easy a rock can be drilled. The parameters utilized to describe the drillability are not well recognized by the oil and gas industry. Mainly, it is referred to UCS and CCS of the rock to define the rock strength during drilling, but at the same time it is worth noting that various type of rocks like anhydrite, limestone, sandstone and shale show similar UCS values, but thoroughly dissimilar behaviour during drilling. In other words, a different set of properties are necessitated to relate drillability of the rocks.

The various rock properties which may be used to describe the drillability of rock are: density, porosity, mineralogy, grain size, UCS [36].

3.3 Specific Energy (SE) Concept

Specific Energy (SE) is the energy required to destroy a given volume of the rock during the drilling process (Eq. 3-1). In a given drilling environment, lower specific energy shows a more efficient drilling process. The MSE measured at atmospheric pressure conditions could have an approximate value of the UCS of the rock, when drilling with maximum efficiency [8], [9], [10]. MSE is not considered as a fundamental intrinsic property of a rock as it depends on the type of the drill bit and the bit design. In addition, Teale [9] stated that energy spent will become very high if we break the cuttings into "smaller fragments than necessary". It will require more particles to be broken without any need and specific energy will considerably rise as the broken particle size is decreased. MSE can directly be observed to enhance the overall performance of the drilling process and discover any variations in the drilling efficiency, and to adjust the affected drilling parameters. SE is highly dependent on the equipment used and the nature of rock breakage. In fact, a rock's drilling SE is affected by several parameters, for instance [37]:

- ✓ Rock strength
- ✓ Rock stiffness
- ✓ Presence of structural discontinuities
- ✓ Abrasivity and hardness of the minerals present in the rock
- ✓ Nature of rock matrix
- ✓ Nature of mineral grain

$$SE = \frac{Total\ Energy\ Input}{Volume\ Removed} \qquad \text{Eq. 3-1}$$

Previously, several experimental research works have been carried out to correlate the drilling efficiency with the given rock characteristics. Most of the drillability parameters, as mentioned before, have a major drawback. In fact, all the drilling conditions have an inherent degree of difficulty in drilling that is only associated to that well or location. However, no drilling performance parameter takes care of the fact that the drilling situation is totally dissimilar in all part of world and there is no relationship between the reservoir properties to benchmark drilling performance.

It is well understood from previous studies that rock hardness has higher effect on the drilling process than other rock properties; therefore, in comparison, drilling into a hard rock section takes longer time than drilling into a soft rock. Yet, it is not possible to compare the drilling process only by considering rock hardness for the reason that other factors (like lithology, abrasivity, and borehole pressure) that affect the drilling process are not similar [38]. In other

words, any comparison just on the basis of drilling time per unit depth is useless if we do not account for the change in drilling parameters in hard versus soft rock.

The ROP is directly affected by rock strength [39] and rock strength logs are applied to conduct different types of analysis such as deciding on completion design methods, controlling sand production and preventing wellbore failure. One of the earliest model was defined by Maurer (Eq. 3-3) [40]. Therefore, UCS is a good candidate to be used as an index to drillability. Additionally, it is obvious that ROP is also dependent on borehole pressure and on formation pore pressure as well. An increase in borehole pressure reduces the ROP in impermeable rock [41], [42]. In the same approach, an increase in difference between pore pressure and borehole pressure lowers ROP in permeable rock [43], [44].

$$ROP = k\frac{RPM\times(W_r - W_{r-0})^2}{d_b^2\times UCS^2} \qquad \text{Eq. 3-2}$$

In the same manner, CCS, can be used as a drillability or performance parameter. The increase in CCS caused by increasing confining pressure is slow as compared to the decrease in ROP owing to increase in confining pressure [45]. Furthermore, the not well documented, non-linear relationship between increasing compressive strength and confining pressure of rock forces us reluctant to employ compressive strength of rock as a drillability parameter.

3.4 MSE Background Knowledge

Pessier and Fear [11] classified drilling efficiency, MSE input, and a minimum specific energy that is close to rock strength as three fundamental components of drilling process when looked as an energy-balanced system. The authors carried out their experiments on grout and Mancos shale under hydraulic pressure. They stated that during the drilling of grout with water as drilling fluid under a bottom hole pressure of 2,000-psi, specific energy was found close to the compressive strength of the grout at the same pressure and mechanical efficiency was found to be 80%. However, the values of specific energy are nearly the twice of that monitored at atmospheric pressure. The results obtained from Mancos shale shows significant changes at 2000 psi which is drilling with 9.6-ppg Lignosulfonate mud. Values of Specific energy started at 40000-psi and increased up to 80000-psi when experiment has to be terminated due to very high weight on bit (100,000-lbs). A decrease in efficiency from 30% to 20% is observed. Additionally, bottom balling and bit balling were monitored in the Mancos shale.

Moreover, the authors mentioned that specific energy is high and the efficiency is low when drilling at low Depth of Cut (DOC) because a minimum has to be achieved to start cuttings generation. Below this DOC, only rock fines are generated. Caicedo et al. [12], [13] stated that the rocks' UCS can only be employed when drilling is performed with clear fluids which is

almost not the case in any drilling process and also use of CCS in impermeable formation is to some extent flawed. The CCS of the rock for impermeable and permeable rocks individually were calculated. For permeable rocks CCS is computed using rock internal angle of friction and differential pressure (Eq. 3-3). Differential pressure is determined by subtracting pore pressure from equivalent circulation density pressure. On the other hand, for impermeable rocks pore pressure is calculated using Skempton model in the expanded rock (Eq. 3-4). In general, effective porosity is used to quantify the impermeable and permeable end points and CCS is determined by linearly interpolating the two extreme cases of impermeable rock and permeable rock (Eq. 3-5). Several correlations are applied to determine rate of penetration and then specific energy, which makes the method unreliable as a result of accumulated errors of various correlations.

$$if\ \varphi \geq 0.2\ \longrightarrow\ ARS_1 = UCS + \left(p_w - p_f\right)\frac{1+sin\,\emptyset}{1-sin\,\emptyset} \qquad \text{Eq. 3-3}$$

$$if\ 0.05 \geq \varphi\ \longrightarrow\ ARS_2 = UCS + \left(p_w - \left(p_f - \frac{\sigma_v - p_w}{3}\right)\right)\frac{1+sin\,\emptyset}{1-sin\,\emptyset} \qquad \text{Eq. 3-4}$$

$$if\ 0.2 > \varphi > 0.05\ \longrightarrow\ ARS_3 = \frac{ARS_1(\varphi - 0.05)}{0.15} + \frac{ARS_2(0.2-\varphi)}{0.15} \qquad \text{Eq. 3-5}$$

Detournay and Atkinson [46] modelled the rock cutting by a PDC bit with using the Merchant model for metal cutting. They ended up with a linear relation between specific energy of cutting the rock and the difference between the bottom hole pressure and the average pore pressure on the shear plane. They related pore pressure at the shear plane to the virgin pore pressure by equating the rate of pore volume increase of the rock due to dilatancy and volume of the fluid supplied to the shear plane. They assumed that pore pressure variation in the rock is governed by diffusion.

Additionally, Detournay and Tan (2002) stated that the MSE for a perfectly sharp cutter that moves with constant velocity and constant depth of cut is related linearly to confining pressure (P) as shown in Eq. 3-6. The angular coefficient (m) of this linear relationship can vary between 3 and 25 for cutters with back rake angle of 15 degrees [42].

$$MSE = MSE_0 + mP \qquad \text{Eq. 3-6}$$

Detournay and Atkinson [47] defined a parameter λ, based on which three regimes of drilling can be defined. A value of more than 10 dictates the high speed regime and a value of less than 0.001 shows a low speed regime. In the high speed regime, rock fails in the shear plane in the undrained manner that means cavitation will occur in the shear plane since there is no change in the fluid content in the pores. Similarly, in the low regime, rock fails in drained manner and the pore pressure in the shear plane and in the intact rock just ahead of the cutter will be almost the same.

They [47] illustrated that cutting shale is in the high speed regime and pore pressure drop is very high and close to undrained pore pressure drop. This high pore pressure drop causes cavitation. Due to cavitation specific energy is not dependent on the virgin pore pressure. In the same manner they showed that cutting permeable sandstone is in low speed regime. Finally, they concluded that the necessary condition of cavitation is that the rock is shear dilatant and cutting process lies in high pressure regime. Later on, Detournay and Tan [42] showed that in shale, due to cavitation specific energy will only be dependent on bottom hole pressure. They assumed that the inelastic pore volume increase associated with shearing of the rock dominates its volumetric response. They expected that with increase in confining pressure, shear dilatant volumetric strain and inelastic pore volume increase will be progressively reduced and the dilatancy will be eventually suppressed.

Kolle [48] carried out his single cutter experiments under pressure and presented results in terms of drilling strength (indentation load divided by area of cut) and specific energy (tangential load divided by area of cut). In Mancos shale, drilling strength was shown to increase with increase in pressure until 25 MPa was reached and after that rate of increase in drilling strength started decreasing. Carthage Marble showed a strong effect of pressure on specific energy and drilling strength initially; however, after 25 MPa there was no significant change. Bonne Terre dolomite exhibited rapid increase in cutter load until 10 MPa but no considerable change beyond that was observed. Colton sandstone showed a rapid increase in drilling strength up to 10 MPa and a more gradual increase thereafter. Berea sandstone exhibited little or no effect of pressure on drilling strength at low traverse rates due to its relatively high permeability. Kolle [48] could not explain the varying strengthening rates due to the high pressure. He finally presented the theory of dynamic confinement to explain the strengthening of rock with dilation theory.

Judzis et al. [49] conducted full scale laboratory testing on Crab Orchard sandstone, Carthage Marble and Mancos shale. They observed that specific energy in drilling experiments is significantly greater than the compressive strength of the rock at a confining pressure equal to bottom hole pressure. They suspected that other than the work being done due to rock becoming stronger under the confining effect additional unproductive work was also done. This unproductive work may include re-grinding of the cuttings which are held in place on the bottom due to local pressure difference.

3.5 MSE Model

The concept of MSE was first introduced by Teale (1964) [9], Specific energy or the energy density is an important parameter to characterize the efficiency of drilling and helps to track

the energy expended to remove a unit volume of rock in unit time, or in simple text, MSE is defined as Energy-In divided by Volume-Out (Eq. 3-1).

Volume of a drill hole is simply the cross sectional area multiplied by the depth of penetration (Δh), and work energy can be described as force multiplied by distance. In drilling there are two forces acting on the bit; weight on bit (axial force) and torque (rotational force). These are additive to MSE, so there are two terms in the MSE equation (Eq. 3-7 and Eq. 3-8).

$$MSE = \frac{Vertical\ Energy\ Input}{Volume\ Removed} + \frac{Rotational\ Energy\ Input}{Volume\ Removed} \quad \text{Eq. 3-7}$$

$$MSE = \frac{W_b \times \Delta h}{A_b \times \Delta h} + \frac{Torque \times 2\pi \times RPM}{A_b \times \Delta h} \quad \text{Eq. 3-8}$$

Where:

MSE = Mechanical Specific Energy (psi)

W_b = Weight On Bit (lb)

RPM = Rotations Per Minute

Torque = Rotational torque (ft-lb)

A_b = Cross sectional area of bit or borehole area (in^2)

ROP = Rate of Penetration (ft/hr)

The distance travelled by the bit (Δh) during a given interval is the penetration per time (ROP) divided by rotations per time. This is also known as depth of cut or as penetration per revolution. On a per-minute basis (Eq. 3-9),

$$\Delta h = Depth\ of\ Cut = \frac{Penetration\ Per\ Minute}{RPM} = \frac{ROP}{RPM} \quad \text{Eq. 3-9}$$

Teale (1964) then defined the drilling specific energy with the following expression (Eq. 3-10):

$$SE = \frac{W_b}{A_b} + \left(\frac{2\pi}{A_b}\right)\left(\frac{RPM \times Torque}{ROP}\right) \quad \text{Eq. 3-10}$$

Eq. 3-10 is composed of two parts; The thrust force or weight on bit component and the rotary speed component. Rabia, (1985), presented a simplified version of the specific energy correlation for bit selection [50], as follows (Eq. 3-11):

$$SE = \frac{20 \times W_b \times RPM}{d_b \times ROP} \quad \text{Eq. 3-11}$$

The parameter not only helps to select and optimize the drilling parameters but also helps to design drill bits more efficiently.

The MSE equation can be expressed when drill rotation mode (Eq. 3-12) and when drill with Down Hole Motor (DHM) [51] in terms of drilling parameters (Eq. 3-13) as:

$$MSE = \frac{W_b}{A_b} + \frac{120 \times \pi \times Torque \times RPM_{Sur}}{A_b \times ROP} \quad \text{Eq. 3-12}$$

$$MSE = \frac{W_b}{A_b} + \frac{120 \times \pi \times (RPM_{Sur} + RPM_{DHM} \times FlowIn)\left(\frac{T_{DHM}}{\Delta P_{DHM}}\right)\left(\frac{\Delta P}{1000}\right)}{A_b \times ROP} \quad \text{Eq. 3-13}$$

In Eq. 3-12 and Eq. 3-13 torque is used as a variable in the MSE calculation formula. Torque at the bit can be measured by a MWD system but in most cases no bit torque measurements exist. Bit specific coefficient of sliding friction (μ) is introduced by Pessier et al 1992 [11] to express torque as a function of the WOB and to let the MSE to be calculated in the absence of reliable torque measurement (Eq. 3-14):

$$TOB = \frac{\mu . W_b . d_b}{36} \quad \text{Eq. 3-14}$$

By combining Eq. 3-12 and Eq. 3-14, MSE_{Mod} is defined as:

$$MSE_{Mod} = W\left(\frac{13.33 \times \mu \times \mathrm{RPM}}{d_b \times ROP} + \frac{1}{A_b}\right) \quad \text{Eq. 3-15}$$

For field application, μ is usually assumed to be equal to 0.25 for tricone bits, and 0.5 for PDC bits.

To improve the usefulness of MSE surveillance in field operations, based on field observations, Dupriest et. al. 2005 assumed a uniform drilling efficiency (Eff_M) equal to 35% regardless of bit type or WOB [52] [53]. Including this assumption, Teale's original equation becomes:

$$MSE_{adj} = MSE \times Eff_M \quad \text{Eq. 3-16}$$

Regardless of the fact that this value is known from laboratory data to commonly vary from 0.30 to 0.40, the value of error introduced was assumed to be adequate. Although MSE calculations from surface sensors show even larger sources of error, but due to only a qualitatively trending curve are used in the field plots, the curve uniformly will shift because of any error in Eff_M. Therefore, the MSE value may be incorrect, but the uniformity of the shift enables the curve to still be used effectively as a useful visual trending tool to analyse bit performance and ROP optimization in real time.

The minimum specific energy is roughly equal to the compressive strength of the rock being drilled. Nevertheless, the calculated specific energy practically rarely equals the strength of the rock due to other inefficiencies within the drilling system like friction and drilling vibration.

Miguel 2008 added a bit hydraulic (Hydraulic Power per Square Inch)-related term on the MSE correlation and defined ***Drilling Specific Energy (DSE)*** as the work done to excavate and remove, underneath the bit, a unit volume of rock [54].

Mohan et al (2009) modified Miguel (2008) to consider the impact of the fluid jet on the formation exerts an equal and opposite "***pump-off***" force on the bit [55]. The pump-off force is in accordance with Newton's third law (for every action; therefore, there is an equal and opposite reaction). Consequently, the effective WOB is reduced.

Pessier et al. suggested a simple mathematical relationship to show ROP and MSE in a single graph as a ***Power Graph*** (Figure 3-1) [56], [57], [58]. For simplicity, in Eq. 3-12, the first term ($\frac{W}{A_b}$) can be ignored as it is dominated by the second term. Further, utilizing the relationship between torque and μ in Eq. 3-14 can allow Eq. 3-12 to be expressed in terms of W and μ in the event that the torque provided to the drill string is not available and as is shown in Eq. 3-17:

$$MSE = \frac{13.33\mu W_b \times RPM}{d_b \times ROP} \qquad \text{Eq. 3-17}$$

The data's distribution brings to mind a simple mathematical relationship in the form of:

$$ROP = \frac{c}{MSE} \qquad \text{Eq. 3-18}$$

Where c is a constant which is equal to the product of the $R \times MSE$. This represents the area specific mechanical power MPSI which is the total available power (P) divided by the borehole area (A):

$$MPSI = \frac{ROP \times MSE}{1.98e6} = \frac{P}{A \times 1.98e6}\ [HP/in^2] \qquad \text{Eq. 3-19}$$

The unit for MPSI is obtained by dividing the product of ROP x MSE by the constant 1.98e6 to convert $\left[\frac{ft-lb}{hr}\right]\ to\ \left[\frac{HP}{in^2}\right]$.

If the constant MPSI lines are superimposed on the same ***Power Graph***, then the total available horsepower could be easily estimated. The total power in the system could be calculated by multiplying MPSI by the borehole area (A).

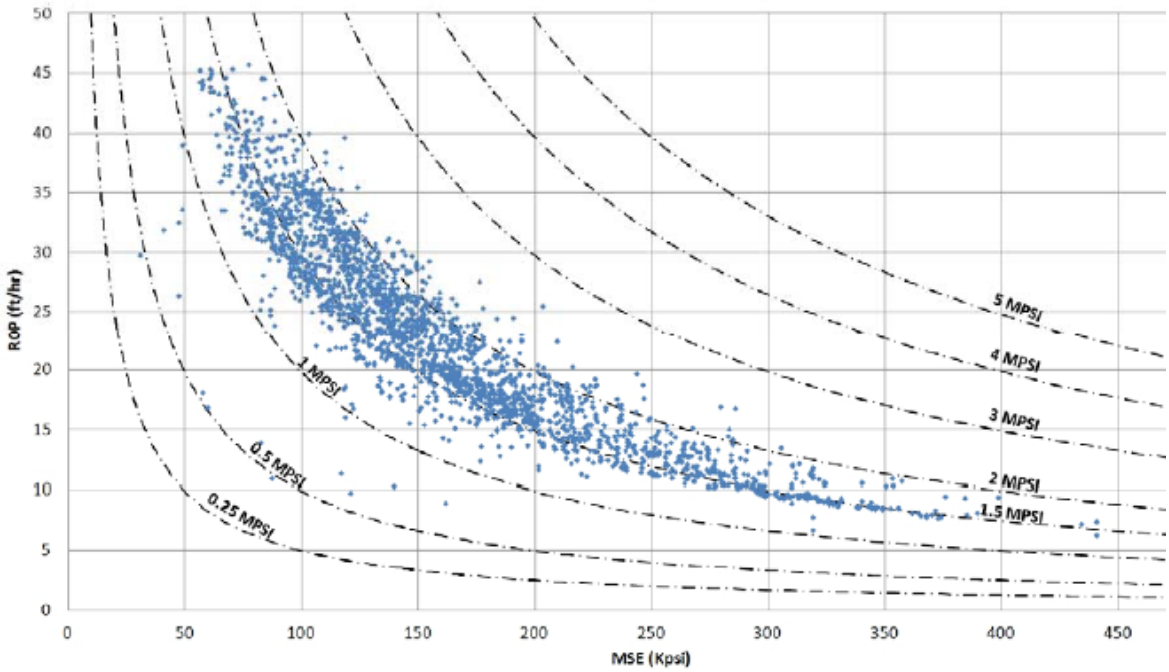

Figure 3-1 Power Graph, [56], [57]

The power input stays constant; however, the distribution of the power changes with depth, lithology, well path, bit type and drilling practices. In other words, when the system can only deliver a fixed amount of power we have a zero sum problem in which ROP and MSE vary depending on the distribution of the power in the system.

4 Thermoporoelastic Theory

4.1 Introduction

When a wellbore is drilled, such as in oil and gas well drilling operations, the removed rock mass, which carried in situ stress, is abruptly replaced by a drilling mud that employs a given hydrostatic pressure in the wellbore. As a consequent, the stress state around the borehole rock redistributes governed by three major mechanisms: thermal, mechanical and chemical effects. The focus of this study is mainly on thermal and mechanical effects.

Normally, the mud pressure is less than the in-situ least principal stress that acts on the well along with the intermediate and maximum principal stresses. Consequently, an immediate stress alteration creates near the wellbore, specifically at the wellbore wall [59]. In addition to the instant ***poroelastic*** effects, two time-dependent behaviors can be considered when influencing the perturbed stress state around the well [60]:

1 In case of a permeable wall of wellbore, drilling fluid pressure diffuses from the well into the formation (Mode 2 effect [61]).
2 The stress alteration lead to an immediate change in pore pressure (the undrained loading effect or mode 3 effect), which dissipates with time.

In addition, the rock comprised of an elastic solid matrix and fluid filled pores is exposed to changes in temperature due to the temperature difference between the drilling mud and the formation. [62]. This temperature variation influences wellbore stability in two ways. Firstly, induced thermal stresses cause to alter the stress profile around the wellbore. Secondly, temperature changes affect the pore pressure distribution [60], [63].

Thermoporoelasticity creates the coupling between pore pressure, thermal stresses and temperature with rock mechanical properties. Thermal energy transmission follows the same diffusion law as does the pore fluid movement. Therefore, it is targeted to model the time-

dependent effects of wellbore heating or cooling using similar equations as are applied for poroelasticity. However, this is potentially valuable because cooling a well decreases the circumferential stress and thus temporarily reduces the probability of breakout formation at the same time it increases the risk for drilling-induced tensile failure. This may result in a weakening zone around the wellbore implying that BHE tool needs less power to destroy the rock. Thermo-poroelasticity is developed on the basis of poroelasticity and thermo-elasticity. It couples the time-dependent processes of fluid diffusion and heat diffusion to mechanical behaviour. Heat transfer between the wellbore and the formation depends on the boundary conditions. Specifically, in the case of the permeable wall, both convection and conduction can cause heat transfer into the surroundings. In low permeability formations, like shale, conduction is the dominant mechanism, while in high permeability formations convection has considerable impact.

According to literature, in case of ***permeable boundary condition*** hydraulic diffusion can be fully coupled with thermal diffusion [64], [65]. Thus, the pore pressure is dependent upon not only the wellbore pressure but also the temperature change [60].

Besides that, for low-permeable formation, such as shale, regardless of wellbore wall condition, the diffusivity equations can be decoupled by ignoring the effect of pore pressure changes on temperature variations. By including the undrained loading effect [61], thermal effects can be included in the fully coupled poroelastic solutions [66].

An impermeable boundary condition can create if a filter cake on the wellbore wall prevents fluid pressure invasion into the formation. Moreover, it can occur if water-wet shale is drilled with an oil-based fluid, as a result of the high capillary entry pressure. In fact, temperature distributions stay the same apart from the wellbore boundary condition. For this scenario, the pore pressure depends only on the temperature field.

Using a loading decomposition system, the fully coupled thermoporoelastic analysis is divided into three different loading modes (Figure 4-2): a) a plane-strain thermoporoelastic medium, b) an elastic uniaxial c) an elastic anti-plane shear problem. Finally, the solutions for each loading mode can be superimposed to establish a complete solution for a wellbore under either impermeable or permeable boundary conditions [60], [67], [68], [65]. In this work, focus will be on the conductive and the convection heat flow and the induced pore pressure diffusion because of an instantaneous pressure and temperature variation.

4.2 Problem Definition

The problem under attention is an infinitely extended circular borehole which is excavated in an infinite poroelastic medium. The borehole is exposed to a non-hydrostatic in-situ stress field, wellbore fluid pressure and a constant temperature along the wellbore wall [66]. Figure

4-1 shows the problem for a linear thermoporoelastic system of an inclined borehole. It is mentioned that $S_{x'}$, $S_{y'}$ and $S_{z'}$ are the in-situ principal compressive stresses in the global coordinate system. $x'y'z'$; p_f and T_f are the virgin formation pore pressure and temperature; p_m and T_m are the wellbore pressure and temperature applied by the drilling fluid, respectively. The local borehole coordinate system, xyz, with its $z-axis$ coinciding with the borehole axis, are related to $x'y'z'$ by an azimuth angle, ω formed by rotating an angle ω about the $z'-axis$; and then by an inclination angle γ, toward the $x-axis$. The borehole coordinate system xyz is selected as the solution domain for the convenience of borehole failure analyses. It should be mentioned that the cube's surfaces are presented in order to easy visualization of far-field stresses. Otherwise, they do not exist as the domain is infinite. The transformation must be used to convert the in-situ principal stresses to the borehole coordinate system (Eq. 4-1 and Eq. 4-2) [69], [70].

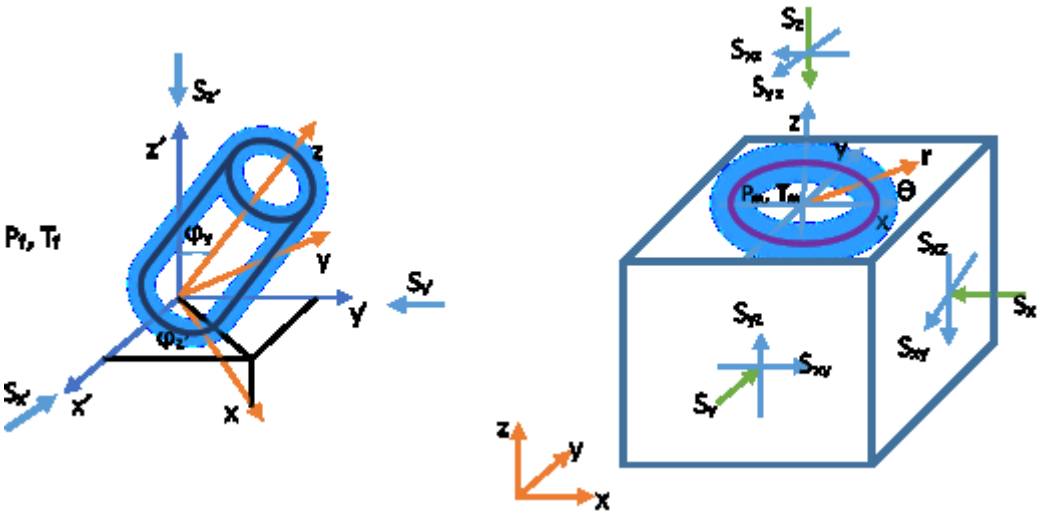

Figure 4-1 Problem definition

$$\begin{bmatrix} S_x \\ S_y \\ S_z \\ S_{xy} \\ S_{yz} \\ S_{xz} \end{bmatrix} = \begin{bmatrix} l_{xx'}^2 & l_{xy'}^2 & l_{xz'}^2 \\ l_{yx'}^2 & l_{yy'}^2 & l_{yz'}^2 \\ l_{zz'}^2 & l_{zy'}^2 & l_{zz'}^2 \\ l_{xx'}l_{yx'} & l_{xy'}l_{yy'} & l_{xz'}l_{yz'} \\ l_{yx'}l_{zx'} & l_{yy'}l_{zy'} & l_{yz'}l_{zz'} \\ l_{zx'}l_{xx'} & l_{zy'}l_{xy'} & l_{zz'}l_{yz'} \end{bmatrix} \begin{bmatrix} S_{x'} \\ S_{y'} \\ S_{z'} \end{bmatrix} \quad \text{Eq. 4-1}$$

$$\begin{bmatrix} l_{xx'} & l_{xy'} & l_{xz'} \\ l_{yx'} & l_{yy'} & l_{yz'} \\ l_{zx'} & l_{zy'} & l_{zz'} \end{bmatrix} = \begin{bmatrix} \cos\omega\cos\gamma & \sin\omega\cos\gamma & -\sin\gamma \\ -\sin\omega & \cos\omega & 0 \\ \cos\omega\sin\gamma & \sin\omega\sin\gamma & \cos\gamma \end{bmatrix} \quad \text{Eq. 4-2}$$

As part of the solution procedure, the rock is assumed to be instantly removed and the wellbore wall is subjected to a different temperature and pressure and that the following initial conditions and boundary conditions are applicable for far field, or drainage radius (r_e), and also at wellbore (r_w):

In the far field

$$\sigma_{xx} = -S_x$$
$$\sigma_{yy} = -S_y$$
$$\sigma_{zz} = -S_z$$
$$\sigma_{xy} = -S_{xy}$$
$$\sigma_{yz} = -S_{yz}$$
$$\sigma_{xz} = -S_{xz}$$
$$p = p_f$$
$$T = T_f$$

Eq. 4-3

At the borehole wall, $r = r_w$, where r_w is the borehole radius, surface tractions and pore pressure are assumed to vanish at the instant of excavation:

Along the borehole

$$\sigma_{rr} = -S_r H(-t)$$
$$\sigma_{r\theta} = -S_{r\theta} H(-t)$$
$$\sigma_{rz} = -S_{rz} H(-t)$$
$$p = p_m H(t) + p_f H(-t)$$
$$T = T_m H(t) - T_f$$

Eq. 4-4

S_r, $S_{r\theta}$, and S_{rz} are the far-field compressive stress components in cylindrical coordinates. Therefore:

$$S_r = \frac{S_x + S_y}{2} + \frac{S_x - S_y}{2}\cos 2\theta + S_{xy}\sin 2\theta \quad \text{Eq. 4-5}$$

$$S_{r\theta} = S_{xy}\cos 2\theta - \frac{S_x - S_y}{2}\sin 2\theta \quad \text{Eq. 4-6}$$

$$S_{rz} = S_{xz}\cos 2\theta + S_{yz}\sin 2\theta \quad \text{Eq. 4-7}$$

Where r_e is the drainage radius for a production process and is the constant pressure outer boundary for an injection process. p_m is the wellbore pressure and p_f is the reservoir pressure. p_m can be the wellbore (or injection) pressure during over-balanced drilling (or injection) or the wellbore flowing pressure (or wellbore static pressure) during under-balanced drilling (or production). $\left(p_m - p_f\right)$ is a positive magnitude for over-balanced drilling (or an injection) operation. However, a negative magnitude denotes for under-balanced drilling (or a production) operation. Note in a high permeability formation, the effect of temperature changes

on pressure change is negligible when pore fluid flow is significantly faster than the heat transfer.

In the above, $H(t)$ denotes the Heaviside unit step function, and $H(-t)$ is defined as $1 - H(t)$ such that:

$$H(-t) = \begin{cases} 1 \; for \; t \leq 0 \\ 0 \; for \; t > 0 \end{cases} \quad \text{Eq. 4-8}$$

4.3 Governing Equations

Governing equations for an isothermal quasi-static state media of a fluid saturated poroelastic solid have been first derived and improved by Biot (1941, 1955, 1956) [71], [72], [73] and Biot et al (1957) [74]. The governing equations are presented here following Rice and Cleary's formulation [75], Kurashige [64], Li [66], Cui [76], Li [77], Chen [78], Chen [60], Tao [62], Detournay [79], … developed Biot's (1941) theory to non-isothermal poroelastic systems.

4.3.1 Conservative Laws

The second governing equations are the conservation laws for the mass, momentum, and energy to be used for the quasi-static thermoporoelasticity as follow:

Mass $$\frac{\partial m}{\partial t} + q_{i,i} = 0 \quad \text{Eq. 4-9}$$

Momentum $$\sigma_{ij,j} = 0 \quad \text{Eq. 4-10}$$

Energy $$\frac{\partial T}{\partial t} = -\frac{1}{\rho_m c_m} h_{i,i} - \frac{1}{\rho_f \varphi_0} (T q_i)_{,i} \quad \text{Eq. 4-11}$$

In which ρ_m is the density of the bulk material, c_m is specific heat of the bulk material, $h_{i,i}$ is the heat flux, q_i is the fluid mass flux, m is the fluid mass, t is time, σ is the stresses, T is temperature, ρ_f is the fluid density, φ_0 is the rock porosity. Eq. 4-10 has been expressed, in terms of the total stress approach, while disregard any inertial and body forces.

4.3.2 Constitutive Laws

Referring to the formulation of Rice and Cleary (1976) [75], the pore pressure variation p and total stress σ_{ij} are selected as the basic static variables. The corresponding conjugate kinematic quantities are the variation in pore fluid mass per unit reference volume, m and the solid strains ε_{ij}. By introducing temperature change T from an initial equilibrium temperature,

the mentioned relation can be improved to the non-isothermal conditions [64], result in the following constitutive relations for the porous solid:

$$\sigma_{ij} = 2G\left[\varepsilon_{ij} - \frac{v}{1-2v}\varepsilon_{kk}\delta_{ij}\right] - \alpha\delta_{ij}P_f - \frac{2G(1+v)}{3(1-2v)}\alpha_m^T\delta_{ij}T \qquad \text{Eq. 4-12}$$

And the change in fluid mass per unit volume $\Delta m = \Delta\varphi.\rho_0 + \varphi_0.\Delta\rho$:

$$\Delta m = \rho_f\left[\frac{\alpha(1-2v)}{2G(1+v)}\sigma_{kk} + \frac{\alpha^2(1-2v)^2(1+v_u)}{2G(1+v)(v_u-v)}p_f - \emptyset_0(\alpha_f^T - \alpha_m^T)T\right] \qquad \text{Eq. 4-13}$$

where σ_{kk} is the overall stress tensor, ε_{kk} is the total strain tensor, p_f is the pore pressure, $\Delta m = m - m_0$ is the variation in fluid mass per unit volume of material from its initial conditions, T is the temperature change from the initial status, G is the shear modulus, α is Biot's coefficient of effective stress, v and v_u are the drained and undrained Poisson's ratio, $\emptyset_0$ is the initial porosity, ρ_f is the fluid density, α_m^T is the volumetric thermal expansion factor of the porous matrix and α_f^T is the volumetric thermal expansion factor of the pore fluid.

4.3.3 Diffusivity Laws

Darcy's and Fourier's laws are used for the pore fluid and heat transfer, respectively:

Darcy $$q_i = -\frac{k}{\mu}p_{,i} \qquad \text{Eq. 4-14}$$

Fourier $$h_i = -\kappa^T T_{,i} \qquad \text{Eq. 4-15}$$

Where k is the intrinsic permeability, μ is the fluid viscosity, k^T is the bulk thermal conductivity. It has been defined as [80]:

$$\kappa^T = \emptyset_0\kappa_f^T + (1-\emptyset_0)\kappa_m^T \qquad \text{Eq. 4-16}$$

Where κ_f^T and κ_m^T are the thermal conductivities of the pore fluid and the matrix, respectively.

4.4 Field equations

The field governing equations can be obtained by combining the constitutive and diffusion equations with the force balance, heat and mass conservation equations. The field governing equations are composed of the Navier-type displacement equations, the fluid diffusivity and heat diffusivity equations as follows:

4.4.1 Deformation Equation

A Navier-type equation for the displacement u_i is given by replacing into the conservative law (Momental), Eq. 4-10, the constitutive relations for the porous solid (Eq. 4-12), with ε_{ij} stated in terms of the displacement gradient as $\varepsilon_{ij} = \frac{u_{ij}+u_{ji}}{2}$. It is given as:

$$Gu_{i,jj} + \frac{G}{1-2v}u_{j,ji} - \alpha P_{,i} - \frac{2G(1+v)}{3(1-2v)}\alpha_s T_{,i} = 0 \qquad \text{Eq. 4-17}$$

Where u_i is the displacement vector.

4.4.2 Fluid Diffusion Equation

The second field equation is the fluid diffusion equation which can be expressed in terms of the pore pressure change as:

$$\frac{\partial p}{\partial t} = \frac{2G(v_u - v)}{\alpha^2(1-2v)(1-2v_u)}\left\{\frac{k}{\mu}p_{f,jj} - \alpha\frac{\partial \varepsilon_{kk}}{\partial t} + \left[\alpha.\alpha_m^T + \left(\alpha_f^T - \alpha_m^T\right)\emptyset_o\right]\frac{\partial T}{\partial t}\right\} \qquad \text{Eq. 4-18}$$

The last term on the right-hand side of Eq. 4-18 denotes the impact of the temperature variation effect on the pore pressure. It depends on two factors [77]:

1 The differential thermal expansion between the porous matrix and pore fluids

2 The formation porosity

4.4.3 Heat Diffusion Equation

The final field equation is the thermal diffusivity equation which can be expressed as [64], [65]:

$$\frac{\partial T}{\partial t} = c_T T_{ii} + \frac{k}{\mu.\emptyset_o}(Tp_i)_i \qquad \text{Eq. 4-19}$$

The first term on the right-hand side of Eq. 4-19 represents heat transfer because of conduction and becomes dominant in low fluid mobility systems. The last term denotes the temperature variation induced by the pore fluid flow and dominates in high-fluid-mobility systems. In order to simplify solution procedure of problem, this term must be ignored; then, these field equations can describe a linear thermoporoelastic system. This solution is appropriate to the borehole problem in low-permeability rock, where heat convection is negligible.

Where c_T is thermal diffusivity is given by:

$$c_T = \frac{k^T}{\rho_m c_m} \quad \text{Eq. 4-20}$$

As it was explained, the pore pressures, displacements and temperature changes are coupled with each other through Eq. 4-17, Eq. 4-18 and Eq. 4-19, where the temperature and pore pressure coupling involves nonlinearity.

4.5 The Fully Coupled in Polar Coordinates

The fully coupled field equations (Eq. 4-17 to Eq. 4-19) are complex to solve analytically in the closed form. In most cases, however, a simplified form of these equations can be expressed. In particular, for the case of a non-rotational displacement field in an infinite media, the fluid and heat diffusion equations Eq. 4-18 and Eq. 4-19, respectively, can be decoupled from the deformation field [65], which are still coupled with each other. In this case, the fully coupled diffusion equations for temperature and pore pressure can be expressed in terms of polar coordinates (Eq. 4-22 and Eq. 4-21):

$$\frac{\partial T}{\partial t} = c_T \left(\frac{\partial^2 T}{\partial r^2} + \frac{1}{r}\frac{\partial T}{\partial r} \right) + c_T' \left[\frac{\partial T}{\partial r}\frac{\partial p}{\partial r} + T\left(\frac{\partial^2 p}{\partial r^2} + \frac{1}{r}\frac{\partial p}{\partial r} \right) \right] \quad \text{Eq. 4-21}$$

$$\frac{\partial p}{\partial t} = c_f \left(\frac{\partial^2 p}{\partial r^2} + \frac{1}{r}\frac{\partial p}{\partial r} \right) + c_{ft}\frac{\partial T}{\partial t} \quad \text{Eq. 4-22}$$

The axisymmetric case of a wellbore in an infinite media is a crucial problem with these conditions can be applied [65].

Where B is the Skempton coefficient, c_T' and c_{ft} are coupling coefficients:

$$c_T' = \frac{k}{\mu . \emptyset_0} \quad \text{Eq. 4-23}$$

$$c_{ft} = \frac{\mu . c_f}{k}\left[\frac{2\alpha_m^T (v_u - v)}{B(1+v_u)(1-v)} + (\alpha_f^T - \alpha_m^T)\emptyset_o \right] \quad \text{Eq. 4-24}$$

c_f is the fluid diffusivity coefficient which can be obtained by:

$$c_f = \frac{2kB^2 G(1-v)(1+v_u)^2}{9\mu(1-v_u)(v_u - v)} \quad \text{Eq. 4-25}$$

In order to facilitate the analysis, Eq. 4-21 and Eq. 4-22 can also be written in a dimensionless form:

$$\frac{\partial T_d}{\partial t_d} = A_0 \left(\frac{\partial^2 T_d}{\partial r_d^2} + \frac{1}{r_d}\frac{\partial T_d}{\partial r_d} \right) + A_0' \left[\frac{\partial T_d}{\partial r_d}\frac{\partial p_d}{\partial r_d} + T\left(\frac{\partial^2 p_d}{\partial r_d^2} + \frac{1}{r_d}\frac{\partial p_d}{\partial r_d} \right) \right] \quad \text{Eq. 4-26}$$

$$\frac{\partial p}{\partial t_d} = \left(\frac{\partial^2 p}{\partial r_d^2} + \frac{1}{r_d}\frac{\partial p_d}{\partial r_d}\right) + A' \frac{\partial T_d}{\partial t_d} \quad \text{Eq. 4-27}$$

Where:

$$A_0 = \frac{c_T}{c_f} \quad \text{Eq. 4-28}$$

$$A_0' = \frac{c_T'}{c_f}\Delta p_0 = \frac{9(v_u - v)(1 - v_u)}{2GB^2\emptyset_0(1 + v_u)^2(1 - v)}\Delta p_0 \quad \text{Eq. 4-29}$$

$$A' = \frac{\Delta T_0}{\Delta p_0} c_{ft} \quad \text{Eq. 4-30}$$

$$T_d = \frac{T}{\Delta T_0}, \quad p_d = \frac{p}{\Delta p_0}, \quad r_d = \frac{r}{r_w}, \quad t_d = \frac{c_f . t}{r_w^2} \quad \text{Eq. 4-31}$$

In order to calculate the temperature distributions, one must consider both heat conduction and heat convection. The c_T term in Eq. 4-21, which contains the second derivative of temperature, represents the impact of heat conduction to temperature changes. The first part of the c_T' term including fluid flux and the first derivative of temperature, represents the effect of heat convection on temperature changes. The second part of the c_T' term represents the effect of pressure diffusion on temperature changes. The c_f term in Eq. 4-21 denotes the pore pressure diffusion, and the c_{ft} term represents the effect of temperature variations on pore pressure changes. It is worth noting that depending upon the relative value of the four coefficients and the value of their correspondent terms, the fully coupled equations can be partly decoupled in some cases hence that they can be solved analytically.

Generally, for high permeability formations, the term c_T' in Eq. 4-21 is significantly higher than the c_T term, which means that the influence of temperature changes on the pore pressure changes may be very low, and the pore pressure may be considered independent of temperature changes. In other words, the pore pressure front moves much faster than the temperature front, or the localized pore pressure has reached equilibrium before the temperature changes. Under this conditions, the pore pressure change may be considered as steady state. In a high permeability formation $(> 1e-15\, m^2\ or\ 1\ millidarcy)$ heat convection may dominate, while in an intermediate permeability formation $(1e-18\, m^2\ to\ 1e-15\, m^2, or\ 1\ microdarcy\ to\ 1\ millidarcy)$ both of the conduction and convection may happen. Unless temperature change is assumed a steady-state, then the analytical solution of temperature and thermally induced effect can only be presented in the Laplace domain.

In contrast, for a low-permeability shale, the c_f term in Eq. 4-21 may be much smaller than the c_{ft} term and it may possible to ignore the transient pore pressure diffusion. In this case, pore pressure will be a steady-state function of temperature variations for certain radial distances. This simplified method may only be used for large distance and long time, under which temperature reaches a pseudo-steady-state distribution. Kurashige (1989) also partially decoupled Eq. 4-21 for granite rocks, sandstones, and Berea sandstone using rock properties provided in his paper [64].

4.6 Loading Decomposition

For a linear thermoporoelastic system for instance the one explained above, the problem depicted in Figure 4-1 can be decomposed into three sub-loading problems and virgin formation as shown in Figure 4-2 [61], [66], [77], [70]. The boundary conditions, in the far field and at wellbore wall, for each of the sub-loading problem are as follows:

4.6.1 Problem I

As shown in Figure 4-2-(b), problem I is a thermoporoelastic plane-strain problem. In fact, it is a modified plane strain problem considering the in-plane shear and normal stresses and the pore pressure and temperature distributions. This problem presents full coupling of the heat and fluid transfer with the deformation. The boundary conditions for this problem are given as follows:

In the far field ($\boldsymbol{r = r_e}$)

$$\sigma_{xx} = -S_x$$

$$\sigma_{yy} = -S_y$$

$$\sigma_{zz} = -v(S_x + S_y) - \alpha(1-2v)p_f$$

$$\sigma_{xy} = -S_{xy} \qquad \text{Eq. 4-32}$$

$$\sigma_{yz} = \sigma_{xz} = 0$$

$$p = p_f$$

$$T = T_f$$

Along the borehole well ($\boldsymbol{r = r_w}$)

$$\sigma_{rr} = -S_r H(-t) \qquad \text{Eq. 4-33}$$

$$\sigma_{r\theta} = -S_{r\theta}H(-t)$$

$$\sigma_{rz} = 0$$

$$p = p_m H(t) + p_f H(-t)$$

$$T = T_m H(t) - T_f$$

Furthermore, the solution for the first problem is given by a decomposition of the boundary conditions into three sub-loading modes [61] [70], [76] (Figure 4-2). Of these, the hydrostatic effect contributing to the boundary stresses is considered as mode 1, both the pore pressure and temperature profiles are taken into account as mode 2, and the thermoporoelastic deviatoric stress loading problem is considered as mode 3. However, only modes 2 and 3 depend on time, in that mode creates the coupling between the pore fluid and heat transportation processes. Whereas mode 3 presents behaviour of full poroelastic coupling without the influence of temperature variations. The boundary conditions at the borehole wall, $r = r_w$ are given as follows:

✓ Mode 1

$$\sigma_{rr}^{(1)} = P_0 H(t) - p_m;\ \sigma_{r\theta}^{(1)} = 0;\ p^{(1)} = 0;\ T^{(1)} = 0 \qquad \text{Eq. 4-34}$$

✓ Mode 2

$$\sigma_{rr}^{(2)} = 0;\ \sigma_{r\theta}^{(2)} = 0;\ p^{(2)} = p_m - p_0 H(t);\ T^{(2)} = T_m - T_f \qquad \text{Eq. 4-35}$$

✓ Mode 3

$$\sigma_{rr}^{(3)} = -S_0 H(t)\cos 2(\theta - \theta_r);\ \ \sigma_{r\theta}^{(3)} = S_0 H(t)\sin 2(\theta - \theta_r);\ \ p^{(3)} = 0;\ T^{(3)} = 0 \qquad \text{Eq. 4-36}$$

In which the expressions for $T^{(2)}$, $p^{(1)-(3)}$and $\sigma_{ij}^{(1)-(3)}$ are the temperature, pore pressure and stress distributions for sub-loading modes 1 to 3, according to the superscripts (1) to (3).

At the far field, all stresses, pore pressure and temperature vanish.

4.6.2 Problem II

Problem II, as shown in Figure 4-2-(c), is a uniaxial loading problem and the anti-plane problem [70], [81], is merely elastic as it does not cause heat or fluid transfer. The boundary conditions for this problem are as follows:

In the far field ($\boldsymbol{r = r_e}$)

$$\sigma_{zz} = -S_z + v(S_x + S_y) + \alpha(1 - 2v)p_f \qquad \text{Eq. 4-37}$$

$$\sigma_{xx} = \sigma_{yy} = \sigma_{xy} = \sigma_{yz} = \sigma_{xz} = p = T = 0 \quad \text{Eq. 4-38}$$

Along the borehole well ($r = r_w$)

$$\sigma_{rr} = \sigma_{r\theta} = \sigma_{rz} = p = T = 0 \quad \text{Eq. 4-39}$$

4.6.3 Problem III

Problem III, as shown in Figure 4-2-(d), is an anti-plane and shear problem. In addition, like the aforementioned problem II, since it does not affect the heat and fluid transfer, it is essentially elastic [70], [81]. The boundary conditions for this problem are:

In the far field ($r = r_e$)

$$\sigma_{xx} = \sigma_{yy} = \sigma_{zz} = \sigma_{xy} = p = T = 0$$
$$\sigma_{rz} = -S_{yz} \quad \text{Eq. 4-40}$$
$$\sigma_{xz} = -S_{xz}$$

Along the borehole well ($r = r_w$)

$$\sigma_{rr} = \sigma_{r\theta} = p = T = 0$$
$$\sigma_{rz} = -S_{rz}H(-t) \quad \text{Eq. 4-41}$$

It is noted that the summation of boundary conditions (4.6) are reproduced by the summation of the above far-field and boundary conditions (Eq. 4-3 and Eq. 4-4).

4.7 Semi-Analytical Solutions

It has been determined that by using the decomposition showed before, the solutions can be acquired elegantly as superposition of existing results, without a formal mathematical method that can result in lengthy, semi-analytical terminologies and can be derived by combining the aforementioned equations:

- ✓ Boundary conditions (at the borehole wall and far field)
- ✓ Deformation equation
- ✓ Fluid diffusion equation
- ✓ Heat diffusion equation
- ✓ Force balance equation

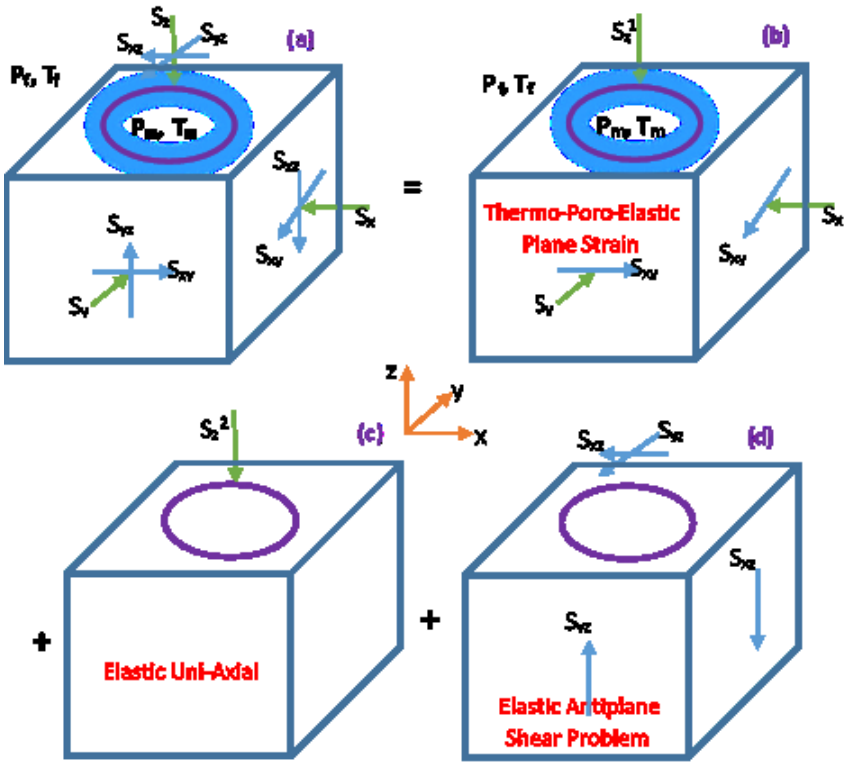

Figure 4-2 Loading decomposition scheme

4.7.1 Problem I

The first problem is designed to be a thermoporoelastic plane-strain problem, namely the out-of-plane displacement (u_z), flux (q_z) and heat flux (h_z) will vanish. It is a plane-strain borehole subjected to a non-hydrostatic stress field, a constant borehole pressure and a constant temperature difference along the borehole wall. These conditions can be admitted only because they are fully compatible with the natural result of a plane-strain solution:

$$\sigma_{zz} = v\left(\sigma_{xx} + \sigma_{yy}\right) - \alpha(1-2v)p$$

$$\sigma_{yz} = \sigma_{xz} = 0 \qquad \text{Eq. 4-42}$$

The problem can be solved by further decomposing the problem into three sub-loading modes (Detournay and Cheng, 1988). Since the solution of Detournay et. al. is given in a coordinate system, assumingly named $x''y''z''$, with its x'' axis coinciding with the in-plane (the plane that is perpendicular to the borehole axis) minimum principal stress $\sigma_{x''x''}$ (Figure 4-3), there is an angular difference between the coordinate systems xyz and $x''y''z''$, that is:

$$\theta'' = \theta - \theta_r \qquad \text{Eq. 4-43}$$

Where θ and θ'' are the polar angles in the xyz and $x''y''z''$ coordinate systems respectively; and,

$$\theta_r = \frac{1}{2}\tan^{-1}\left(\frac{2\sigma_{xy}}{\sigma_{xx} - \sigma_{yy}}\right) \qquad \text{Eq. 4-44}$$

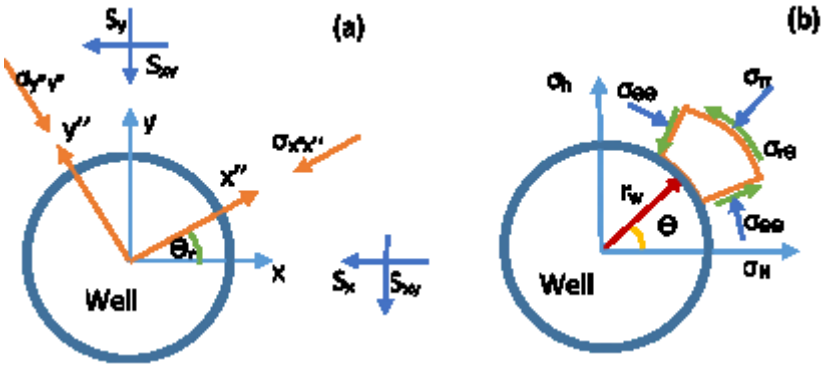

Figure 4-3 (a) Relationship between the two local coordinate systems, (b) stress components acting in the plane perpendicular to the borehole in cylindrical coordinate system

The far field conditions become:

$$\begin{gathered}\sigma_{x''x''} = -(P_0 - S_0) \\ \sigma_{y''y''} = -(P_0 + S_0) \\ \sigma_{x''y''} = 0 \\ p = p_0\end{gathered} \qquad \text{Eq. 4-45}$$

Where P_0 is the mean compressive stress and S_0 the deviatoric stress given by:

$$\begin{gathered}P_0 = \frac{\sigma_{xx} + \sigma_{yy}}{2} \\ S_0 = \sqrt{\left(\frac{\sigma_{xx} - \sigma_{yy}}{2}\right)^2 + \sigma_{xy}^2}\end{gathered} \qquad \text{Eq. 4-46}$$

The final solution for problem I in a polar coordinate system, complying with the xyz coordinates, can be expressed as:

$$\begin{gathered}\sigma_{rr}^{(I)} = -P_0 + S_0 \cos 2(\theta - \theta_r) + \sigma_{rr}^{(1)} + \sigma_{rr,hydraulic}^{(2)} + \sigma_{rr,thermal}^{(2)} + \sigma_{rr}^{(3)} \\ \sigma_{\theta\theta}^{(I)} = -P_0 - S_0 \cos 2(\theta - \theta_r) + \sigma_{\theta\theta}^{(1)} + \sigma_{\theta\theta,hydraulic}^{(2)} + \sigma_{\theta\theta,thermal}^{(2)} + \sigma_{\theta\theta}^{(3)} \\ \sigma_{zz}^{(I)} = v\left(\sigma_{rr}^{(I)} + \sigma_{\theta\theta}^{(I)}\right) - \alpha(1 - 2v)p^{(I)} - \frac{E\alpha_m}{3}T \\ \sigma_{r\theta}^{(I)} = -S_0 \sin 2(\theta - \theta_r) + \sigma_{r\theta}^{(3)} \\ \sigma_{rz}^{(I)} = \sigma_{\theta z}^{(I)} = 0\end{gathered} \qquad \text{Eq. 4-47}$$

$$p^{(I)} = p_f + p^{(2)}_{hydraulic} + p^{(2)}_{therm} + p^{(3)}$$

$$T^{(I)} = T^{(2)}$$

Where the superscript (I) represents the solution for Problem I.

4.7.1.1 Loading mode 1

The mode 1 loading does not cause any volumetric strain; hence no pore pressure is generated. The solution is purely elastic as given by the classical Lamé solution:

$$\sigma^{(1)}_{rr} = H(t)(P_0 - p_w)\left(\frac{r_w}{r}\right)^2$$

$$\sigma^{(1)}_{\theta\theta} = -H(t)(P_0 - p_w)\left(\frac{r_w}{r}\right)^2 \qquad \text{Eq. 4-48}$$

4.7.1.2 Loading mode 2

Solutions for mode 2 is given in the Laplace domain and are inverted to the time-domain using the Stehfest algorithm [82] for different permeability range.

High permeability formation (Permeability > 1md)

For an overbalance drilling (or injection) or an underbalance drilling (or production) operation in a high permeability sandstone, the fluid flow can be considered as steady state. In other words, fluid pressure distribution may become independent of time after a certain time, regardless of the temperature distribution. Kurashige (1989) [64] presented the simplified pressure equation for the spherical geometry. For steady state fluid flow in the cylindrical geometry, the second equation in Eq. 4-21 becomes:

$$\frac{\partial^2 p}{\partial r^2} + \frac{1}{r}\frac{\partial p}{\partial r} = 0, or\ \frac{d^2 p_d}{dr_d^2} = 0 \qquad \text{Eq. 4-49}$$

For a cylindrical coordinate system, the finite boundary conditions for an injection or a production process can be written as:

$$p(r_w) = p_m - p_f$$

$$p(r_e) = 0 \qquad \text{Eq. 4-50}$$

The solutions are summarized as permeable and impermeable boundary conditions. Note in a high permeability formation, the effect of temperature changes on pressure change is negligible when pore fluid flow is significantly faster than the heat transfer.

✓ Permeable boundary condition

The solution for the steady-state fluid flow can be written as:

$$p_{hydraulic}^{(2)} = \frac{p_m - p_f}{\ln\left({}^{r_e}/_{r_w}\right)} \ln\left({}^{r_e}/_{r}\right) = -A_p \ln\left({}^{r_e}/_{r}\right)$$

$$p_{thermal}^{(2)} = 0 \qquad \text{Eq. 4-51}$$

$$A_p = -\frac{p_m - p_f}{\ln\left({}^{r_e}/_{r_w}\right)}$$

Note $p^{(2)} > 0$ for an underbalance drilling (or an injection) process and $p^{(2)} < 0$ for an under-balanced drilling (or a production) process.

$$\sigma_{rr,hydraulic}^{(2)} = \eta A_p \left\{ \left(\ln\left({}^{r}/_{r_e}\right) - \frac{1}{2} \right) - \left(\frac{r_w}{r}\right)^2 \left(\ln\left({}^{r_w}/_{r_e}\right) - \frac{1}{2} \right) \right\} \qquad \text{Eq. 4-52}$$

$$\tilde{\sigma}_{rr,thermal}^{(2)} = -\frac{\eta_T (T_m - T_f) c_T}{s\xi} \left(\frac{r_w}{r}\right)^{\frac{\bar{\omega}}{2}} \frac{K_{v\pm1}(\xi_T) - \left(\frac{r_w}{r}\right)^{1\pm v} K_{v\pm1}(\beta_T)}{K_v(\beta_T)} \qquad \text{Eq. 4-53}$$

$$\sigma_{\theta\theta,hydraulic}^{(2)} = \eta A_p \left\{ \left(\ln\left({}^{r}/_{r_e}\right) + \frac{1}{2} \right) + \left(\frac{r_w}{r}\right)^2 \left(\ln\left({}^{r_w}/_{r_e}\right) - \frac{1}{2} \right) \right\} \qquad \text{Eq. 4-54}$$

$$\tilde{\sigma}_{\theta\theta,thermal}^{(2)} = -\frac{\eta_T (T_m - T_f) c_T}{s\xi} \left(\frac{r_w}{r}\right)^{\frac{\bar{\omega}}{2}} \frac{K_{v\pm1}(\xi_T) - \left(\frac{r_w}{r}\right)^{1\pm v} K_{v\pm1}(\beta_T)}{K_v(\beta_T)} \qquad \text{Eq. 4-55}$$

$$\sigma_{zz}^{(2)} = 2\eta \left(p_{hydraulic}^{(2)} + p_{thermal}^{(2)} \right) + \frac{E\alpha_m}{3} T \qquad \text{Eq. 4-56}$$

$$\sigma_{zz} = \sigma_{zz}^{i} + v \begin{pmatrix} \sigma_{rr}^{(1)} + \sigma_{rr}^{(3)} \\ +\sigma_{\theta\theta}^{(1)} + \sigma_{\theta\theta}^{(3)} \end{pmatrix} + \alpha(1-2v) p^{(3)} + 2\eta \left(p_{hydraulic}^{(2)} + p_{thermal}^{(2)} \right) + \frac{E\alpha_m}{3} T \qquad \text{Eq. 4-57}$$

Where:

$$\begin{cases} v \pm 1 = v + 1 \; when \; \bar{\omega} < 0 \\ v \pm 1 = v - 1 \; when \; \bar{\omega} > 0 \end{cases}$$

$$\bar{\omega} = \frac{\acute{c}_T A_p}{c_T}$$

✓ Impermeable boundary condition

An impermeable boundary may be appropriate for an oil base mud drilling operation. In this occasion, the pore fluid will maintain a constant pressure in the near-wellbore area. For an impermeable boundary, the hydraulic terms such as $\sigma_{rr,hydraulic}^{(2)}$ and $\sigma_{\theta\theta,hydraulic}^{(2)}$, will disappear but thermal effects still apply. The temperature distribution in the near-wellbore area for the initial and boundary conditions expressed in (Eq. 4-3 and Eq. 4-4) can then be solved using the well-known heat conduction approach (Carslaw and Jaeger, 1959) [83]. The solution

is shown in the next section. The thermally-induced radial, hoop and axial stresses are then given by the following equations.

$$p^{(2)} = 0 \quad \text{Eq. 4-58}$$

$$\sigma^{(2)}_{rr,hydraulic} = 0 \quad \text{Eq. 4-59}$$

$$\tilde{\sigma}^{(2)}_{rr,thermal} = \frac{\eta_T}{s}\left(T_m - T_f\right)\left[\left(\frac{r_w}{r}\right)^2 \frac{K_1\left(\beta_T\right)}{\beta_T K_0\left(\beta_T\right)} - \left(\frac{r_w}{r}\right)\frac{K_1\left(\xi_T\right)}{\beta_T K_0\left(\beta_T\right)}\right] \quad \text{Eq. 4-60}$$

$$\sigma^{(2)}_{\theta\theta,hydraulic} = 0 \quad \text{Eq. 4-61}$$

$$\tilde{\sigma}^{(2)}_{\theta\theta,thermal} = \frac{\eta_T}{s}\left(T_m - T_f\right)\left[-\left(\frac{r_w}{r}\right)^2 \frac{K_1\left(\beta_T\right)}{\beta_T K_0\left(\beta_T\right)} + \left(\frac{r_w}{r}\right)\frac{K_1\left(\xi_T\right)}{\beta_T K_0\left(\beta_T\right)} + \frac{K_0\left(\xi_T\right)}{K_0\left(\beta_T\right)}\right] \quad \text{Eq. 4-62}$$

Where:

$$\eta_T = \frac{E\alpha_s}{3(1-v)} \quad \text{Eq. 4-63}$$

$$\xi = r\sqrt{\frac{s}{c}} \quad \text{Eq. 4-64}$$

$$\beta = a\sqrt{\frac{s}{c}} \quad \text{Eq. 4-65}$$

$$\xi_T = r\sqrt{\frac{s}{c_T}} \quad \text{Eq. 4-66}$$

$$\beta_T = r\sqrt{\frac{s}{c_T}} \quad \text{Eq. 4-67}$$

Low-permeable formation (0.001md < Permeability < 1md)

The term c_T in Eq. 4-21 is significantly higher than c_T' for a low permeability shale formation. Therefore, this term can be ignored and the diffusivity equations can be partially decoupled:

$$\frac{\partial T}{\partial t} = c_T\left(\frac{\partial^2 T}{\partial r^2} + \frac{1}{r}\frac{\partial T}{\partial r}\right) \quad \text{Eq. 4-68}$$

$$\frac{\partial p}{\partial t} = c_f\left(\frac{\partial^2 p}{\partial r^2} + \frac{1}{r}\frac{\partial p}{\partial r}\right) + c_{ft}\frac{\partial T}{\partial t} \quad \text{Eq. 4-69}$$

The solutions for Eq. 4-68 and Eq. 4-69 with IC and BC expressed in (Eq. 4-3 and Eq. 4-4) are summarized as follow:

$$\tilde{p}^{(2)}_{hydraulic} = \frac{\left(p_w - p_f\right)}{s}\frac{K_0(\xi)}{K_0(\beta)} \quad \text{Eq. 4-70}$$

$$\tilde{p}^{(2)}_{therm} = \frac{c_{ft}}{1 - {c_f}/{c_T}}\frac{\left(T_m - T_f\right)}{s}\left[\frac{K_0(\xi)}{K_0(\beta)} - \frac{K_0\left(\xi_T\right)}{K_0\left(\beta_T\right)}\right] \quad \text{Eq. 4-71}$$

$$\tilde{T} = \frac{\left(T_m - T_f\right)}{s}\frac{K_0(\xi_T)}{K_0(\beta_T)} \quad \text{Eq. 4-72}$$

$$\begin{aligned}\tilde{\sigma}^{(2)}_{rr,hydraulic} = &-\frac{2\eta}{s}\left[\left(p_w - p_f\right) + \frac{c_{ft}}{1 - {c_f}/{c_T}}\left(T_m - T_f\right)\right] \\ &\times\left[\left(\frac{r_w}{r}\right)^2\frac{K_1(\beta)}{\beta K_0(\beta)} - \left(\frac{r_w}{r}\right)\frac{K_1(\xi)}{\beta K_0(\beta)}\right] \\ &+\frac{2\eta}{s}\frac{c_{ft}}{1 - {c_f}/{c_T}}\left(T_m - T_f\right)\left[\left(\frac{r_w}{r}\right)^2\frac{K_1\left(\beta_T\right)}{\beta_T K_0\left(\beta_T\right)}\right. \\ &\left.-\left(\frac{r_w}{r}\right)\frac{K_1\left(\xi_T\right)}{\beta_T K_0\left(\beta_T\right)}\right]\end{aligned} \quad \text{Eq. 4-73}$$

$$\tilde{\sigma}^{(2)}_{rr,thermal} = \frac{\eta_T}{s}\left(T_m - T_f\right)\left[\left(\frac{r_w}{r}\right)^2\frac{K_1\left(\beta_T\right)}{\beta_T K_0\left(\beta_T\right)} - \left(\frac{r_w}{r}\right)\frac{K_1\left(\xi_T\right)}{\beta_T K_0\left(\beta_T\right)}\right] \quad \text{Eq. 4-74}$$

$$\begin{aligned}\tilde{\sigma}^{(2)}_{\theta\theta,hydraulic} = &\frac{2\eta}{s}\left[\left(p_w - p_f\right) + \frac{c_{ft}}{1 - {c_f}/{c_T}}\left(T_m - T_f\right)\right] \\ &\times\left[\left(\frac{r_w}{r}\right)^2\frac{K_1(\beta)}{\beta K_0(\beta)} - \left(\frac{r_w}{r}\right)\frac{K_1(\xi)}{\beta K_0(\beta)} - \frac{K_0(\xi)}{K_0(\beta)}\right] \\ &+\frac{2\eta}{s}\frac{c_{ft}}{1 - {c_f}/{c_T}}\left(T_m - T_f\right)\left[-\left(\frac{r_w}{r}\right)^2\frac{K_1\left(\beta_T\right)}{\beta_T K_0\left(\beta_T\right)}\right. \\ &\left.+\left(\frac{r_w}{r}\right)\frac{K_1\left(\xi_T\right)}{\beta_T K_0\left(\beta_T\right)} + \frac{K_0\left(\xi_T\right)}{K_0\left(\beta_T\right)}\right]\end{aligned} \quad \text{Eq. 4-75}$$

$$\begin{aligned}\tilde{\sigma}^{(2)}_{\theta\theta,thermal} = &\frac{\eta_T}{s}\left(T_m - T_f\right)\left[-\left(\frac{r_w}{r}\right)^2\frac{K_1\left(\beta_T\right)}{\beta_T K_0\left(\beta_T\right)} + \left(\frac{r_w}{r}\right)\frac{K_1\left(\xi_T\right)}{\beta_T K_0\left(\beta_T\right)}\right. \\ &\left.+\frac{K_0\left(\xi_T\right)}{K_0\left(\beta_T\right)}\right]\end{aligned} \quad \text{Eq. 4-76}$$

$$\sigma_{r\theta} = 0 \quad \text{Eq. 4-77}$$

When hydraulic diffusivity is identical to thermal diffusivity, a singularity will occur for the solutions of both the permeable and the impermeable boundaries, the terms including the inversion of $\left(1 - {}^{c_f}/_{c_T}\right)$ can be replaced with the following expressions in the pore pressure and stress solutions to remove the singularity. The solutions can be written as follows:

$$\tilde{p}_{therm}^{(2)} = \frac{c_{ft}\left(T_m - T_f\right)}{2s}\left[\frac{\xi K_1(\xi)}{K_0(\beta)} - \frac{K_0(\xi)}{K_0(\beta)}\frac{\beta K_1(\beta)}{K_0(\beta)}\right] \qquad \text{Eq. 4-78}$$

Impermeable formation

For an impermeable boundary, the hydraulic terms such as $\sigma^{(2)}_{rr,hydraulic}$ and $\sigma^{(2)}_{\theta\theta,hydraulic}$, will vanish, but thermal effects and pore pressure still apply. The temperature solution for the partially decoupled equation Eq. 4-68 and Eq. 4-69 will stay the same as low permeability formation. In case of impermeable wellbore wall, the boundary condition at the borehole wall will become:

$$\frac{\partial p}{\partial r}(r_w, t) = 0 \qquad \text{Eq. 4-79}$$

Therefore, solution for pore pressure and temperature induced radial and tangential stress are given as follow:

$$\tilde{p}^{(2)}_{thermal} = \frac{c_{ft}}{1 - {}^{c_f}/_{c_T}} \frac{(T_m - T_f)}{s} \left[\frac{K_0(\xi_T) - \sqrt{\frac{c_f}{c_T}} K_0(\xi) \frac{K_1(\beta_T)}{K_1(\beta)}}{K_0(\beta_T)} \right] \qquad \text{Eq. 4-80}$$

$$\begin{aligned} \tilde{\sigma}^{(2)}_{rr,thermal} = {} & \frac{2\eta(T_m - T_f)}{s} \frac{c_{ft}}{1 - {}^{c_f}/_{c_T}} \left[\sqrt{\frac{c_f}{c_T}} \frac{K_1(\beta_T)}{K_0(\beta)} \left(\frac{r_w}{r} \frac{K_1(\xi)}{K_1(\beta)} - \left(\frac{r_w}{r}\right)^2 \right) \right] \\ & - \frac{1}{\beta_T} \left[\frac{r_w}{r} \frac{K_1(\xi_T)}{K_o(\beta_T)} - \left(\frac{r_w}{r}\right)^2 \frac{K_1(\beta_T)}{K_o(\beta_T)} \right] \\ & + \frac{2\eta}{s} \frac{K\alpha_m}{\alpha} (T_m - T_f) \left[\frac{r_w}{r} \frac{K_1(\xi_T)}{\beta_T K_o(\beta_T)} - \left(\frac{r_w}{r}\right)^2 \frac{K_1(\beta_T)}{\beta_T K_o(\beta_T)} \right] \end{aligned} \qquad \text{Eq. 4-81}$$

$$\begin{aligned} \tilde{\sigma}^{(2)}_{\theta\theta,thermal} = {} & \frac{2\eta(T_m - T_f)}{s} \frac{c_{ft}}{1 - {}^{c_f}/_{c_T}} \left\{ \frac{K_0(\xi_T) - \sqrt{\frac{c_f}{c_T}} K_0(\xi) \frac{K_1(\beta_T)}{K_1(\beta)}}{K_0(\beta_T)} \right. \\ & \left. - \left[\sqrt{\frac{c_f}{c_T}} \frac{K_1(\beta_T)}{K_0(\beta)} \left(\frac{r_w}{r} \frac{K_1(\xi)}{K_1(\beta)} - \left(\frac{r_w}{r}\right)^2 \right) \right] \right\} \\ & - \frac{1}{\beta_T} \left[\frac{r_w}{r} \frac{K_1(\xi_T)}{K_o(\beta_T)} - \left(\frac{r_w}{r}\right)^2 \frac{K_1(\beta_T)}{K_o(\beta_T)} \right] \\ & + \frac{2\eta}{s} \frac{K\alpha_m}{\alpha} (T_m - T_f) \left[\frac{r_w}{r} \frac{K_1(\xi_T)}{\beta_T K_o(\beta_T)} - \left(\frac{r_w}{r}\right)^2 \frac{K_1(\beta_T)}{\beta_T K_o(\beta_T)} \right. \\ & \left. + \frac{K_0(\xi_T)}{K_o(\beta_T)} \right] \end{aligned} \qquad \text{Eq. 4-82}$$

When hydraulic and thermal diffusivity are the same, a singularity will occur for the solutions of both the permeable and the impermeable boundaries, the terms including the inversion of $\left(1-{}^{c_f}/_{c_T}\right)$ can be replaced with the following expressions in the pore pressure and stress solutions to remove the singularity. The solutions can be written as follows:

$$\tilde{p}^{(2)}_{thermal}=\frac{c_{ft}\left(T_m-T_f\right)}{2s}\left[\frac{\xi K_1(\xi)}{K_0(\beta)}-\frac{\beta K_0(\xi)}{K_1(\beta)}\right] \quad \text{Eq. 4-83}$$

$$\tilde{\sigma}^{(2)}_{rr,thermal}=\frac{2\eta c_{ft}\left(T_m-T_f\right)}{s}\frac{K_1(\beta)}{\xi K_0(\beta)}\left[-\frac{K_1(\xi)}{K_1(\beta)}+\frac{r_w}{r}-\frac{\xi K_0(\xi)}{2K_1(\beta)}+\frac{\beta K_0(\beta)K_1(\xi)}{2[K_1(\beta)]^2}\right] \quad \text{Eq. 4-84}$$

The hoop stress can be calculated using the solution of pore pressure and radial stress.

4.7.1.3 Loading mode 3

The mode 3 effect can be significant for a low permeability formation like shale (for a certain time period), but it will only appear within a very short period for a high-permeability rock. Under an axisymmetric loading condition, this loading mode effect is not present.

$$\tilde{\sigma}^{(3)}_{rr}=\frac{S_0\cos 2(\theta-\theta_r)}{s}\left\{\frac{B(1+v_u)}{3(1-v_u)}C_1\left[\frac{1}{\xi}K_1(\xi)+\frac{6}{\xi^2}K_2(\xi)\right]-\frac{C_2}{1-v_u}\left(\frac{r_w}{r}\right)^2-3C_3\left(\frac{r_w}{r}\right)^4\right\} \quad \text{Eq. 4-85}$$

$$\tilde{\sigma}^{(3)}_{\theta\theta}=\frac{S_0\cos 2(\theta-\theta_r)}{s}\left\{\frac{B(1+v_u)}{3(1-v_u)}C_1\left[\frac{1}{\xi}K_1(\xi)+\left(1+\frac{6}{\xi^2}\right)K_2(\xi)\right]+3C_3\left(\frac{r_w}{r}\right)^4\right\} \quad \text{Eq. 4-86}$$

$$\tilde{\sigma}^{(3)}_{r\theta}=\frac{S_0\cos 2(\theta-\theta_r)}{s}\left\{\frac{2B(1+v_u)}{3(1-v_u)}C_1\left[\frac{1}{\xi}K_1(\xi)+\frac{3}{\xi^2}K_2(\xi)\right]-\frac{C_2}{2(1-v_u)}\left(\frac{r_w}{r}\right)^2-3C_3\left(\frac{r_w}{r}\right)^4\right\} \quad \text{Eq. 4-87}$$

$$\tilde{p}^{(3)}=\frac{S_0\cos 2(\theta-\theta_r)}{s}\left\{\frac{B^2(1-v)(1+v_u)^2}{9(1-v_u)(v_u-v)}C_1K_2(\xi)+\frac{B(1+v_u)C_2}{3(1-v_u)}\left(\frac{r_w}{r}\right)^2\right\} \quad \text{Eq. 4-88}$$

Where the overbars represent the Laplace transform C_1, C_2 and C_3 are constants obtained from boundary conditions:

$$C_1 = -\frac{12\beta(1-v_u)(v_u-v)}{B(1+v_u)(D_2-D_1)} \quad \text{Eq. 4-89}$$

$$C_2 = \frac{4(1-v_u)D_2}{(D_2-D_1)} \quad \text{Eq. 4-90}$$

$$C_3 = -\frac{\beta(D_2-D_1)+8(v_u-v)k_2(\beta)}{\beta(D_2-D_1)} \quad \text{Eq. 4-91}$$

$$D_1 = 2(v_u-v)k_1(\beta) \quad \text{Eq. 4-92}$$

$$D_2 = \beta(1-v)k_2(\beta) \quad \text{Eq. 4-93}$$

In which k_0, k_1 and k_2 are the second kind of Bessel functions with zero, one and two order, respectively.

Other parameters:

$$\eta = \frac{\alpha(1-2v)}{2(1-v)} \quad \text{Eq. 4-94}$$

The Mode 3 effect can be significant for a low-permeability formation like shale, but it will only appear within a very short period for a high-permeability rock. Under an axisymmetric loading condition, the Mode 3 effect is not present.

4.7.2 Problem II

For the second problem, because the boundary conditions at the wellbore wall are zero, as presented in Eq. 4-38, the drilling and the following pressurization of the borehole do not produce any turbulences for this particular case, i.e. the solution is elastic or time independent conditions [76]. In fact, the solution is uniaxial and is given by a constant vertical stress (σ_{zz}) everywhere:

$$\sigma_{zz}^{(II)} = -S_z + \left[v\left(S_x+S_y\right)+\alpha(1-2v)p_0\right]$$
$$\sigma_{rr}^{(II)} = \sigma_{\theta\theta}^{(II)} = \sigma_{r\theta}^{(II)} = \sigma_{rz}^{(II)} = \sigma_{\theta z}^{(II)} = p^{(II)} = T^{(II)} = 0 \quad \text{Eq. 4-95}$$

4.7.3 Problem III

For the third problem, the disturbance on stress status due to drilling is introduced by the sudden drop of surface traction σ_{rz} on the borehole wall from the value $-S_{rz}$ to zero. This anti-plane shear variation does not produce any mean normal stress; thus no pore pressure will be created by the Skempton's effect; and the solution is the same as the elastic one. Following Bradley (1979) [59], the solution for problem III can be expressed as:

$$\sigma_{rz}^{(III)} = -\left(\sigma_{xz}\cos\theta + \sigma_{yz}\sin\theta\right)\left(1 - \left(\frac{r_w}{r}\right)^2\right)$$

$$\sigma_{\theta z}^{(III)} = \left(\sigma_{xz}\cos\theta - \sigma_{yz}\sin\theta\right)\left(1 + \left(\frac{r_w}{r}\right)^2\right) \qquad \text{Eq. 4-96}$$

$$\sigma_{rr}^{(III)} = \sigma_{\theta\theta}^{(III)} = \sigma_{zz}^{(III)} = \sigma_{r\theta}^{(III)} = p^{(III)} = T^{(III)} = 0$$

4.8 Superposition

Superimposing the solutions for Problems I to III results in the final solution of the overall problem (omitting the zero components):

$$\sigma_{rr} = \sigma_{rr}^{(I)}$$

$$\sigma_{\theta\theta} = \sigma_{\theta\theta}^{(I)}$$

$$\sigma_{zz} = \sigma_{zz}^{(I)} + \sigma_{zz}^{(II)}$$

$$\sigma_{r\theta} = \sigma_{r\theta}^{(I)} \qquad \text{Eq. 4-97}$$

$$\sigma_{rz} = \sigma_{rz}^{(III)}$$

$$\sigma_{\theta z} = \sigma_{\theta z}^{(III)}$$

$$p = p^{(I)}$$

$$T = T^{(I)}$$

4.9 Result in Time Domain

Due to the complexity of the integrands involved in conducting Laplace inversions, the stress components in the time domain have to be obtained numerically. This is performed by applying approximate numerical schemes. The Stehfest method which has received high marks for its accuracy, efficiency and stability, is used to solve the partial equations. The Stehfest formula is:

$$f(t) = \frac{\ln 2}{t}\sum_{n=1}^{N} C_n \tilde{f}\left(n\frac{\ln 2}{t}\right)$$

With the coefficient C_n is given by:

$$C_n = (-1)^{n+N/2} \sum_{j=\left[(n+1)/2\right]}^{min(n,N/2)} \frac{j^{N/2}(2j)!}{(N/2 - j)!\, j!\, (j-1)!\, (n-j)!\, (2n-j)!} \qquad \text{Eq. 4-98}$$

The number of terms N in the series is even and generally a selection of $N = 8$ provides reasonable results.

In the next chapter, the least effective stress out of these stresses (Eq. 4-97) will be used to estimate Apparent Rock Strength (ARS) according to Mohr-Coulomb criteria. Then, the result will be used to calculate Analytical Mechanical Specific Energy (AMSE) and compare the performance of the bit and the combination of the bit-reamer in order to make decision to choose the efficient method (lower MSE) in the certain formation.

5 Experimental Design

This chapter presents the planning required for the experiments. The design of experiments and tools preparation is a time-consuming and expensive process of this project. However, it is important as it provides assistance as a proposal for implementing the experiment, and for the interpretation of its outcomes.

The design is based on the thesis objective and hypotheses supporting it, following which the research design was then evaluated. Following that, the details of the experimental process were explained containing the key parameters, variables, planning, objects, instrumentation and systems for data gathering and analysis. Finally, the validity of the experimental design was evaluated.

5.1 Experiment Goal

The aim of these experiments is to analyze the thermoporoelastic approach of assessing the efficiency of Multidiameter tools in order to improve the decision making process concerning tools with respect to the performance of drilling predictions.

5.2 Hypothesis

The hypothesis claims that rock around the wellbore weaken due to stress alteration, pore pressure and temperature variation (the latter as a result of drilling fluid penetration into formation). A Matlab code using equations developed in chapter 4 and this section was developed to estimate the extent of the weakening zone based on the thermoporoelastic method (Eq. 4-97) of AMSE calculation.

There are different variables to consider in a reamer/pilot combination, such as dynamic vibration, weight on pilot and reamer distribution, and torque on bit and reamer distribution etc. This test proposal focuses on effect of rock strength on reamer/pilot size ratio.

Drilling experts normally apply MSE (It has been discussed in chapter 3 in detail) in order to evaluate drilling efficiency, bit performance, etc. An analytical method will be described here to estimate MSE and base on can be seen whether drilling performance improve or not. Apparent Rock Strength (ARS) can be determined according to Mohr-Coulomb criteria [12] [13](discussed in section 3.4: Eq. 3-3 to Eq. 3-5):

$$ARS = \mathrm{UCS} + S_3 \tan^2 \emptyset \qquad \text{Eq. 5-1}$$

Which: UCS is the Unconfined Strength of the rock, S_3 is the least effective stress out of the section 4.8 (Eq. 4-97), $\emptyset$ is the friction angle. Considering the small amount of rock around the wellbore (Figure 5-1), the average ARS for an element surrounded by four nodes $(i,j),(i,j-1),(i-1,j)\ and\ (i-1,j-1)$ is determined by:

$$ARS_{ave,i} = \frac{ARS_{i,j} + ARS_{i,j-1} + ARS_{i-1,j-1} + ARS_{i-1,j}}{4} \qquad \text{Eq. 5-2}$$

Moreover, the area of the element is:

$$Area_i = \frac{\Delta\theta}{2}\left(r_i^2 - r_{i-1}^2\right) \qquad \text{Eq. 5-3}$$

Therefore, Analytical Mechanical Specific Energy (AMSE) can be extrapolated for certain radius of wellbores as:

$$AMSE_i = \frac{\sum\left(ARS_{ave,i} \times Area_i\right)}{\sum Area_i} \qquad \text{Eq. 5-4}$$

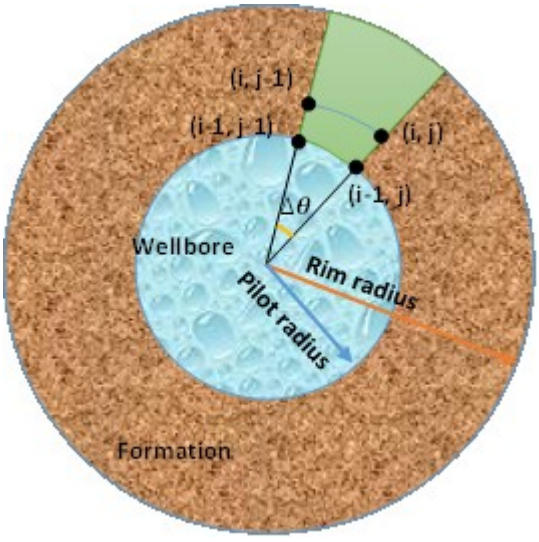

Figure 5-1 Rock strength estimation in the vicinty of wellbore

I utilized Matlab, in order to derive AMSE based on equations mentioned in chapter 4 and above. The calculation was conducted for three different formations (Table 5-1) which their properties were collected from the academic literature ([60], [62]).

Table 5-1 Test Key Parameters (Lab operational condition, [60], [62])

Property	***low-permeable***	***Medium/High P.***	***High permeable***
Vertical stress. σ_v, Psi	**4500**	**4500**	**4500**
Max. horizontal stress, σ_H, Psi	**5500**	**5500**	**5500**
Min. horizontal stress, σ_h, Psi	**5500**	**5500**	**5500**
Pore pressure, P_p, Psi	**17400**	**1740**	**1740**
Wellbore pressure, P_m, Psi	**3000**	**3000**	**3000**
Temperature difference, ΔT, ℃	**-40.00**	**-40.00**	**-40.00**
Biot's coefficient, α	**0.97**	**0.44**	**0.99**
Drained poisson's ratio, v	**0.22**	**0.25**	**0.30**
Undrained poisson's ratio, v_u	**042**	**0.33**	**0.46**
Skempton's coefficient	**0.92**	**0.81**	**0.92**
Thermal diffusivity [m2/s]	**1.6e-6**	**5.1e-6**	**7.15e-7**
Fluid diffusivity [m2/s]	**6e-8**	**6.26e-5**	**7.15e-3**
Coupling coefficient [MPa/C]	**0.17**	**0.41**	**0.31**
UCS	**35.00**	**35.00**	**35.00**
Friction angle	**20.00**	**20**	**20.00**
Wellbore radius [in]	**8.50**	**8.50**	**8.50**
Drainage radius [in]	**-**		**60.00**

Figure 5-2a displays the associated transient pore pressure distribution with a thermal effect and hydraulic diffusion for the very low permeable formation. The pore pressure is kept equal to mud pressure at the borehole wall, because of the permeable boundary condition. However, a significant pore pressure drop develops near the borehole from a very early stage. The drop decomposes over time, and moves away from the wellbore. In the case of borehole cooling, this implies a considerable pore pressure decline near the wellbore when cooling commences, and the reduction pore pressure will vanish with increasing time. On the other hand, if the mud temperature is higher than the formation temperature, it indicates a notable pore pressure peak near the wellbore wall at the beginning of heating; however, the initially increased/decreased pore pressure will adjust with time toward its initial condition.

Figure 5-2b illustrates the comparison of the transient AMSE and rock strength below the pilot bit according to the method was presented by Caicedo et al, 2005 [12], [13]. The bold blue line (at the top of graph) indicates the result for the impermeable rock below the pilot and the bold red line (at the bottom of graph) shows the rock strength for the permeable formation below the pilot bit. These figures reveal that the effect of pore pressure on the AMSE is significant. At an initial stage, when pore pressure is very low in the thermoporoelastic condition, a significant reduction in AMSE near the borehole wall is observed. Over time, this rock weakening will move inside the formation and cover a larger radius.

In addition, the time frame can be interpreted as distance by referring to it as ROP. Hence for a typical ROP (assume 30-m/hr.) a 5% larger reamer should be placed 0.5-meters above the pilot bit. If a 10% bigger reamer is considered, then it must be placed 75-meters above the bit in order to benefit from the rock weakening process generated by the pilot. In other words, if an advantage is to be gained from lower strength rendered from the pilot hole with a reamer size only 10% bigger than the pilot, the rim must set 75 meters above the pilot bit. It is a fact that with increasing distance between bit and reamer other uncertainties come into play, such as drilling into a non-homogenous formation which causes fluctuations of the neutral point, vibrations, drilling tools failure, etc. Such dysfunctions lead to increased NPT.

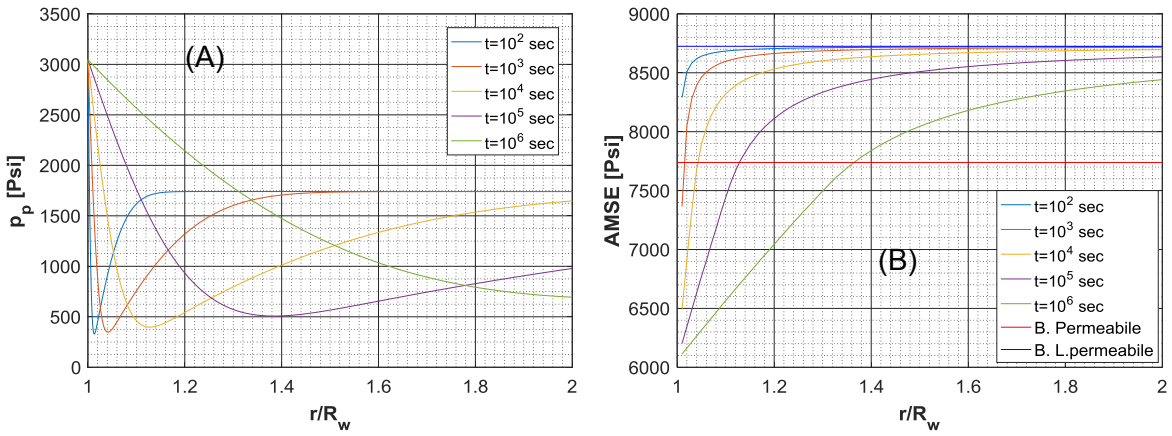

Figure 5-2 Low permeable thermoporoelastic induced transient pore pressure distribution (a) and AMSE profile (b) [84], [85]

Figure 5-3 presents isochrones of the pore pressure and AMSE around the borehole for the medium permeable formation. The finding show that the pore pressure generally increases as time progresses, deviating gently from its original value. For all the time space considered, the induced pore pressure monotonically declines declining as it moves inside the formation, and drops uniformly to the initial pore pressure. It is worth mentioning that all the five pore pressure curves display the identical pressure at the borehole wall as a result of the fixed wellbore pressure boundary conditions. The constant pressure at the wellbore may be maintained with the wellbore drilling fluid (e.g., overbalance drilling and or underbalance drilling).

As a means of providing a comparison between ARS of the wellbore with in situ rock just below the bit, the minimum and maximum values of ARS for permeable and impermeable formations (according to the method as presented by Caicedo et al, 2005 [12],. [13]) are plotted on the same figure (top and bottom bold line). Teasdale (2014) suggested that the stress alteration zone around the wellbore is in line with the results of this graph [6]. The conclusion drawn from this figure is that the weakening zone extension is a function of time. (Time as a result of Laplace transformation comes into effect). Therefore, at an early stage after drilling the pilot hole reamer size should be just a little bigger than pilot bit in order to gain benefit from

the weakening rock. However, if the subsequent hole enlargement process continues after a longer time, then the weakening zone will expand as a consequence of hydraulic and thermal diffusivity. This allows bigger reamer size, since it may actively use this change in rock strength to its advantage.

In the same way as low permeable formation, in order to derive benefits from a weakening zone to a multi-diameter system, it is possible to conclude there is a certain reamer/bit size ratio and distance between them. For example, for expected 30m/hr. ROP, a reamer which is 20% larger than the pilot bit, should be placed 15 meters above the pilot bit.

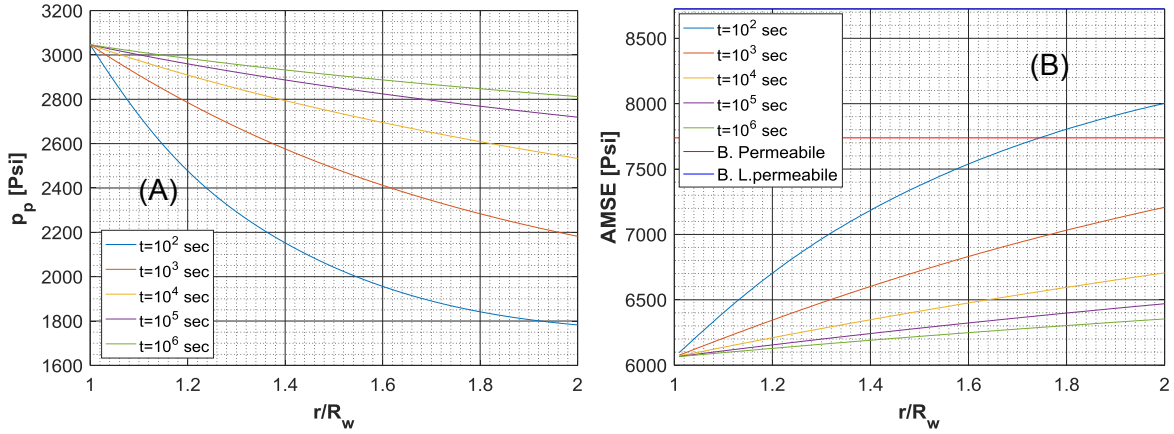

Figure 5-3 Medium/high permeable thermoporoelastic induced transient pore pressure distribution (a) and AMSE profile (b).

The simulation run for high permeable is different from low/medium permeable formations, as one consequence of hydraulic diffusion is the dominant factor; causing the pore pressure reach an equilibrium within a very short space of time. For instance, for a permeable formation with 1-md permeability, the final stage may be attained within 30 minutes [78]. This critical time depends on rock permeability. The Figure 5-4 illustrates the simulation results for the permeable formation. It is possible to see that the AMSE always falls below the rock strength just below the bit in the DOC zone, thereby confirming it to be a good candidate for the pilot and reamers combination application.

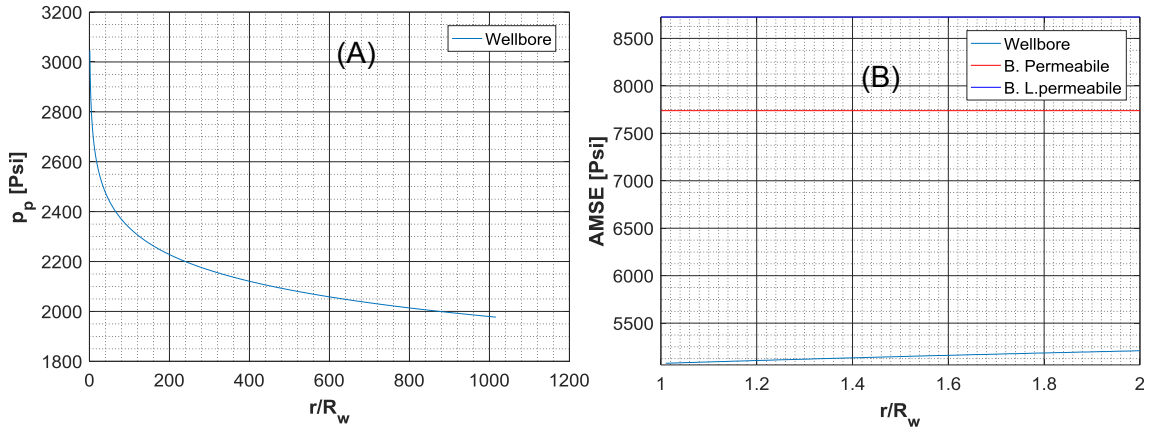

Figure 5-4 Very High permeable formation pore pressure distribution (a) and AMSE distribution (b).

5.3 Lab Facility

Mines de Paris/ARMINES, as an independent research center, is able to develop many full-scale tests to obtain a full laboratory PDC and Roller Drill Bit Characterization, and underlines the potential of each type of Drill Bit. This research center is located in the south of France, near the Pyrenees. The Mines de Paris Drilling Laboratory performs research projects and provides services for customers in the oil and gas drilling fields.

The Drilling Test Facility (DTF) allows evaluating roller cones or fixed cutter bits up to 8 ½" in diameter, and it is also able to simulate the deep hole drilling conditions. The tests consist of drilling rock samples under constant WOB or constant ROP. The rock can be held in a pressure vessel and after the test, the bit and the bottom hole pattern can be examined immediately.

As stated earlier, the portion of rock in direct contact with the drill bit is under a complex state of stress. The four stress conditions are:

(a) The greatest, compressive horizontal stress along the x-direction.

(b) The vertical principal litho-static stress (overburden); directed parallel to the well-bore axis in the z-direction.

(c) The drill-string weight vertically applied uniformly at the bottom of the drill bit;

(d) The well-bore mud or fluid pressure applied perpendicularly to all the borehole free surfaces [86]. This lab can provide these parameters as mentioned in Table 5-2.

Table 5-2 Sample cells

Bit size	<6 ½”	<8 ½”
Inside mud pressure	50 MPa	10 MPa
Over burden pressure	70 MPa	20 MPa
Confining pressure	50 MPa	10 MPa
Pore pressure	50 MPa	10 MPa
Rock sample length	480 mm	450 mm
Drilling length	480 mm	450 mm

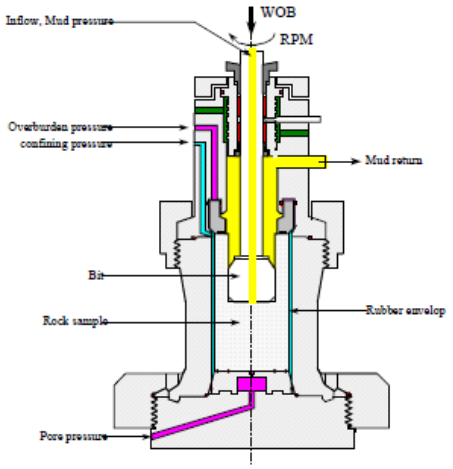

Figure 5-5 Principle of the Drilling Test Facility (DTF)

Figure 5-6 Cross-section of the drilled sample

Figure 5-7 Drilling Test Facility

5.4 Parameters

The proposed data for the calculation and experimental work take into account the capability of Drilling Test Facility at Mines Lab research center and summarized in Table 5-1.

The drilling mode can be controlled automatically by ROP or WOB display. The Maximum allowable WOB is 25 tons and the maximum ROP is 90 m/h. The rotation with continuous variation is possible from 0 to 900 rpm. The mud flow rate ranges between 0 and 600 l/min. In addition, all mud types are equipped with a temperature variation system (>100°C). DTF is able to measure 100 points, of which 30 are recorded. The acquisition frequency varies from 1 to 3000 Hz.

There are six rock samples in this center, 1 Shale, 2 Limestone and 3 Sandstones. The high permeable sandstone was chosen for our laboratory tests.

5.5 Proposed Design of Pilot-Reamer Arrangement

For several decades, there have been several different types and sets of pilot bits and reamers. In order to reduce costs, the decision was taken to combine them by means of a sophisticated crossover sub (XOS), instead of buying new pilot and reamer bits. Since the

DTF's connection is dressed with a 2 3/8" Regular Box thread, the XOS was designed in such a way, allowing the integration to connect with the DTF and the pilot and reamer (Figure 5-8) concurrently. Furthermore, the two extensions (5-cm and 10-cm) were designed to provide more options for the pilot and reamer arrangement (Figure 5-9).

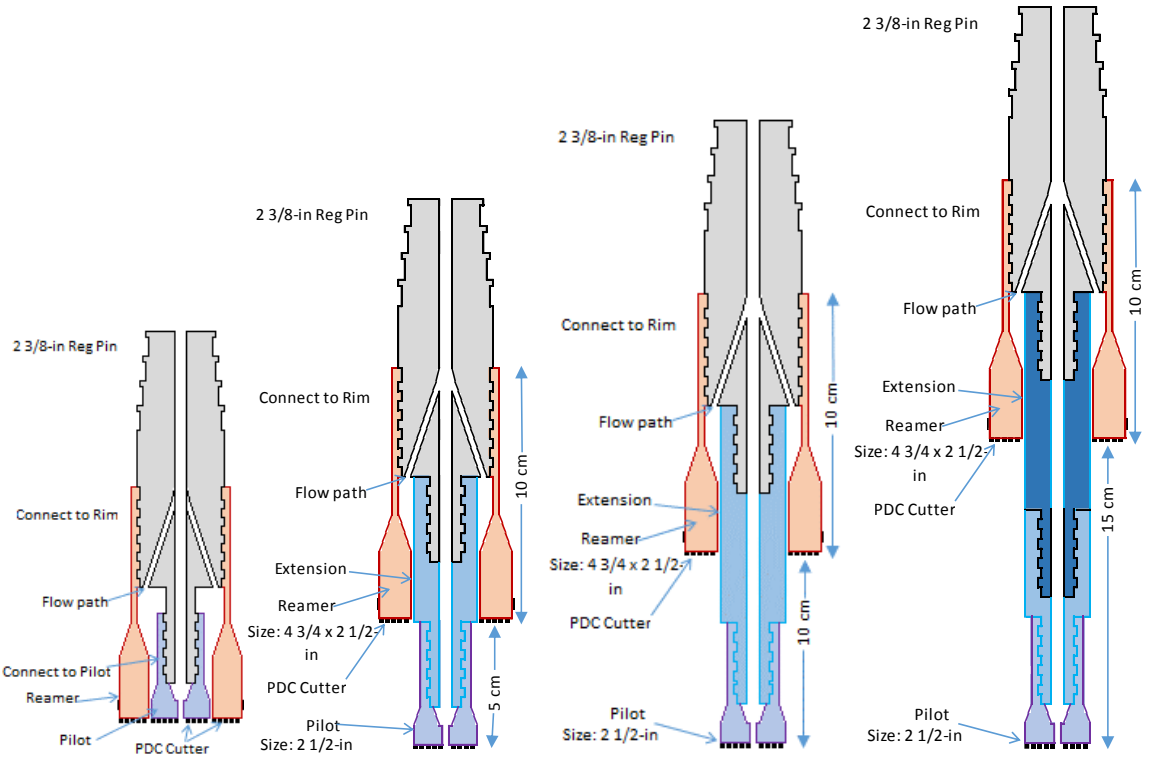

Figure 5-8 The XOS, Pilot bit and Reamer arrangment

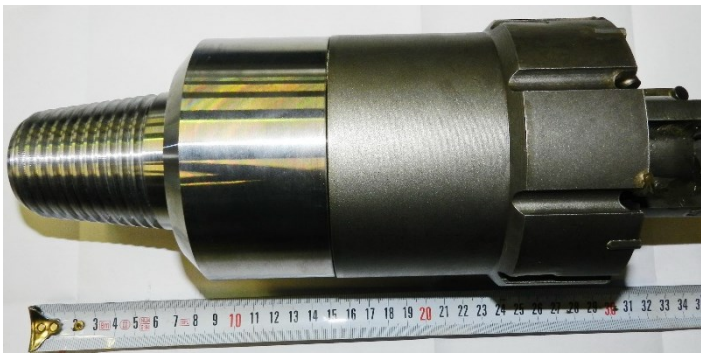

Figure 5-9 XOS, Pilot bit and Reamer

5.6 Test Procedure

According to analytical calculations, different approaches can be suggested in order to confirm the effect of reamer size and distance.

In the first scenario, a standard (4 ¾") bit is used to compare the power required to drill the same volume of rock with 2 ½" bit followed by (2 ½" x 4 ¾") reamer (Figure 5-8) after different time periods. MSE is defined as the required energy for destroying a unit volume of rock. If pilot and reamer can be run separately, then total MSE of pilot-reamer is given by:

$$MSE_{p-r} = \frac{MSE_p \times area_p + MSE_r \times area_r}{area_p + area_r} \qquad \text{Eq. 5-5}$$

As extensively discussed in chapter 2 of this thesis, a hole that it is crucial to mitigate drillstring vibrations is to be established in the pilot hole. In other words, if the pilot bit is attached onto the reamer, then it will promptly heighten drillstring dynamics. Therefore, this scenario will more likely lead to vibrations occurring in the drillstring.

In the second scenario, a reamer (2 ½" x 4 ¾") drills through an intake rock sample, and its required power is compared with the same reamer on the rock sample which has been already drilled with 2 ½" pilot bit (Figure 5-11). The existing facility in this research center is not able to drill more than 5-cm for this scenario.

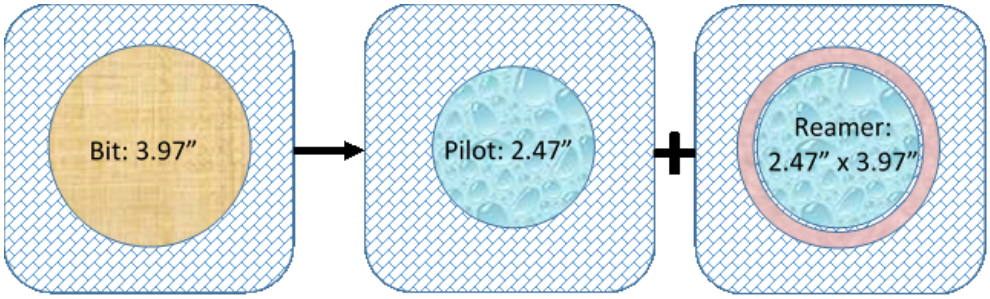

Figure 5-10 Problem definition (First scenario)

In the third scenario, drilling is performed with the pilot bit, which is placed 15-cm ahead of the rim for 15-cm deep in formation; then drilling is stopped for a certain period. While drilling is stopped, only WOB is reduce to zero, and other parameters must be kept identical with drilling conditions. This provides the same mud pressure and a diffusivity similar to drilling (Figure 5-9).

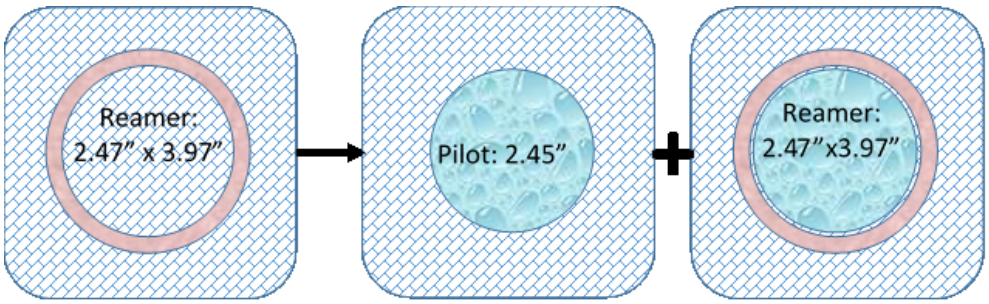

Figure 5-11 Problem definition (Second scenario)

Time zone for drilling in high permeable formation: 1, 3, 5, and 20 minutes

Temperature Effect: There are two options: (1) Circulate high temperature mud prior to test to heat up rock sample, (2) Heat up rock sample in oven.

The third scenario was chosen as there was less influence from vibrations.

6 Results and Discussions

In principle, while on the bottom, the driller can control only three parameters: weight on bit (WOB), rotary speed (RPM) and mud flow rate. Without a mud motor in the drill string, and especially in my case a laboratory drillability test - the flow rate has a limited effect on ROP. Therefore, the optimization is two dimensional in WOB and revolutions/min (RPM). Table 6-1 sums up the test configurations, bit types and reamers that were used, and operating parameters.

Table 6-1 Summary of the test condition (Rock sample: Sandstone Vosges)

TEST	DATE	BIT	ROP (M/HR)		WOB (TON)	RPM	CON P [MPA]	OB PRE [MPA]	PP [MPA]	MUD P [MPA]	MUD TEMP	ROCK TEMP
1	20160525_01	FH	2	16	2	90	20	20	12	20	20	40
2	20160802_01	FH	2	14	1	90	20	20	12	20	20	40
3	20160803_01	FH	2	14	1	90	20	20	0	20	20	80
4	20160803_01R	FH	2	14	1	90	20	20	0	20	20	80
5	20160803_01RR	FH	2	14	1	90	20	20	0	20	20	80
6	20160803_02	FH	2	14	1	90	20	20	0	20	20	20
7	20160804_01	FH	2	14	1	90	20	20	12	20	20	20
8	20160804_02	P+R	5	5	1	90	20	20	0	20	20	80
9	20160804_02R	P+R	5	5	1	90	20	20	0	20	20	80
10	20160804_03	P+R	5	5	1	90	20	20	12	20	20	20
11	20160804_03R	P+R	5	5	1	90	20	20	12	20	20	20

6.1 1st test

Objective:

Define a set of reference parameters and get familiar with DTF

Procedure:

The most common method to optimize drilling performance is the 'drill rate' test, which consists of simply experimenting with various WOB and RPM settings and observing the results. The parameters were then set, which resulted in the highest ROP. A variety of processes was possible for optimizing ROP at the existing facility in Paris De Mines. Mud was prepared in two tanks. One was heated up to 60 °C and another one was kept at ambient temperature. High temperature mud was used to increase the rock temperature and pressurized it prior to starting drilling. Cold mud circulated while drilling through the rock.

For the 1st test, a simple configuration of the pilot bit and the reamer was chosen, like a conventional bit. The RPM was set at 90-RPM for the first 280-sec and then increased in two stages to 150-RPM (Figure 6-1). Meanwhile ROP was raised to different levels (Figure 6-2); consequently, WOB was adjusted automatically by machine (Figure 6-3).

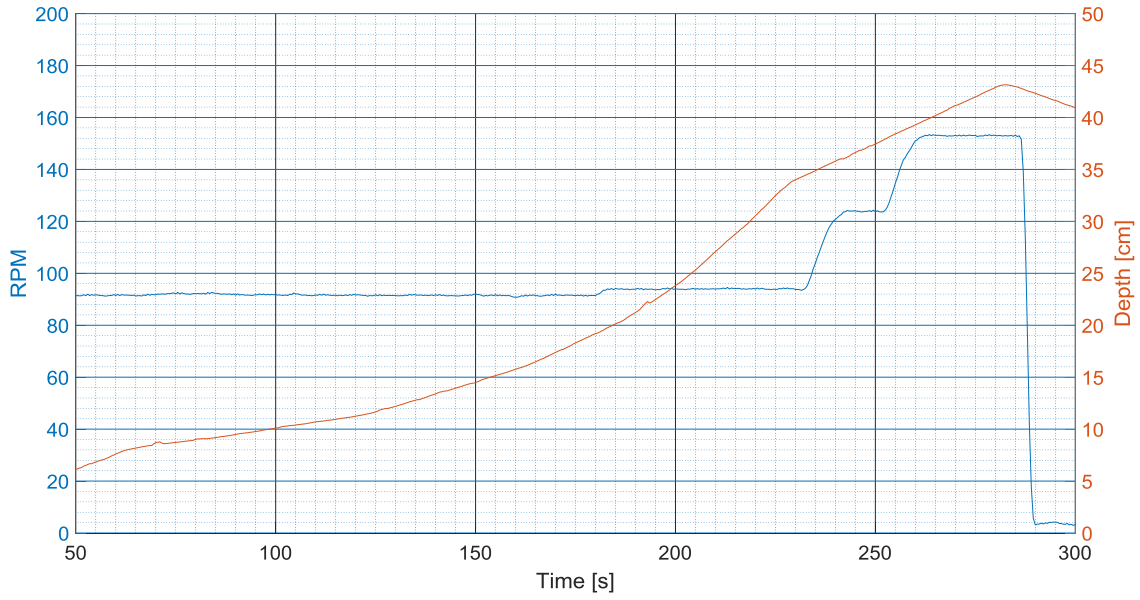

Figure 6-1 Drilling parameters: RPM, Depth

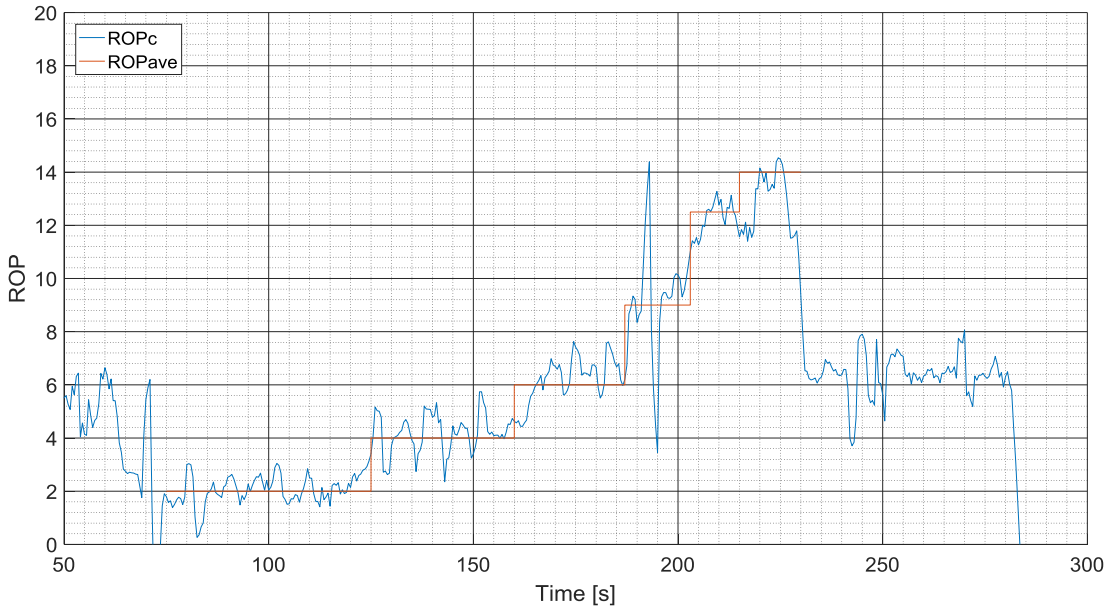

Figure 6-2 Drilling parameters: ROP (ROPc: calculated) was increased to different levels

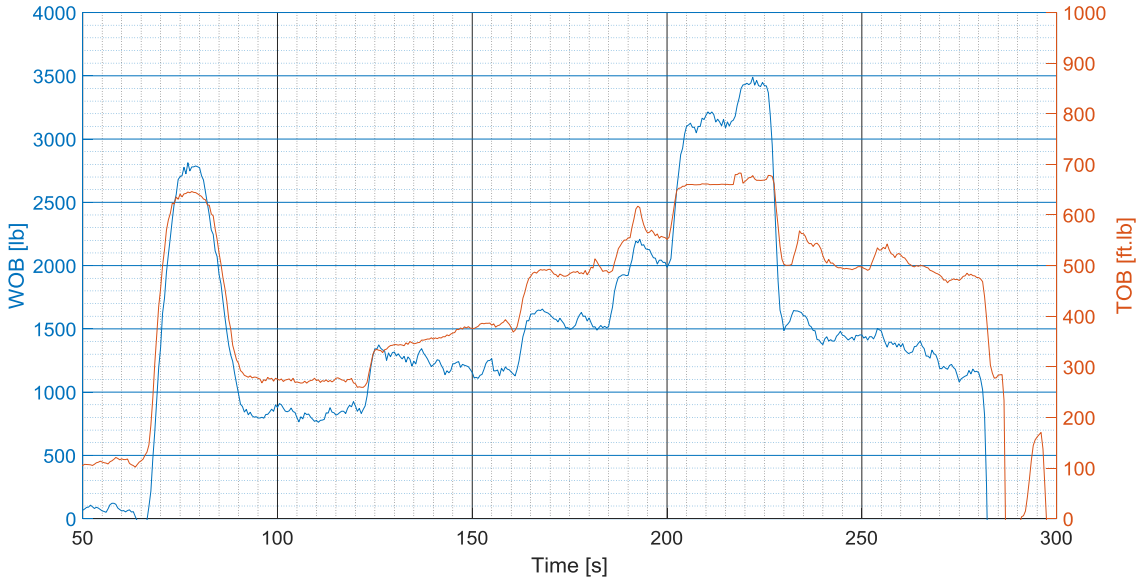

Figure 6-3 Drilling parameters: WOB, TOB

Results and Discussions of 1st test

A Matlab code was programmed to provide cross-linked displays of different drilling parameters. The three variables combined (RPM, WOB & TOB) determine the Depth of Cut (DOC), Mechanical Specific Energy (MSE) and DOC.

Mechanical Specific Energy (MSE)

MSE surveillance proved to be valuable as an educational and optimization tool. Drilling is at its most efficient in energetic terms when the MSE is at a minimum – the lower the specific energy, the more efficient the drilling process. When drilling with optimal efficiency under atmospheric conditions, the numerical value of the MSE will usually be close to the unconfined compressive strength (UCS) of the rock. Typically, the MSE tends to increase as the hydrostatic pressure rises. The pressure variables were set as follows:

Confining pressure:	3100 psi
Overburden pressure:	6000 psi
Pore pressure:	1900 psi

Highly permeable sandstone from the Vosges with the following properties was used:

UCS:	5802 psi
CCS at 5800 psi:	23000 psi
CCS at 8700 psi:	27122 psi

Ten drilling zones are identifiable in the graphs, depending on the drilling parameters. One and ten are not taken into consideration due to unstable conditions (Figure 6-4). Zone seven shows the minimum MSE (23000 psi), which is close to CCS, at 5800 psi.

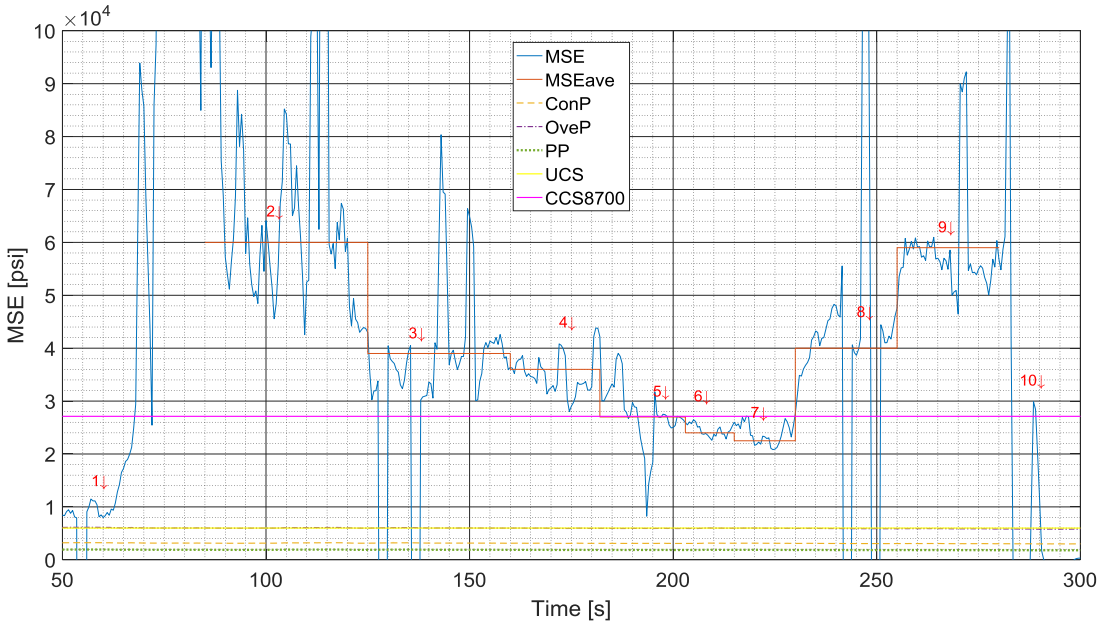

Figure 6-4 Mechanical Specific Energy (MSE) and Pressures

Another way to show the relationship between ROP and MSE is to plot the two variables in a single graph (Figure 6-5). The product of ROP x MSE represents the total available power (P) divided by the bit area (A) in horsepower per square inch (HSI). Figure 6-5 shows the ROP vs the MSE with lines of constant HSI superimposed. It shows that the total available

horsepower is relatively constant between 22HSI and 140HSI, while the ROP and MSE values vary over a wide range. Zone two received less power and is evidently not at all efficient. Zones six, seven and eight show the same power. However, zone seven displays higher ROP and lower MSE.

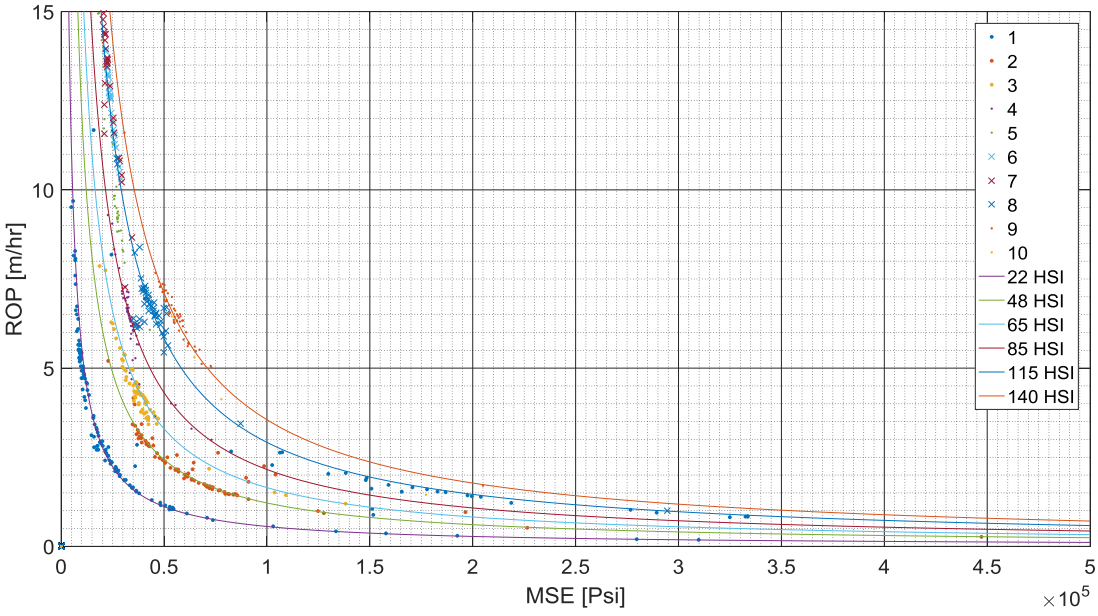

Figure 6-5 ROP vs MSE: Zones 6, 7 and 8 show higher performance, any zone placed on a particular power curve which means power loss is very low

Depth of Cut (DOC) variation

At shallow DOC, MSE is high and Eff_M is low because it has to reach a minimum threshold to start generating cutting debris and chips (Figure 6-6).

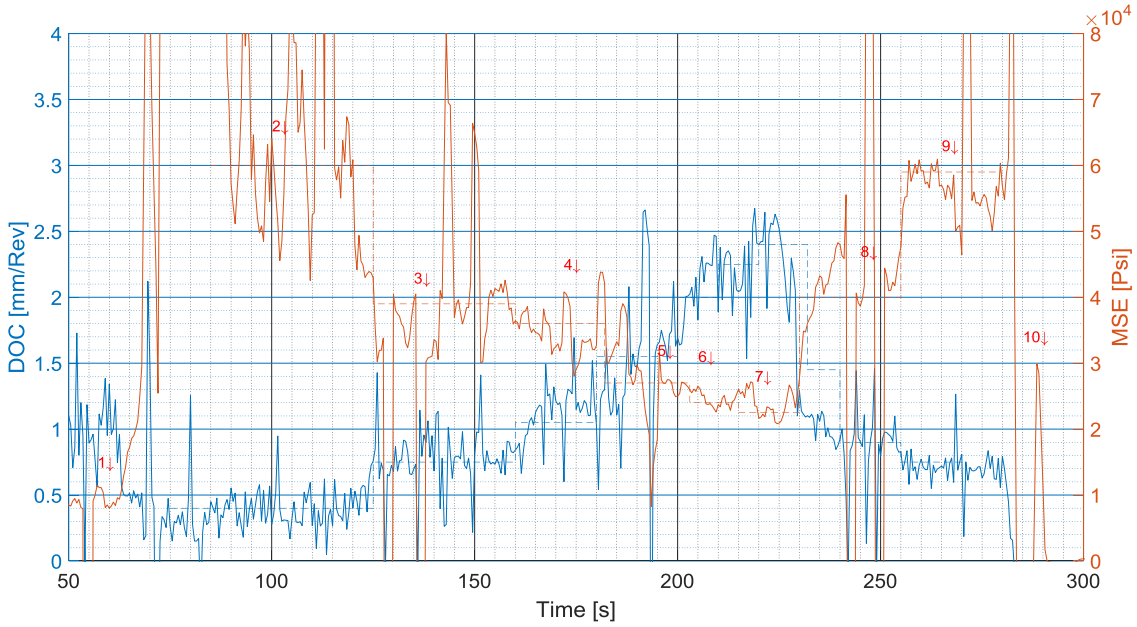

Figure 6-6 Depth of Cut vs MSE: there is a riverse relation between DOC and MSE

Torque vs WOB

Figure 6-7 shows the relationship between Torque and WOB. As depth of cut increases, the rock beneath the contact area will fail, and the contact area will be larger. This continues until a critical depth of cut is reached. Beyond the critical depth of cut, any WOB increase transfers into the bit's matrix body. Therefore, the bit body supports some of the WOB. The bit incrementally behaves as a sharp bit until it reaches the founder point. When the bit body is exposed to rock, a clear wear ring on the pilot is an indication of this condition (Figure 6-8). Hence, the technical limit of WOB for this bit's configuration is 2200-lb.

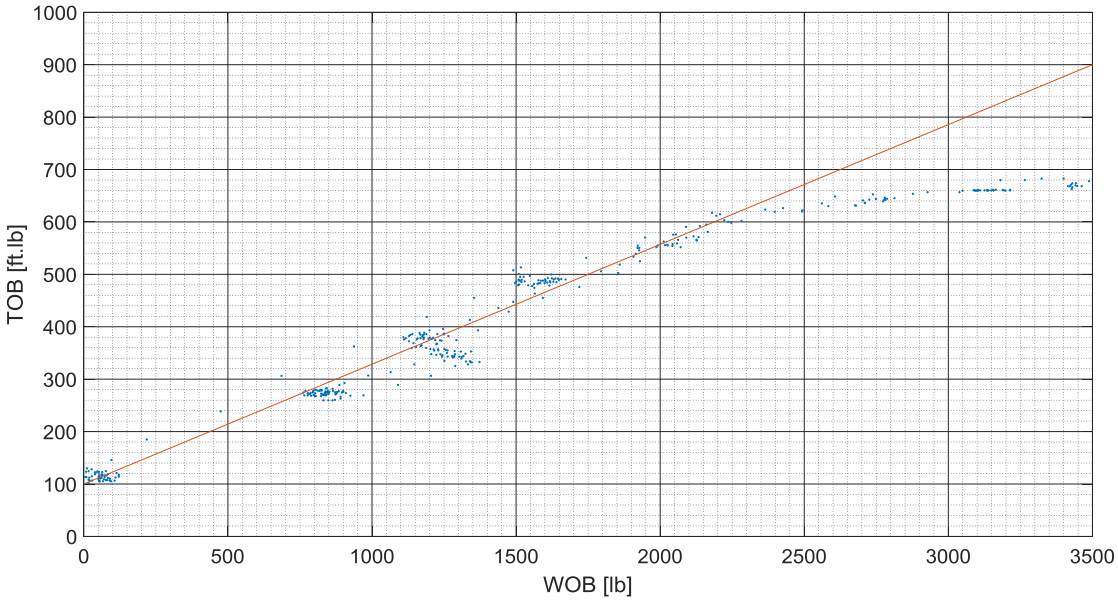

Figure 6-7 Torque vs WOB: Beyond the critical depth of cut, any WOB increase transfers into the bit's matrix body.

Figure 6-8 Wear ring on body bit indication of high WOB

Conclusion and recommendations for next test

MSE surveillance and the power graph demonstrated clearly that the existing facility is efficient. It also highlighted that only a small degree of vibrations affected the drill string, and

precise data measurement. Based on the results from the first drilling test, drilling parameters are recommended as a technical limit for future work:

WOB	= 2200 lb
	= 1 ton
RPM	= 90
Max ROP	= 12 m/hr

When drilling with the DTF, almost no vibrations were observed. This can be proved by looking at the bottom hole patterns and wellbore that form. Figure 6-9 demonstrates a picture taken from the inside of the rock sample that correspond to the test 1. A concentric, circular and smooth pattern was observed, which substantiates the stable performance of the bit drilling approach.

Figure 6-9 Smooth bottom hole, indicates very low vibration frequency/rate

Another possibility to evaluate the downhole bit dynamics is look at the power graph analysis. Figure 6-5 shows well sorted data which reflects no power has been lost due to vibrations.

One type of rock sample will be used with two configurations of the pilot and reamer. A small part of each test will be considered as a reference for confirmation.

6.2 2nd test

Objective:

Define a set of reference parameters and become familiar with DTF

Procedure:

Following the first test's result, Figure 6-10 shows the plan for the second test. ROP was to increase step-wise from 2-m/hr to 14m/hr; WOB adjusted itself to reach target ROP; RPM was constant. High-temperature and high-pressure mud was circulated above the rock sample in advance to heat up and provide greater pore pressure.

2nd Test
1st Run
R+P 0cm

Depth	WOB Max	RPM	ROP ave
0	1	90	2
4	1	90	2
4	1	90	4
7	1	90	4
7	1	90	6
12	1	90	6
12	1	90	8
18	1	90	8
18	1	90	10
25	1	90	10
25	1	90	12
33	1	90	12
33	1	90	14
33	1	90	14
33	1	90	14
40	1	90	14

Rock Sample Vosges (High permeable)
RPM Constant **ROP** Control **Rock Temp** 60 C **Pore Pressure** 12 Mpa **Confine P** 20 Mpa
WOB Variable **Mud Temp** 20 C **Overburden** 25 Mpa **Mud Pressure** 20 Mpa

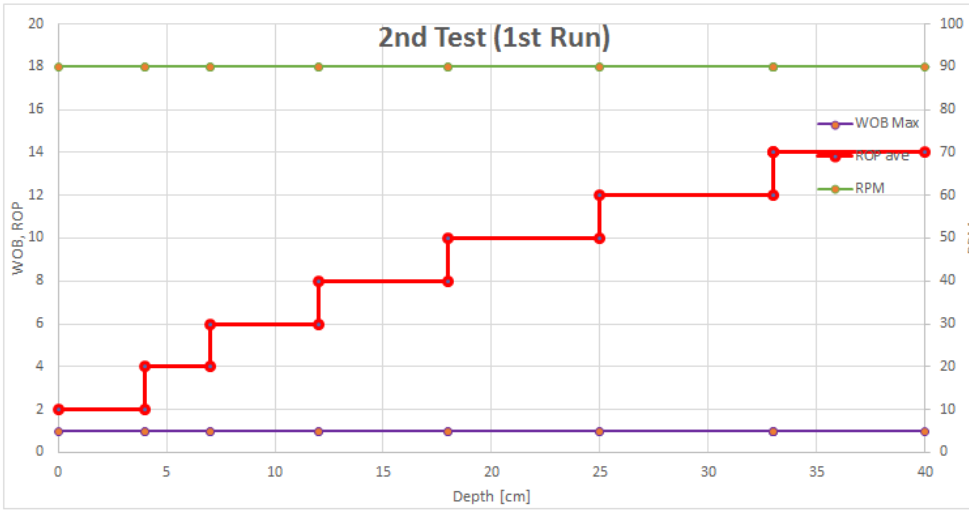

Figure 6-10 2nd test plan: Maintain RPM, increase ROP, WOB will be adjusted by machine to reach target ROP

New sets of the pilot and the reamer were selected due to wear ring signs on the pilot body (Figure 6-11). This set has a smaller cutter size than the first set.

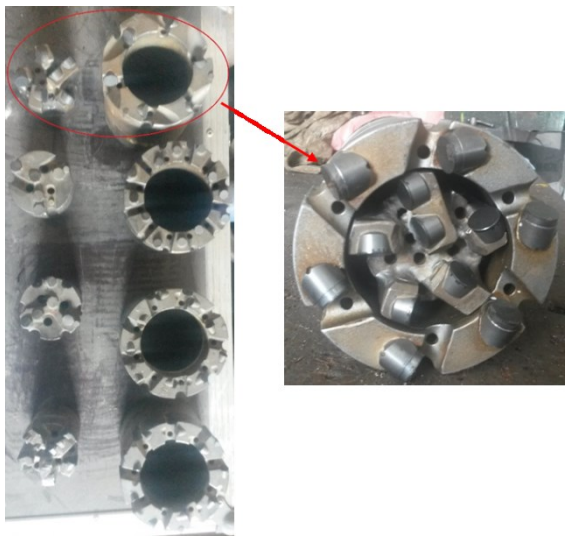

Figure 6-11 2nd pilot and reamer: larger cutter size which leads to lower MSE

Results and Discussions of the second test

✓ As a result of the larger cutter size, less power was required to destroy the rock (Figure 6-12).

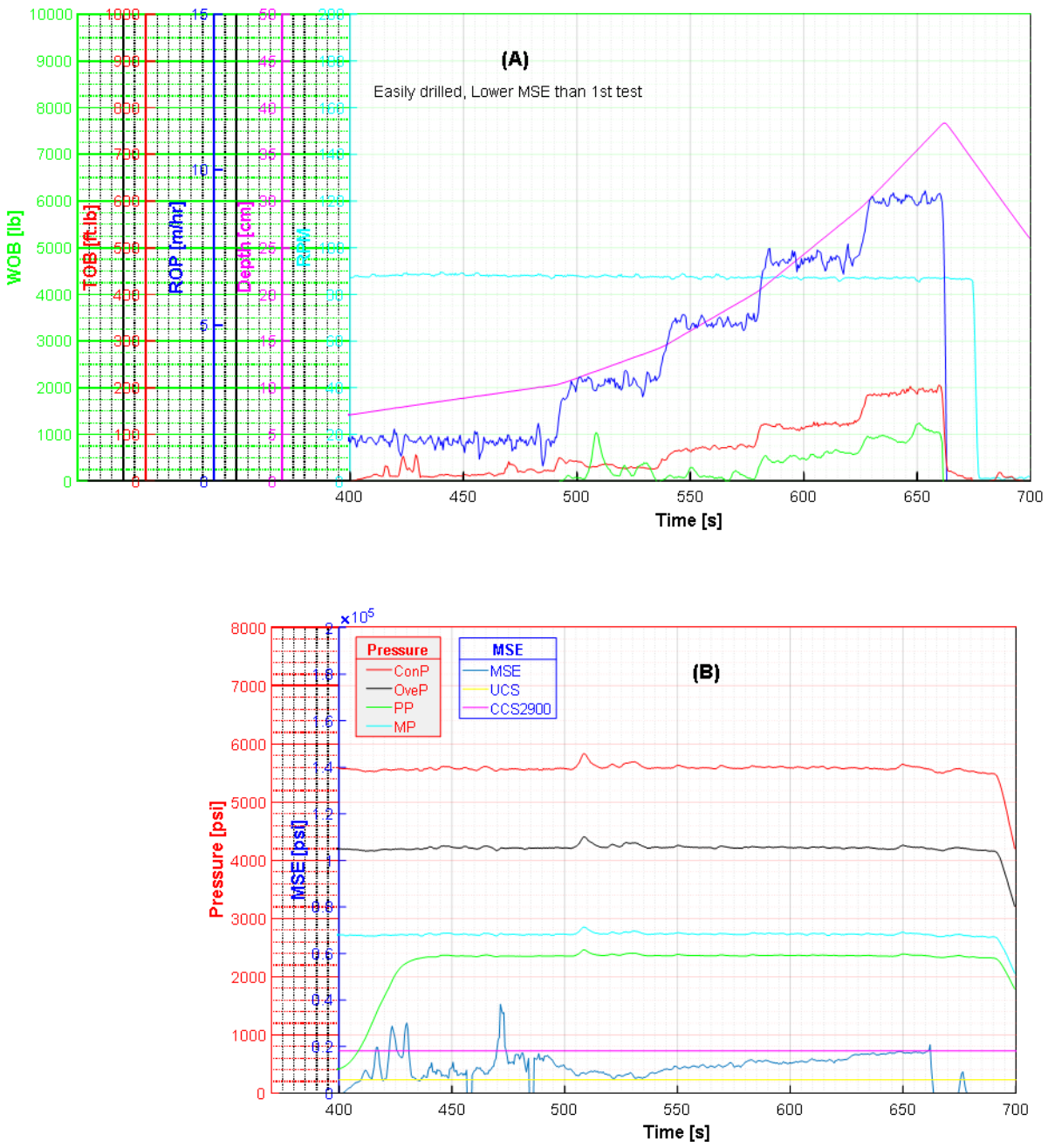

Figure 6-12 Test 2: Full hole, High Pore pressure, High Temperature (A): ROP, Depth, WOB, TOB vs Time, (B) MSE, Confine, Overburden, Pore and Mud pressure vs Time

6.3 Third, fourth and fifth tests

Objective:

The objective was to define a set of reference parameters, become familiar with DTF and evaluate the effects of pore pressure and temperature on the ability to drill rock.

Procedure:

Figure 6-10 shows the plan for the third test. ROP was to increase step wise from 2-m/hr to 14m/hr, WOB adjusted itself to reach target ROP. RPM was constant. Rock sample was heated up to 80°C by keeping it in the oven over night. High temperature, high pressure mud prior to testing was ignored, therefore the rock sample was not pressurized.

This test was repeated three times. The first run was drilled to about 45-cm, but the other two runs were impossible to drill deeper than 35-cm. The rock sample and the drill string are likely to rotate, there by rendering any further drilling impossible.

Result

- ✓ MSE is higher than during the second test, because of greater effective confinement stress than in the second test.
- ✓ Zone one has almost the same ROP in all three runs. The first run shows higher MSE than others, due to the rock sample being kept in the oven over night; yet others were put in the oven for only two hours (Figure 6-13 to Figure 6-15). The temperature difference between the mud and the rock sample for the first run is much larger than in the others.
- ✓ Zone two shows similar behaviour in Figure 6-13 to Figure 6-15

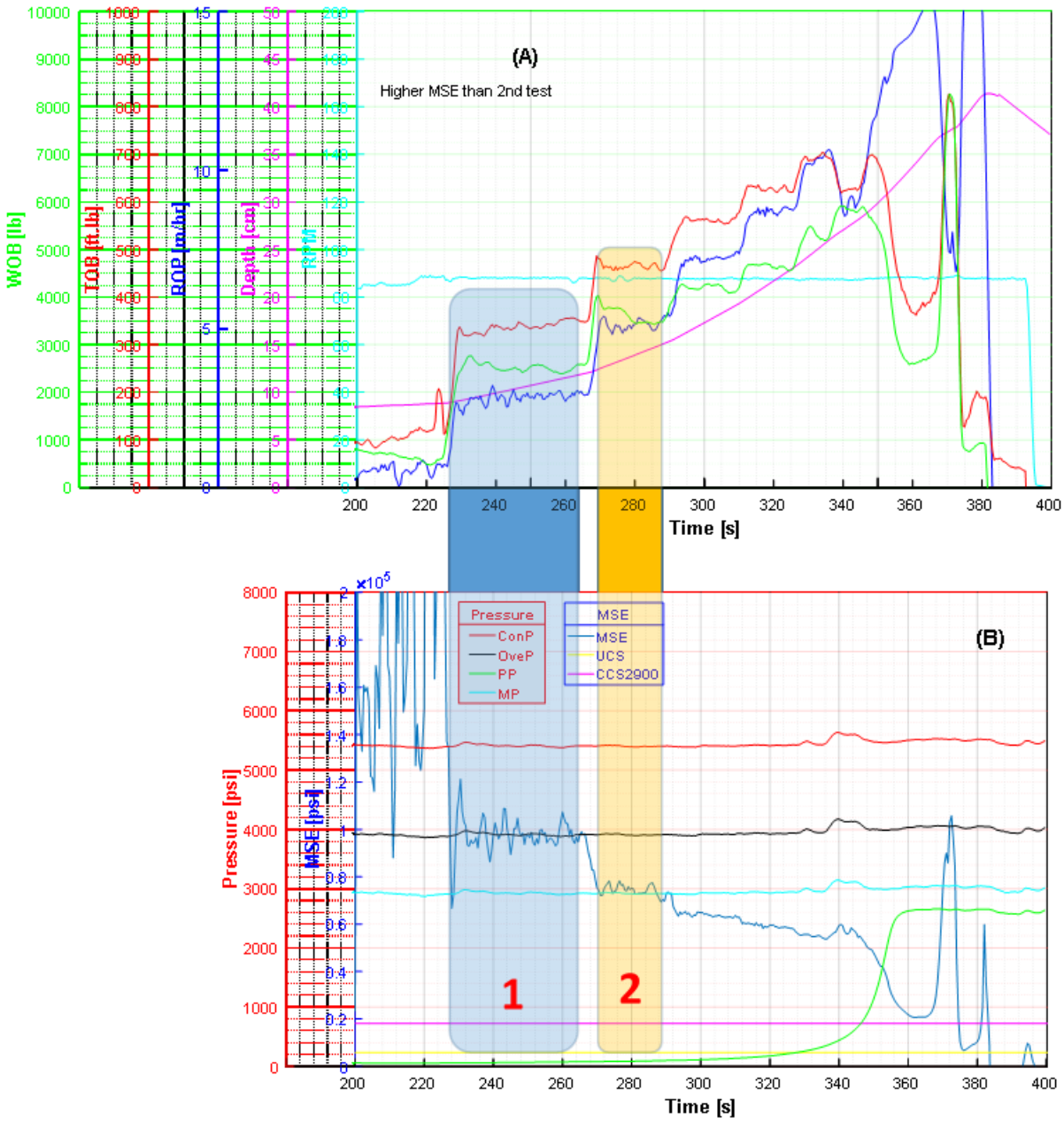

Figure 6-13 Test 3: Full Hole bit, High Pore pressure, High Temperature (A): ROP, Depth, WOB, TOB vs Time, (B) MSE, Confine, Overburden, Pore and Mud pressure vs Time

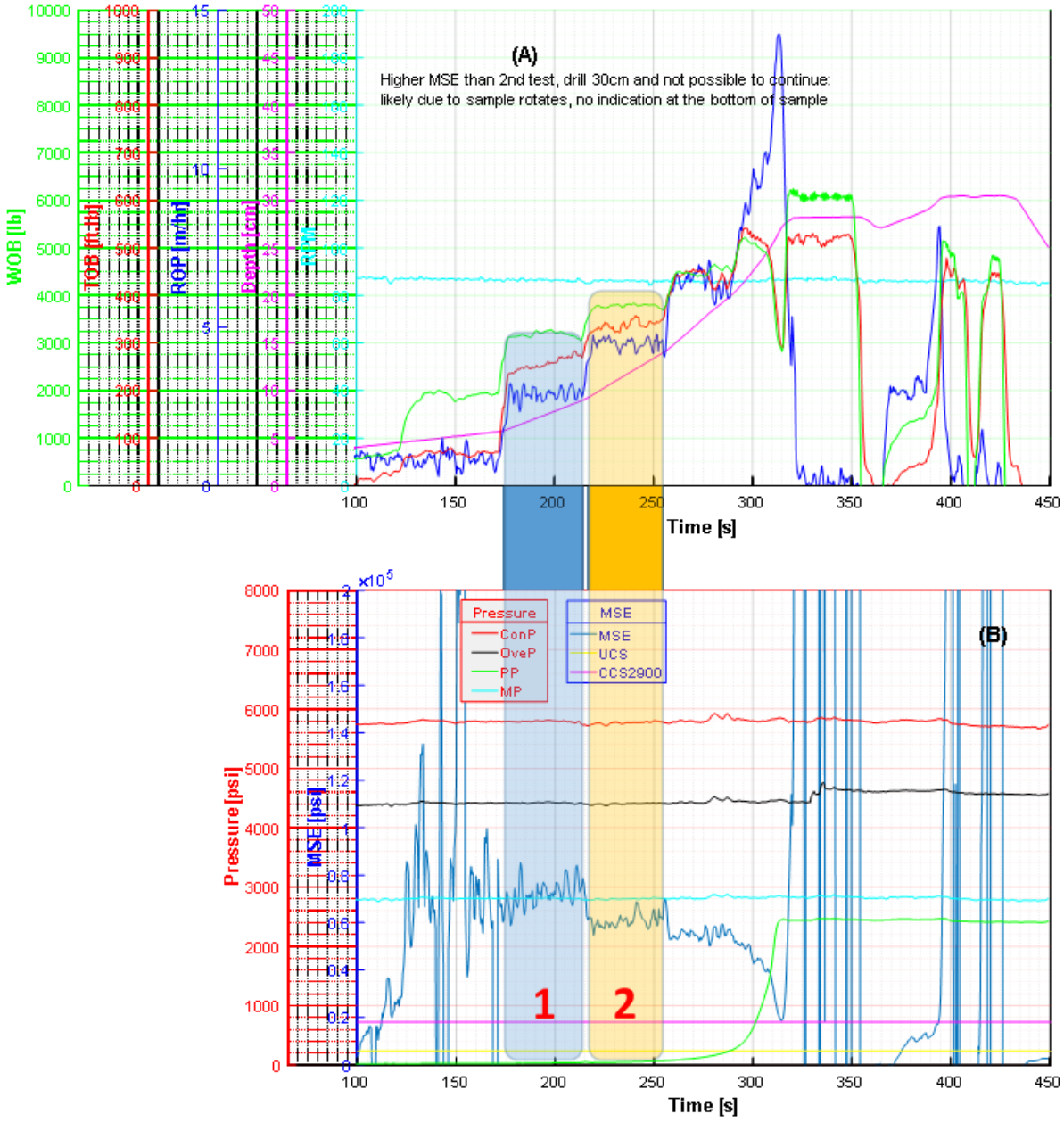

Figure 6-14 Test 4: Full Hole, High Pore pressure, High Temperature (A): ROP, Depth, WOB, TOB vs Time, (B) MSE, Confine, Overburden, Pore and Mud pressure vs Time

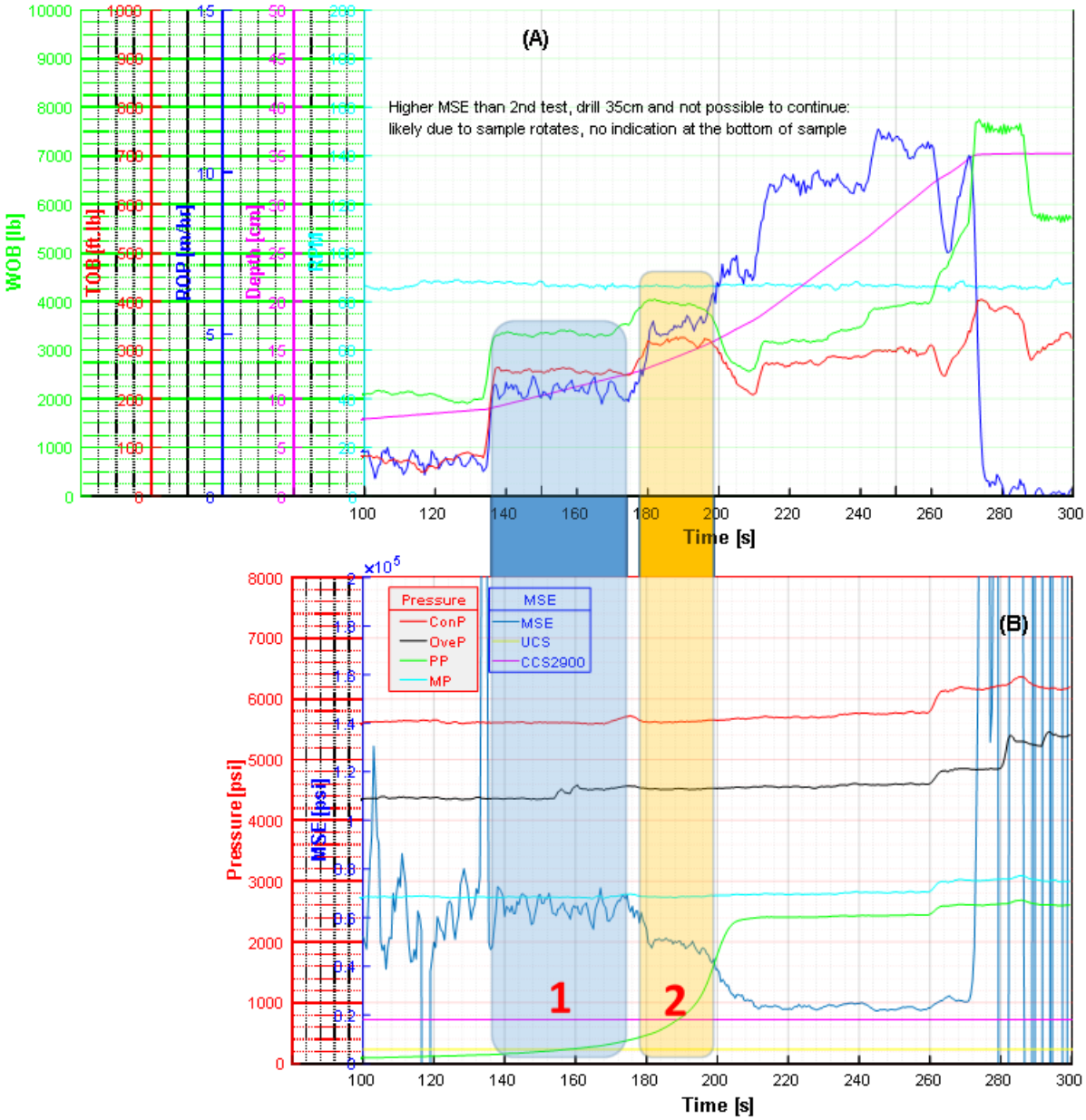

Figure 6-15 Test 5: Full Hole, High Pore pressure, High Temperature (A): ROP, Depth, WOB, TOB vs Time, (B) MSE, Confine, Overburden, Pore and Mud pressure vs Time

6.4 6th and 7th test

Objective:

Evaluate the pilot and the reamer configuration's performance

Procedure:

A rock sample was heated up to 80°C by keeping it in the oven over night. The pilot was projected 10-cm ahead of the reamer (Figure 6-16). Commence drilling with 4-m/hr for 15 -cm. Then stop drilling for 1-minute by removing WOB and maintain RPM and circulation mud. In the next step, continue drilling with same ROP for 10-cm, stop drilling for 3-minutes, proceed by continuing drilling to final depth. Figure 6-18 (a & b) show drilling parameters at different steps. Test 7 repeated this procedure with different a stoppage time in order effect of formation exposer time to drilling fluid and reamer to pilot distance (Figure 6-19).

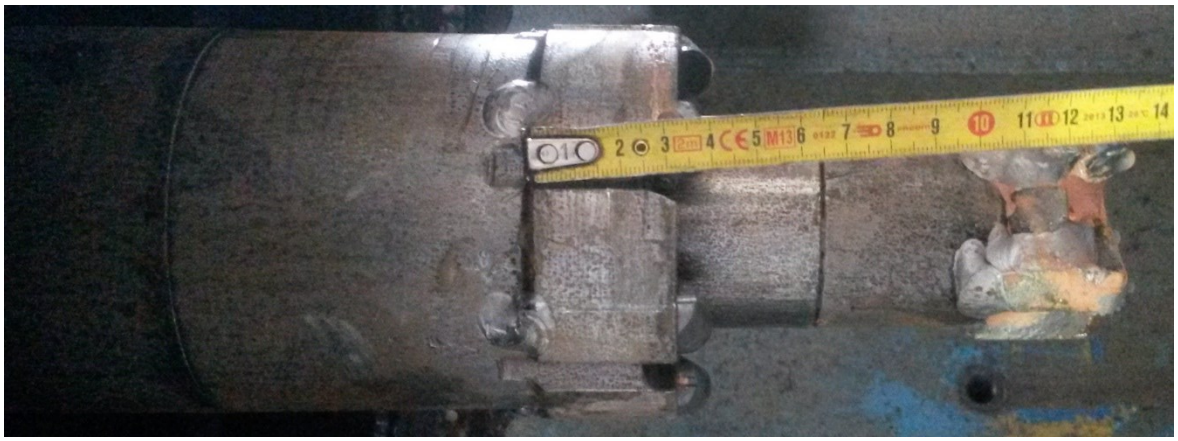

Figure 6-16 Pilot and Reamer configuration: The pilot set 10-cm ahead of the reamer

Result:

Five zones can been seen in Figure 6-18. The first zone shows the drilling parameters that have been set by the pilot alone; the MSE is approximately $0.95 \times 10^5 - Psi$. In the next zone, the reamer begins working and both together drill the rock sample. The resulted MSE decreases to$0.85 \times 10^5 - Psi$. This means that the required power to destroy one unit of rock reduces, mainly due to stress alteration caused by the pilot hole drilled by the pilot bit. Drilling was then stopped (WOB removed), for one minute while circulation and rotary speed were still on in the next zone. The required power drops even more ($0.80 \times 10^5 - Psi$). This reduction in the MSE is due to stress alteration, mud and heat diffusivity. In order to evaluate the effects of exposure time of formation to mud, as well as the distance between the pilot and the reamer, in the next zone, drilling was stopped for longer: 3 minutes. The required power to destroy one unit of the rock decreases to $0.20 \times 10^5 - Psi$.

Figure 6-19 shows a longer stopping time. The first and the second zone in Figure 6-19 show the same trend as the corresponding zones in Figure 6-18. Drilling with the pilot and the reamer combination continued (the fourth zone) after 5 minutes stopping while circulation and RPM were still on (the third zone). The MSE reduces to $0.15 \times 10^5 - Psi$. Drilling stopped for 20 minutes (zone 5) and then continued (zone 6). There is no clear result from this stage for any conclusions to be drawn. Indeed, because of rotation off-bottom for long periods, huge vibrations lead to the rock sample breaking. As a result, the MSE increases. The observation of the sample after the test confirms this condition (Figure 6-17). An extra-large hole size can be seen due to rotation at the same depth during stopping. Even worse, the rock sample broke due to a high level of vibrations during the second stopping phase. The result of these two tests confirm AMSE reduction described in Figure 5-2 to Figure 5-4.

Stopping time translates as the distance between the pilot and the reamer. For example, one minute stopping with 4-m/hr average ROP renders 6.5-cm plus 10-cm distance already exist; therefore a total of 16.5-cm. Equivalently, 3 minutes stopping at the same ROP renders 30-cm, 5-minutes renders 43.3-cm, and 20 minutes renders 143-cm. It must be emphasized that drill string dynamic challenges will increase with a growing distance between the pilot and the reamer.

Figure 6-17 The sample was enlarged and broken due to long period of time off-bottom rotation at the same depth

Figure 6-18 test 6: Pilot - Reamer 10-cm distance, No Pore pressure, High Temperature: MSE reduces as the combination of the pilot-reamer drill and over time. Time can be translated to distance between the pilot and the reamer. It was shown before in section 5.2

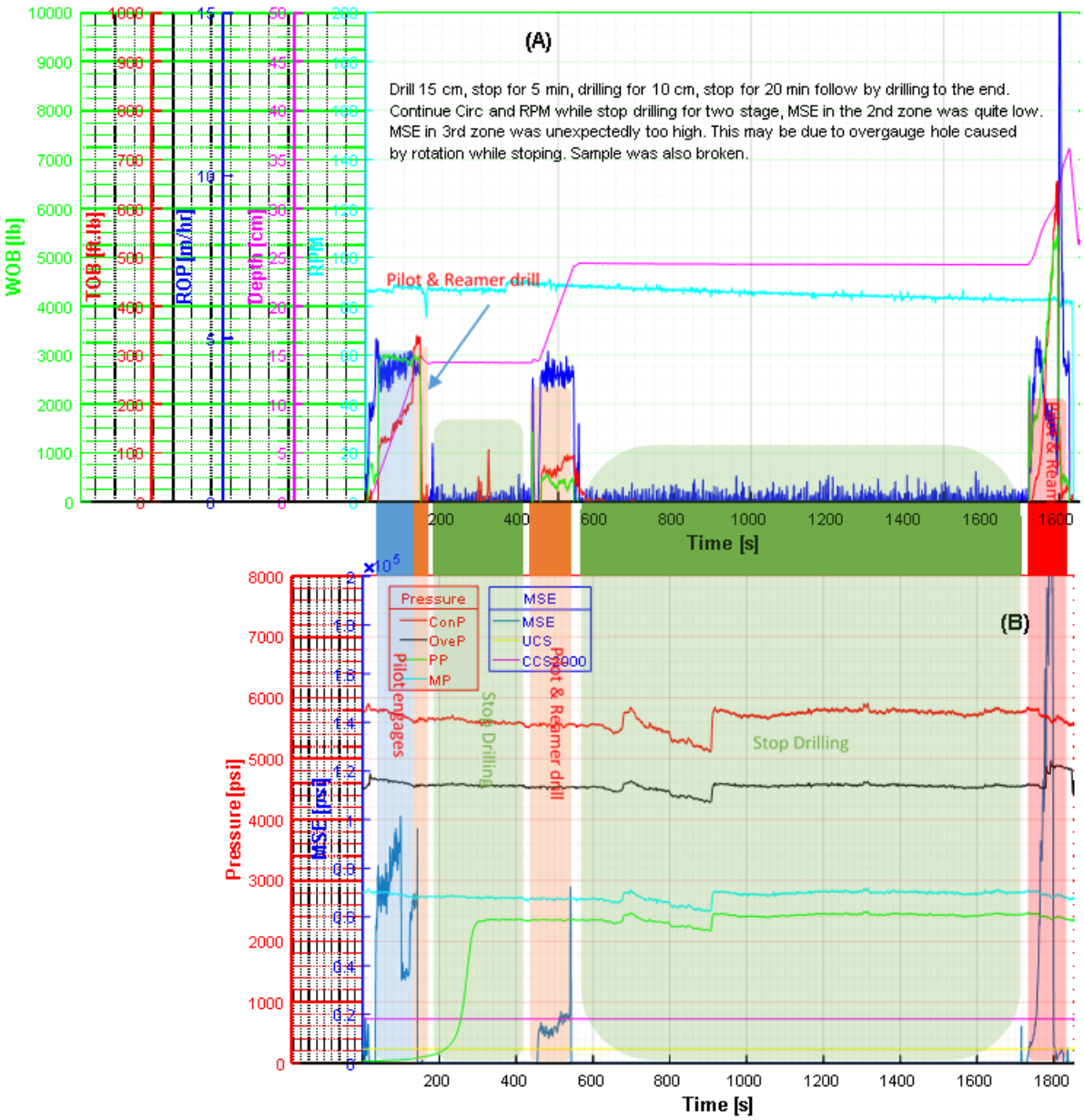

Figure 6-19 test 7: Pilot - Reamer 10-cm distance, No Pore pressure, High Temperature: Reduction of MSE confirms the Hyptothesis in section 5.2

6.5 8th and 9th test

Objective:

Evaluate the pilot and the reamer configuration's performance

Procedure:

The rock sample was pressurized by circulating high-pressure mud at ambient temperature prior to the drilling test. Drilling proceeded at 4-m/hr for 15 -cm with the pilot and the reamer configuration. Then I stopped drilling for 1-minute by removing WOB and keep continue RPM and circulation mud. In the next step, I continued drilling with same ROP for 10-cm, stopped drilling for 3-minutes, followed by continuous drilling to the final depth. Figure 6-20 show drilling parameters at different steps. Test 9 repeated this procedure with different stoppage time in order to check the effect of formation exposer time to drilling fluid and reamer to pilot distance (Figure 6-21).

Result:

Figure 6-20 indicates that the required power to destroy rock in the first and second zone was significantly lower than in tests 6 and 7, because of pore pressure effect on confine pressure and CCS. In the third drilling zone, MSE increased sharply, the possible reason is a broken rock sample (Figure 6-24) caused by extra enlargement and bit eccentricity. The MSE declined in the final drilling phase to lower than a third, as a consequence of a rise in pore pressure and stress alteration. Unfortunately, one of the cutters on the pilot was lost during test 9, (Figure 6-23). Therefore, the higher value of the MSE is evident in the second and third drilling phase in Figure 6-21.

Another problem observed during these tests was bit balling (Figure 6-22). The main factors identified were linked to the hydraulic design (improper placement of the mud flow channels) of the test running procedure (trying to improve the ROP performance, with the mud flow rate not being able to clean the increased number of cuttings being formed), and the bit design itself.

The lower MSE of the combination of the pilot and the reamer than the MSE of the pilot is proven the higher performance of the pilot + reamer combination and confirms the result which is shown in Figure 5-2 to Figure 5-4.

A realistic outcome is to recommend conducting additional research and development for optimizing the pilot and reamer designs. Furthermore, a significant finding is identifying those system constraints, which are based on optimized tool performance in a particular geological environment, and practical ranges of operating parameters. It is clear that with additional tests,

the research team would gain more experience. Consequently, bit design, testing procedures and analytical work will improve results.

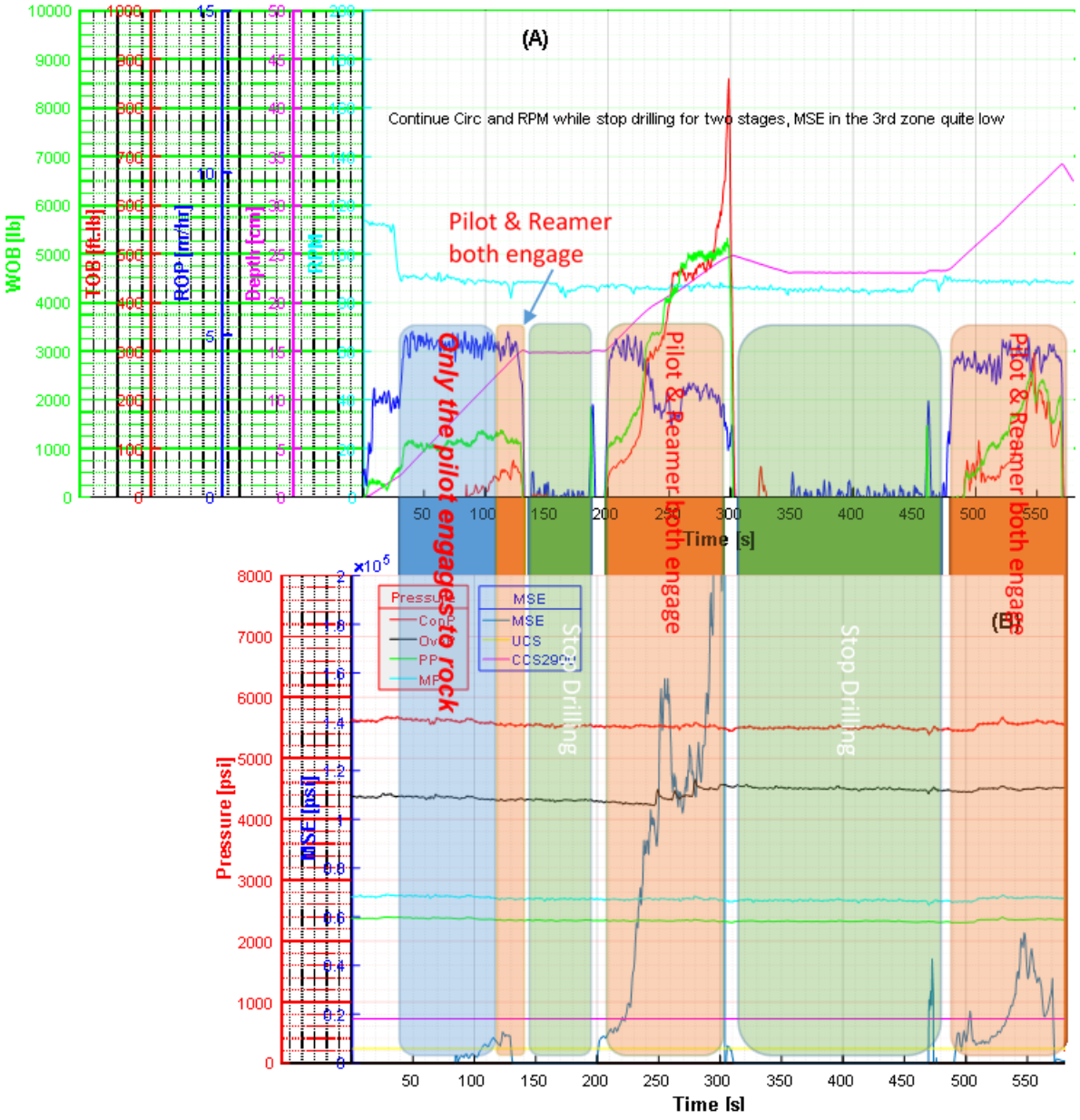

Figure 6-20 Test 8: Pilot - Reamer 10-cm distance, High Pore pressure, Ambient Temperature: The rock sample was broken due to high vibrations,

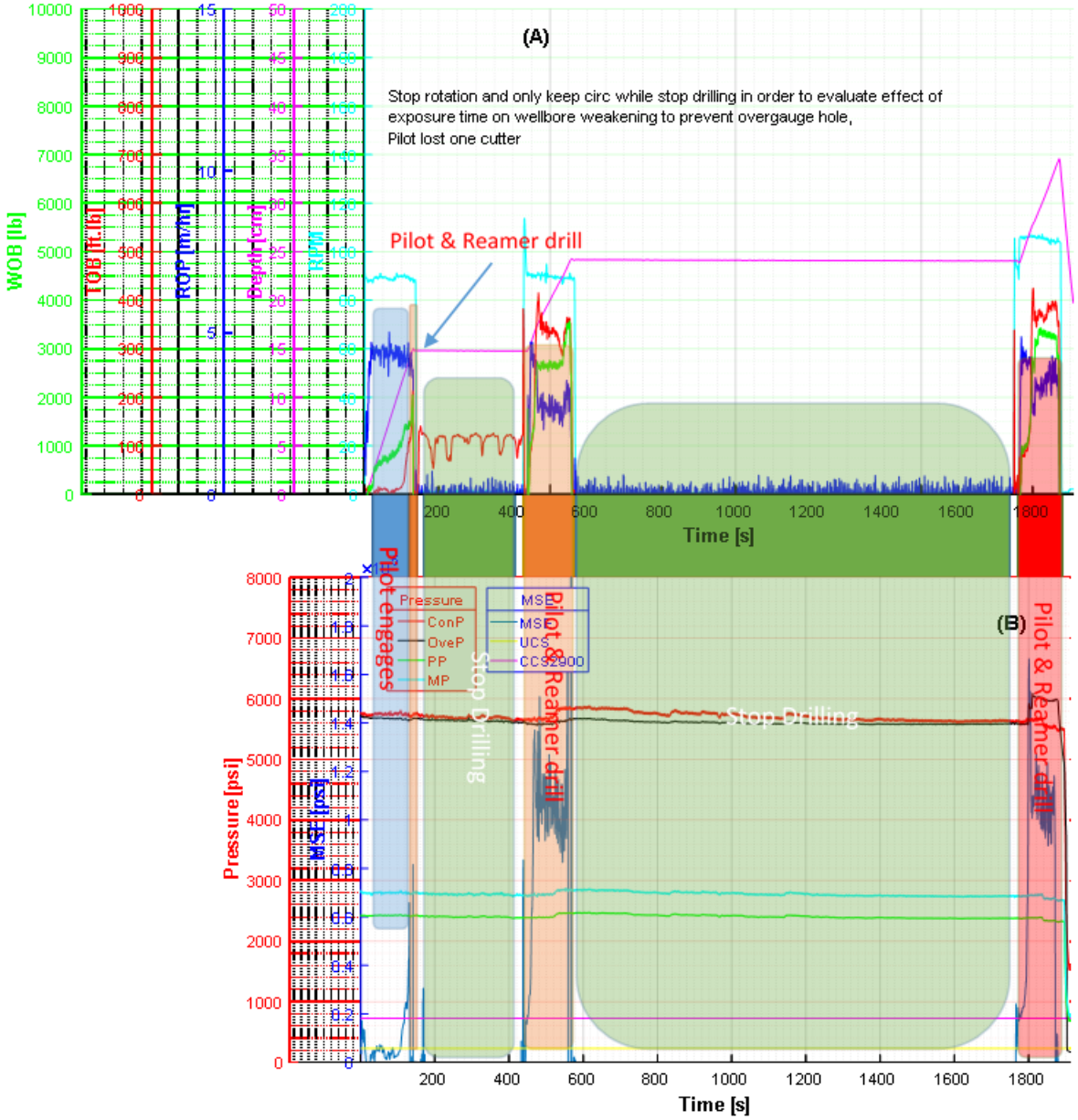

Figure 6-21 Test 9: Pilot - Reamer 10-cm distance, High Pore pressure, Ambient Temperature: One cutter was broken, therefore MSE higher than former test

Figure 6-22 the pilot bit balling (test 9)

Figure 6-23 Broken cutter (test 9)

Figure 6-24 Extreme vibration while rotating off bottom (test 8), unsmooth wellbore is a good indication of viberation

7 Summary and Conclusions

This research presents a thermoporoelastic model for different formation properties, proven by means of laboratory tests. The formations were exposed to a non-hydrostatic stress field and a steady temperature difference between the drilling fluid and the formation. Analytical calculations demonstrate the role of the thermoporoelastic process on the conditions leading to borehole weakening, pursuant drilling under non-isothermal situations. The research indicates that stress alteration, cooling the borehole, hydraulic diffusion and micro-fractured drilling can significantly reduce the MSE, which could correlate with the weakening of the surrounding rock. With time and mud pressure applied, the hydraulic diffusion moves undisturbed inside the core sample. Consequently, the reamer will be able to destroy the rock around the pilot hole more efficiently and with less required energy per unit of volume.

This work discusses detailed laboratory research on how opening a borehole while drilling can improve drilling efficiency. The results of drilling tests in a permeable formation with the pilot & reamer configuration have shown significantly higher efficiency than with standard full body bits with the same equivalent diameter.

The effect of performance by pilot and reamer combination can also be expected during drilling through large scale formations, however, this is yet to be proven in real field applications. In order to gain the advantages from this weakening zone, the following conclusions are drawn:

- ✓ For a typical ROP (assume 30-m/hr.) to drill through low permeable formation, 5% bigger reamer should be placed 0.5-meter above the pilot bit and if 10% bigger reamer is considered, then it must be placed 75-meters above the bit in order to gain benefit of rock weakening process by the pilot. This is a result of time-dependent rock weakening process; due to stress alteration, fluid diffusion and temperature change.

- ✓ This distance in a highly permeable formation is very short. In addition, the required power to destroy a unit volume of rock reduces significantly more than when drilling with multi-diameter tools through not very permeable formations. Less power leads to lower costs and shorter drilling times.
- ✓ However, additional research efforts are still needed for a more sophisticated multi-diameter design. For the full approach, further field tests are required. These will render the potential improvements that are to be achieved with the multi-diameter system.
- ✓ Although a lot of work and laboratory tests remain to be performed, this method and the results show that the concept can be used as guidance for selecting the optimum reamer-bit system for a specific scenario. Investigating the optimum bit to reamer distance has become the major objective.
- ✓ This research focuses solely on presenting the advantages of rock weakening around the with relation to the enlargement tool; however, several schools of thought maintain that it is essential to make a pilot hole and enlarge it simultaneously and efficiently whilst also taking into account aggressiveness, durability, steerability, stability, etc.

8 Further Work

After exhaustive cross-over-sub design and testing efforts, this research project has discovered a new concept as being one possible solution to improve drilling performance. The concept is based on specifically taking advantage of rock weakening around the wellbore by designing multi diameter bits. The bits, which have been combined with a pilot and a reamer, and a cross over sub for different configurations were then tested in the laboratory facility. The facility is able to provide overburden, confine and pore pressure as well as circulating under pressure at the designated temperature. However, continued research is still required to optimize the bit designs. Additional test bit designs and more laboratory test runs could lead to new insights and major design changes. Furthermore, the researchers have managed to gain further know how and experience, which leads to a more effective approach an as well as developing new ideas in drilling.

Further investigation work shall address a mechanism to change the distance that the pilot bit is projecting ahead of the following reamer while drilling. Evidence suggests a variation of plug lengths are required for an optimized drilling performance, for different degrees of rock permeability.

Another area of further investigation addresses a deep understanding of mechanics will not only maximize ROP but also the steerability. It means rotation of the inner part of the bit at different RPM with the outer reamer. The RPM of the reamer can be lower than the pilot as it can provide higher rotational force than the pilot owing to its larger radius.

The necessary loads to make latching/un-latching mechanism of the inner bit should be further investigated.

Nevertheless, to prove the functionality of the overall concept, the field execution of the developed analytical approach is essential.

9 List of Abbreviations

Nomenclature

A_b, A_r	Cross sectional area of the bit / reamer $[L^2]$
A_0	Variable defined in Eq. 4-28
$A_0^{'}$	Variable defined in Eq. 4-29
A'	Variable defined in Eq. 4-30
A_p	Variable defined in Eq. 4-51
AFE	Authority for expenditures
AMSE	Analytical Mechanical Specific Energy $[ML^{-1}T^{-2}]$
ARS	Apparent Rock Strength $[ML^{-1}T^{-2}]$
B	Skempton pore pressure coefficient
BHA	Bottom Hole Assembly
BHE	Bore Hole Enlargement
CCS	Confined Compressive Strength $[ML^{-1}T^{-2}]$
CWD	Casing While Drilling
C_1	Variable defined in Eq. 4-89
C_2	Variable defined in Eq. 4-90
C_3	Variable defined in Eq. 4-91
D_1	Variable defined in Eq. 4-92
D_2	Variable defined in Eq. 4-93
c_T	Thermal diffusivity $[L^2T^{-1}]$
c_f	Fluid diffusivity $[L^2T^{-1}]$
c_{ft}	Coupled thermal-fluid pressure coefficient $[ML^{-1}T^{-2}K^{-1}]$
$c_T^{'}$	Coupling coefficient
c_m	Specific heat $[L^{-2}T^{-2}K^{-1}]$
DBB	Dual Body Bit
DHM	Down Hole Motor
DLS	Dog Leg Severity $[Deg]$
DOC (Δh_b, Δh_r)	Depth Of Cut (Bit, Reamer) $[L]$
DSE	Drilling Specific Energy
DTF	Drilling Test Facility
d_b	Bit diameter $[L]$
Eff_M	Uniform drilling efficiency
ECD	Equivalent Circulation Density
f_w	Weight distribution factor

F_r	Ratio of weight on the reamer
G	Shear modulus $[ML^{-1}T^{-2}]$
GOM	Gulf Of Mexico
h_i	Linear heat flow in the ith direction $[MT^{-3}]$
HSI	Horsepower per Square Inch
$H(t)$	Heaviside unit step function
k	Drillability constant
KPI	Key Performance Indicators
k^T	Thermal conductivity of the solid matrix $[MLT^{-3}K^{-1}]$
k_b	Bit sharpness
K_0	Modified Bessel function of second kind of order zero
K_1	Modified Bessel function of second kind of order one
K_2	Modified Bessel function of second kind of order two
LWD	Logging While Drilling
MPSI	Mechanical Power per Square Inch
MSE	Mechanical Specific Energy $[ML^{-1}T^{-2}]$
MSE_{adj}	Adjusted MSE $[ML^{-1}T^{-2}]$
MSE_{Mod}	Modified MSE $[ML^{-1}T^{-2}]$
MW	Mud Weight
MWD	Measure While Drilling
NPT	Non-Productive Time
PDC	Polycrystalline diamond compact
PDM	Positive Displace Motor
p	Pore pressure $[ML^{-1}T^{-2}]$
p_0	Initial pore pressure $[ML^{-1}T^{-2}]$
p_f	Formation pore pressure $[ML^{-1}T^{-2}]$
p_w	Mud pressure in the borehole $[ML^{-1}T^{-2}]$
P_0	Isotropic compressive stress $[ML^{-1}T^{-2}]$
q_i	Fluid velocity in the ith direction [LT^{-1}]
r	Radial distance to the center of the borehole $[L]$
r_d	Dimensionless radial distance, defined in Eq. 4-31
ROP	Rate Of Penetration $[LT^{-1}]$
RPM	Revolution Per Minute
RSS	Rotary Steerable System
s	Laplace variable
SE	Specific Energy $[ML^{-1}T^{-2}]$
TOB	Torque On Bit
t	Time [T]
t_d	Dimensionless time, defined in Eq. 4-31
T	Temperature [K]
T_f	Formation temperature [K]
T_m	Mud temperature [K]
u	Solid matrix displacement [L]
UCS	Unconfined Compressive Strength $[ML^{-1}T^{-2}]$
WOB	Weight On Bit $[MLT^{-2}]$
W_b, W_r	Weight On Bit / Reamer $[MLT^{-2}]$
W_{r-0}	Threshold weight on bit $[MLT^{-2}]$
XOS	Cross Over Sub
Greek Letters	
$\emptyset$	Rock internal angle of friction $[Degree]$
v	Drained Poisson's ratio $[Dimensionless]$
v_u	Undrained Poisson's ratio $[Dimensionless]$
α	Biot's coefficient $[Dimensionless]$

α_m^T	Volumetric thermal expansion coefficient of the solid matrix $[K^{-1}]$
α_f^T	Volumetric thermal expansion coefficient of the pore fluid $[K^{-1}]$
η_T	Constant defined in Eq. 4-63
η	Constant defined in Eq. 4-94
ξ	Constant defined in Eq. 4-64
β	Constant defined in Eq. 4-65
ξ_T	Constant defined in Eq. 4-66
β_T	Constant defined in Eq. 4-67
δ_{ij}	Kronecker delta
Δ	Change
ε_{ij}	Strain tensor of the solid matrix
γ	Wellbore inclination angle $[Degree]$
ω	Wellbore azimuth angle $[Degree]$
σ_b, σ_r	Compressive strength of the rock below bit / reamer $[ML^{-1}T^{-2}]$
σ_v	Overburden pressure $[ML^{-1}T^{-2}]$
σ_1	Effective maximum principal stress $[ML^{-1}T^{-2}]$
σ_3	Effective minimum principal stress $[ML^{-1}T^{-2}]$
σ_h	Minimum horizontal principal stress $[ML^{-1}T^{-2}]$
σ_H	Haximum horizontal principal stress $[ML^{-1}T^{-2}]$
σ_{ij}	Stress tensor of the solid matrix $[ML^{-1}T^{-2}]$
σ_{kk}	Total principal stresses $[ML^{-1}T^{-2}]$
σ_v	Vertical stress $[ML^{-1}T^{-2}]$
φ	Formation effective porosity
φ_0	Initial porosity
ρ_f	Fluid density
ρ_b	Bulk density
Subscripts	
0	Initial
b	Bulk material
m	Matrix
d	Dimensionless parameter
$\theta\theta$	Tangential
f	Hydraulic or formation
h	Minimum horizontal
H	Maximum horizontal
i, j	Index of coordinate
kk	Bulk value
$r\theta$	Shear
rr	Radial
T	Thermal
v	Vertical
Superscripts	
max	Maximum
T	Thermal
$'$	Effective stress
Over scripts	
$\sim$	Laplace space

10 References

[1] S. Barton and R. Weeden, *Accurate Matching of Bit and Reamer Tools Delivers Optimized Drilling Performance,* Beijing, 2010.

[2] S. Lisa, “Oilfield Review,” Schlumberger, 2011.

[3] M. Fear, F. Abbasian, S. Parfitt and A. McClean, “The Destruction of PDC Bits by Severe Slip-Stick Vibration,” in *SPE/IADC Drilling Conference*, Amsterdam, 1997.

[4] G. Mensa-Wilmot, J. Gagneaux, G. Woldtvedt and A. Osborn, *Innovative Product Concepts and Drilling Practices Improve Bit and Reamer Performances in Harsh Drilling Environments,* London: SPE/IADC-173140-MS, 2015.

[5] G. Mensa-Wilmot and M. J. Fear, “The Effects of Formation Hardness, Abrasiveness, Heterogeneity and Hole Size on PDC Bit Performance,” in *SPE/IADC Drilling Conference*, Amsterdam, 2001.

[6] P. Teasdale, G. John and R. Davis, “Innovative Dual-Diameter PDC Bit Design Provides Unique Solution to Successful Drilling of Challenging Volcanic Interval,” in *IADC/SPE Drilling Conference and Exhibition*, Texas, 2014.

[7] A. Bencic, *Development of Low Cost Dynamically Stable Slimhole Drill and Core Bits,* Leoben: Montanuniversität Leoben, 1998.

[8] R. Simon, “Energy Balance in Rock Drilling,” *Society of Petroleum Engineers Journal,* vol. 3, no. 04, pp. 298 - 306, 1963.

[9] R. Teale, “The concept of Specific Energy in Rock Drilling,” *International Journal of Rock Mechanics and Mining Sciences & Geomechanics Abstracts,* vol. 2, pp. 57 - 73, 1965.

[10] E. Detournay, T. Richard and M. Shepherd, “Drilling response of drag bits: Theory and experiment,” *International Journal of Rock Mechanics and Mining Sciences,* vol. 45, no. 8, pp. 1347 - 1360, 2008.

[11] R. C. Pessier and M. J. Fear, *Quantifying Common Drilling Problems With Mechanical Specific Energy and a Bit-Specific Coefficient of Sliding Friction,* Washington: SPE 24584-MS, 1992.

[12] H. U. Caicedo , W. M. Calhoun and R. T. Ewy, *Unique ROP Predictor Using Bit-specific Coefficient of Sliding Friction and Mechanical Efficiency as a Function of Confined Compressive Strength Impacts Drilling Performance,* Amsterdam: SPE/IADC Drilling Conference, 2005.

[13] H. Caicedo, W. Calhoun and R. Ewy, *Unique Bit Performance Predictor Using Specific Energy Coefficients As a Function of Confined Compressive Strength Impacts Drilling Performance,* Johannesburg: 18th World Petroleum Congress, 2005.

[14] A. Bencic, M. Prohaska, J. de Sousa and K. Millheim, “Slimhole Drilling and Coring - A New Approach,” in *SPE Annual Technical Conference and Exhibition*, Louisiana, 1998.

[15] J. McCarthy, J. Rebellon, S. Barton and R. Rambhai, *A Practical, Application-Based Guide to Borehole Enlargement Tool Selection,* Macae, 2011.

[16] A. Bencic, M. Prohaska, J. de Sousa and K. Milleim, “Slimhole Drilling and Coring - A New Approach,” in *SPE Annual Technical Conference and Exhibition*, New Orleans, Louisiana, 1998.

[17] J. de Sousa, M. Prohaska, A. Bencic and K. Milleim, “Optimization of Slimhole Dual-Body Bits by Experiments and Computational Fluid Dynamics,” in *SPE Western Regional Meeting*, Anchorage, Alaska, 1999.

[18] G. Csonka, M. W. Tweedy, S. Cornel and M. Anderson, *Ream While Drilling Technology Applied Successfully Offshore Australia,* Adelaida: SPE 36990, 1996.

[19] C. H. Dewey and G. C. Miller, *Drilling and Underreaming Simultaneously: A Cost-Effective Option. Society of Petroleum Engineers,* Denver: SPE 36462, 1996.

[20] P. Hyatt, A. Little, A. Sinor and G. Herran, *Ream While Drilling Technology Cuts $1 Million in Nile Delta Well,* Bahrain: SPE/IADC 39248, 1997.

[21] G. C. Miller and R. D. Childers, *Innovative Concentric Reamer Enhances Deepwater Drilling Operations,* Denver: SPE 84247, 2003.

[22] D. F. Courville, R. D. Childers and G. C. Miller, *Wellbore Enlargement for a Deepwater Casing Program: Case Study and Developments,* Dalas: IADC/SPE 87153, 2004.

[23] C. J. Mason, B. Wenande and D.-K. Chen, *Supersize Hole Creates Drilling Opportunity,* Anaheim: SPE 108427, 2007.

[24] S. Jones and J. Sugiura, *Concurrent Rotary-Steerable Directional Drilling and Hole Enlargement Applied Successfully: Case Studies,* Orlando: IADC/SPE 112670, 2008.

[25] T. Ho, C. Alferez, M. Cortez, I. Nott and X. McNary, *Optimal Bit, Reamer Selection and Operating Procedures Improve Hole Enlargement Performance in Deepwater Gulf of Mexico,* Amesterdam: SPE/IADC 163425, 2013.

[26] I. Thomson, S. Radford, J. Powers, L. Shale, C. Hughes and J. M. , *A Systematic Approach to a Better Understanding of the Concentric Hole-Opening Process Utilizing Drilling Mechanics and Drilling Dynamics Measurements Recorded Above and Below the Reamer,* Orlando, Florida: IADC/SPE 112647, 2008.

[27] M. Reich, *Investigation of complex BHA sets with integrated, switchable extension tool,* Ph.D dissertation, Technische Universität Bergakademie Freiberg, 2003.

[28] B. Meyer-Heye, H. Reckmann and G. P. Ostermeyer, *Weight Distribution in Reaming While Drilling BHAs,* New Orlean, Louisina: IADC/SPE 127094, 2010.

[29] T. Warren, L. Sinor and M. Dykstra, *Simultaneous Drilling and Reaming with Fixed Blade Reamers,* Dallas, 1995.

[30] S. Barton and R. Weeden, *Unique Selection Tool Enables Scientific Approach to Matched Reamer Assemblies,* Galveston: SPE 137871, 2010.

[31] S. Barton, F. Baez and R. Gee, *Downhole Matched Solutions: Innovative Scientific Approach to More Efficient Assemlies,* Jakarta: SPE 145980, 2011.

[32] A. Nascimento, A. Elmgerbi, A. Roohi, M. Prohaska, G. Thonhauser and M. H. Mathias, *Dynamic Drill-rate Test Approach Applied to a Pre-salt Case Study,* Quito: SPE-177141-MS, 2015.

[33] M. Rutao, J. Youzhe, W. Hui and H. Fei, *Dual-Factor Method for Calculating Weight Distribution in Reaming While Drilling,* Tianjin: IADC/SPE 155834, 2012.

[34] J. K. Al-Thuwaini, M. Emad, H. Hendrazid, W. Mohamed, R. Chafai and A. D. Murdock, *Combination of unique stabilized Bi-Center bit and Vibration dampening tool improve hole opening performance through interbedded formations in Saudi Arabia,* Abu Dhabi: SPE 117248, 2008.

[35] S. Barton and J. Clegg, *True Matching of Bit and Multidiameter String Tools Delivers Optimized Drilling Performance,* Amesterdam, 2009.

[36] U. Prasad, *Drillability of a Rock In Terms of Its Physico-Mechanical And Micro-Structural Properties,* Asheville: 43rd U.S. Rock Mechanics Symposium & 4th U.S. - Canada Rock Mechanics Symposium, 2009.

[37] D. J. Reddish and E. Yasar, “A New Portable Rock Strength Index Test Based on Specific Energy of Drilling,” *International Journal of Rock Mechanics and Mining Sciences & Geomechanics Abstracts,* vol. 33, no. 5, pp. 543 - 548, 1996.

[38] D. Curry, M. Fear, A. Govzitich and L. Aghazada, *Technical Limit Specific Energy - An Index to Facilitate Drilling Performance Evaluation,* Amsterdam: SPE/IADC Drilling Conference, 2005.

[39] G. Hareland and R. Nygaard, *Calculating Unconfined Rock Strength From Drilling Data,* Vancouver: American Rock Mechanics Association, 2007.

[40] W. Maurer, “The "Perfect - Cleaning" Theory of Rotary Drilling,” *Journal of Petroleum Technology,* vol. 14, no. 11, pp. 1270 - 1274, 1962.

[41] D. Gray-Stephens, J. M. Cook and M. C. Sheppard, “Influence of Pore Pressure on Drilling Response in Hard Shales,” *SPE Drilling & Completion,* vol. 9, no. 04, pp. 263 - 270, 1994.

[42] E. Detournay and C. P. Tan , *Dependence of Drilling Specific Energy on Bottom-Hole Pressure in Shales,* Irving, Texas: SPE/ISRM Rock Mechanics Conference, 2002.

[43] R. Cunningham and J. G. Eenink, “Laboratory Study of Effect of Overburden, Formation and Mud Column Pressures on Drilling Rate of Permeable Formations,” vol. 217, pp. 9 - 17, 1959.

[44] A. D. Black, . H. L. Dearing and B. G. DiBona, “Effects of Pore Pressure and Mud Filtration on Drilling Rates in a Permeable Sandstone,” *Journal of Petroleum Technology,* vol. 37, no. 09, pp. 1671 - 1681, 1985.

[45] A. J. Garnier and N. H. Van Lingen, “Phenomena Affecting Drilling Rates at Depth,” *AIME,* vol. 216, pp. 232 - 239, 1959.

[46] E. Detournay and C. Atkinson, *Influence of Pore Pressure On the Drilling Response of PDC Bits,* Norman, Oklahoma: The 32nd U.S. Symposium on Rock Mechanics (USRMS), 1991.

[47] E. Detournay and C. Atkinson, “Influence of pore pressure on the drilling response in low-permeability shear-dilatant rocks,” *International Journal of Rock Mechanics and Mining Sciences,* vol. 37, no. 7, pp. 1091 - 1101, 2000.

[48] J. J. Kolle, *The Effects of Pressure and Rotary Speed on the Drag Bit Drilling Strength of Deep Formations,* Denver, Colorado: SPE Annual Technical Conference and Exhibition, 1996.

[49] A. Judzis, A. D. Black, D. A. Curry, M. J. Meiners, T. Grant and R. G. Bland, *Optimization of Deep Drilling Performance; Benchmark Testing Drives ROP Improvements for Bits and Drilling Fluids,* Amsterdam: SPE/IADC Drilling Conference, 2007.

[50] H. Rabia, “Specific Energy as a Criterion for Bit Selection,” *Journal of Petroleum Technology,* vol. 37, no. 07, 1985.

[51] Pason. [Online]. Available: http://www.pason.com/. [Accessed 2016].

[52] F. Dupriest and W. L. Koederitz, *Maximizing Drill Rates with Real-Time Surveillance of Mechanical Specific Energy,* Amsterdam: SPE/IADC Drilling Conference, 2005.

[53] F. Dupriest, J. W. Witt and S. M. Remmert, *Maximizing ROP With Real-Time Analysis of Digital Data and MSE,* Doha: International Petroleum Technology Conference (IPTC), 2005.

[54] M. Armenta, *Identifying Inefficient Drilling Conditions Using Drilling-Specific Energy,* Denver, Colorado: SPE Annual Technical Conference and Exhibition, 2008.

[55] K. Mohan, F. Adil and R. Samuel, *Tracking Drilling Efficiency Using Hydro-Mechanical Specific Energy,* Amsterdam: SPE/IADC Drilling Conference and Exhibition, 2009.

[56] R. C. Pessier, S. N. Wallace and H. Oueslati, *Drilling Performance is a Function of Power at the Bit and Drilling Efficiency,* San Diego: IADC/SPE Drilling Conference and Exhibition, 2012.

[57] R. Pessier, S. Wallace and H. Oueslati, "Drilling Performance Is a Function of Power at the Bit and Drilling Efficiency," *Journal of Petroleum Technology,* vol. 64, no. 04, 2012.

[58] R. C. Pessier, S. N. Wallace and H. Oueslati, "Graph to analyze drilling parameters". US Patent US8854373 B2, 7 10 2014.

[59] W. B. Bradley, "Failure of Inclined Boreholes," *Journal of Energy Resources Technology,* vol. 101, pp. 232 - 239, 1979.

[60] G. Chen and R. T. Ewy, "Thermoporoelastic Effect on Wellbore Stability," *SPE Journal,* vol. 10, no. 02, 2005.

[61] E. Detournay and A. H.-D. Cheng, "Poroelastic Response of a Borehole in a Non-hydrostatic Stress Field," *Int. J. Rock Mech. Min. Sci. & Geomech,* vol. 25, no. 3, pp. 171 - 182, 1988.

[62] Q. Tao and A. Ghassemi, "Poro-thermoelastic borehole stress analysis for determination of the in situ stress and rock strength," *Geothermics,* vol. 39, no. 3, pp. 250 - 259, 2010.

[63] H. Shahabadi, M. Yu , S. Z. Miska and N. E. Takach, *Modeling Transient Thermo-Poroelastic Effects on 3D Wellbore Stability,* San Antonio: SPE Annual Technical Conference and Exhibition, 2006.

[64] M. Kurashige, “A Thermoelastic Theory of Fluid-Filled Porous Materials,” *Int. J. Solids Structures,* vol. 25, no. 9, pp. 1039 - 1052, 1989.

[65] Y. Wang and E. Papamichos, “Conductive heat flow and thermally induced fluid flow around a well bore in a poroelastic medium,” vol. 30, no. 12, p. 3375, 1994.

[66] X. Li, L. Cui and J. -C. Roegiers, “Thermoporoelastic Modelling of Wellbore Stability in Non-hydrostatic Stress Field,” *International Journal of Rock Mechanics and Mining Sciences,* vol. 35, no. 4 - 5, pp. 584 - 584, 1998.

[67] L. Cui, S. Ekbote, Y. Abousleiman and J.-C. Roegiers, “Borehole stability analysis in fluid saturated formations with Impermeable Walls,” *International Journal of Rock Mechanics and Mining Science,* vol. 35, no. 4, pp. 582 - 583, 1998.

[68] L. Cui, Y. Abousleiman, A. H.-D. Cheng and J. -C. Roegiers, “Time-Dependent Failure Analysis of Inclined Boreholes in Fluid-Saturated Formations,” *Journal Energy Resources Technology ,* vol. 121, no. 38, 1999.

[69] Y. Abousleiman, S. Ekbote, L. Cui, F. Mody, J. C. Roegiers and M. Zaman, *Time-Dependent Coupled Processes in Wellbore Design and Stability: PBORE-3D,* Houston: Society of Petroleum Engineers, 1999.

[70] Y. Abousleiman and S. Ekbote, “Solutions for the Inclined Borehole in a Porothermoelastic Transversely Isotropic Medium,” *Journal of Applied Mechanics,* vol. 72, no. 1, pp. 102 - 114, 2005.

[71] M. A. Biot, “General theory of three-dimensional consolidation,” *Journal Applied Physics,* vol. 12, no. 2, pp. 155 - 164, 1941.

[72] M. A. Biot, “Theory of elasticity and consolidation for a porous anisotropic solid,” *Journal of Applied Physics,* vol. 26, no. 2, pp. 182 - 185, 1955.

[73] M. A. Biot, “General solutions of the equations of elasticity and consolidation for a porous material,” *Journal of Applied Mechanics,* vol. 78, p. 91 96, 1956.

[74] M. A. Biot and D. G. Willis, “The elastic coefficients of the theory of consolidation,” *Journal of Applied Mechanics,* pp. 594 - 601, 1957.

[75] J. R. Rice and M. P. Cleary, “Some Basic Stress-Diffusion Solutions for Fluid-Saturated Elastic Porous Medium with Compressible Constituents,” *Reviews of Geophysics and Space Physics,* vol. 14, no. 2, pp. 227 - 241, 1976.

[76] L. Cui, A. H.-D. Cheng and Y. Abousleiman, “Poroelastic Solution for an Inclined Borehole,” *Journal of Applied Mechanics,* vol. 64, no. 1, pp. 32 - 38, 1997.

[77] X. Li, L. Cui and J. -C. Roegiers, *Thermoporoelastic Analyses of Inclined Boreholes,* Trondheim: SPE/ISRM Rock Mechanics in Petroleum Engineering, 1998.

[78] G. Chen and R. T. Ewy, *Thermoporoelastic Effect On Wellbore Stresses In Permeable Rocks,* Houston: American Rock Mechanics Association, 2004.

[79] E. Detornay and A. H.-D. Cheng, “Fundamentals of Poroelasticity,” in *Comprehensive Rock Engineering: Principles, Practice and Projects*, Pergamon Press,, 1993, pp. 113 - 171.

[80] P. A. Domenico and F. W. Schwartz, “Physical and Chemical Hydrogeology,” New York, John Wiley, 1990.

[81] A. H.-D. Cheng, “On generalized plane strain poroelasticity,” *International Journal of Rock Mechanics and Mining Sciences,* vol. 35, no. 2, pp. 183 - 193, 1998.

[82] H. Stehfest, “Numerical inversion of Laplace transforms [D5],” *Commun. ACM (Communications of the ACM),* vol. 13, no. 1, pp. 47 - 49, 1970.

[83] H. S. Carslaw and J. C. Jaeger, Conduction of Heat in Solids, Clarendon Press, 1959.

[84] A. Roohi, A. Elmgerbi, A. Nascimento, M. Prohaska and G. Thonhauser, “Mathematical Approach of MSE in Thermo-Poro-Elastic Conditions Improves Decision Making to Use RWD,” in *SPE Bergen One Day Seminar*, Bergen, Norway, 2016.

[85] A. Roohi, A. Nascimento, A. Elmgerbi, M. Prohaska and G. Thonhauser, “A Mathematical Approach Using Thermoporoelastic Model for Reamer While Drilling Efficiency Analysis and Closeness,” *Research Journal of Applied Science, Engineering & Technology,* vol. 13, no. 1, pp. 7 - 14, 2016.

[86] Y. Li and D. R. Schmitt, “Well-Bore Bottom Stress Concentration and Induced Core Fractures,” *AAPG Bulletin,* vol. 81, no. 11, pp. 1909 - 1925, 1997.

[87] L. Ulvedal, J. D. Enterline, D. Scott, S. Radford, J. Clinkscales, L. Shale and M. Croxton, *Operator's Recommendation for a Uniform Dull Grading System for Fixed Cutter Hole Enlargement Tools,* Amsterdam, 2011.

[88] B. C. SketchIer, C. M. Fielder and B. E. Lee, *New Bi-Center Technology Proves Effective in Slim Hole Horizontal Well,* Amsterdam, 1995.

[89] S. Paul Barton and R. William Weeden, *Unique Selection Tool Enables Scientific Approach to Matched Reamer Assemblies,* Galveston, 2010.

[90] S. Barton, W. Jones and H. Rorvik, *Multi-Diameter String Tools Deliver Lower Cost-Per-Foot in Demanding Rotary Steerable Applications,* Orlando: IADC/SPE 112785 , 2008.

[91] T. M. Warren and L. A. Sinor, *Simultaneous Drilling and Reaming with Fixed Blade Reamers,* Dallas, Texas: SPE Annual Technical Conference and Exhibition, 1995.

[92] T. M. Warren, "Penetration Rate Performance of Roller Cone Bits," vol. 2, no. 01, 1987.

[93] H. Rabia, *Rig Hydraulics,* Entrac Software, 1989.

[94] W. K. Amadi and I. Iyalla, *Application of Mechanical Specific Energy Techniques in Reducing Drilling Cost in Deepwater Development,* Galveston, Texas: SPE Deepwater Drilling and Completions Conference, 2012.

[95] B. Rashidi, G. Hareland and R. Nygaard, *Real-Time Drill Bit Wear Prediction by Combining Rock Energy and Drilling Strength Concepts,* Abu Dhabi: International Petroleum Exhibition and Conference, 2008.

[96] R. J. Waughman, J. V. Kenner and R. A. Moore, *Real-Time Specific Energy Monitoring Reveals Drilling Inefficiency and Enhances the Understanding of When to Pull Worn PDC Bits,* Dalas, Texas: IADC/SPE Drilling Conference, 2002.

[97] P. L. Moore, *Drilling Practices Manual,* Tulsa: Penn Well Books, 1974.

[98] H. Abdollahi, S. Moosazadeh and A. Ghazvinian, *Drilling Optimization Using Minimum Energy Concept,* Tehran: the 2nd Iranian Rock Mechanics Conference, 2004.

[99] J. C. Jaeger, N. G. W. Cook and R. W. Zimmerman, "Fundamentals of rock mechanics," Wiley-Blackwell Publishing, 2007.

[100] E. Fjaer, R. M. Holt, P. Horsrud, A. M. Raaen and R. Risnes, “Petroleum Related Rock Mechanics,” Elsvier, 2008.

[101] B. S. Aadnoy and R. Looyeh, “Petroleum Rock Mechanics: Drilling Operations and Well Design,” Elsevier, 2011.

[102] M. D. Zoback, “Resevoir Geomechanics,” Cambridge University Press, 2007.

[103] T. Engleder, “Stress regimes in the lithosphere,” Princeton University Press.

[104] R. H. G. Parry, “Mohr circles, stress paths and geotechnics,” E & FN Spon, Chapman & Hall, 1995.

[105] D. L. Turcotte and G. Schubert, “Geodynamics,” Cambridge University Press, 2002.

[106] J. Handin, “On the Mohr-Coulomb failure criterion,” *Journal of Geophysical Research,* vol. 74, no. 22, pp. 5343 - 5348, 1969.

[107] K. Terzaghi, Theoretical soil mechanics, New York: John Wiley and Sons, 1943.

[108] H. F. Wang, Theory of Linear Poroelasticity with Applications to Geomechanics and Hydrogeology, New Jersey: Princeton University Press, 2000.

[109] M. A. Biot, “Theory of elasticity and consolidation for a porous anisotropic solid,” *Journal of Applied Physics,* vol. 26, no. 2, pp. 182 - 185, 1955.

[110] I. Rumzan and D. Schmitt, *The Influence of well bore fluid pressure on drilling penetration rates and stress dependent strength,* Washington: American Rock Mechanics Association, 2001.